Synchronization phenomena in complex networks of pulse-coupled oscillators: self-generated changes between randomness and order

Dissertation
zur
Erlangung des Doktorgrades (Dr. rer. nat.)
der
Mathematisch-Naturwissenschaftlichen Fakultät
der
Rheinischen Friedrich-Wilhelms-Universität Bonn

vorgelegt von
Alexander Rothkegel
aus
Berlin (West)

Bonn, 2013

Angefertigt mit Genehmigung der Mathematisich-Naturwissenschaftlichen
Fakultät der Rheinischen Friedrich-Wilhelms-Universität Bonn

1. Gutachter: Prof. Dr. Klaus Lehnertz
2. Gutachter: Prof. Dr. Carsten Urbach
Tag der mündlichen Prüfung: 7. Februar 2014
Erscheinungsjahr 2014

Abstract

Complex network comprised of interconnected oscillatory systems are investigated in various contexts in the natural sciences. It is an important goal to understand in which way synchronization phenomena in such networks are determined by the structure of the network itself and by properties of the oscillatory systems. Contrasting the microscopic behavior which often shows fluctuations, many studies have characterized synchronization and desynchronization as convergence towards oscillatory and constant macroscopic behavior, respectively. However, very few models have been developed which show self-generated and recurrent changes between randomness and order.

In this thesis, we study the influence of the connection structure on the dynamical behavior of complex networks of oscillators. More concretely, we consider δ-pulse-coupled, excitatory integrate-and-fire-like oscillators, possibly endowed with refractory periods and time delayed interactions, and study their dynamics when coupled onto random and onto small-world networks, i.e., networks with both short-ranged and long-ranged connections.

In random networks, these oscillators may exhibit both chaotic, asynchronous behavior and synchronous behavior. We define and investigate different types of continuum models which describe the thermodynamic limit of large networks and allow us to characterize different mechanism for the loss of stability of asynchronous behavior. If stability is lost, oscillators may show partially synchronous states and irregular behaviors. We relate the latter to recurrent times at which the firing rate in the networks diverges and a macroscopic amount of oscillators spontaneously fires in unison.

Continuing one of these transitions to synchrony into the small-world regime leads to a rich spectrum of dynamical behaviors which are determined by the interplay between pattern formation and synchronization phenomena. In addition to various kinds of wave-dominated states, we report here on so-called chimera states, in which the networks split into asynchronous and synchronous regions. Depending on oscillator parameters, these regions may be fixed in shape and size, or may evolve constantly leading to macroscopic observables which show non-converging behavior. The latter may take the form of asynchronous firing interrupted by short and rare events of synchronous firing, or of a network rhythm in which more and less synchronous behaviors alternate on a timescale

well below the period duration of oscillators.

The non-converging synchronization phenomena that we describe in this thesis add new aspects to the discussion which may help in unravelling the complicated relationships between the network structure, node dynamics, and the collective network dynamics.

Contents

The following list provides an overview of publications containing material from this thesis.

- A. Rothkegel and K. Lehnertz. "Recurrent events of synchrony in complex net- works of pulse-coupled oscillators". *Europhys. Lett.* 95 (2011), p. 38001.
- A. Rothkegel, C. E. Elger, and K. Lehnertz. "Initiation and termination of seizure- like activity in small-world networks of integrate-and-fire neurons". In: *Epilepsy: The Intersection of Neurosciences, Biology, Mathematics, Engineering, and Physics*. Ed. by I. Osorio, H. P. Zaveri, M. G. Frei, and S. Arthurs. Boca Raton, USA: CRC Press, 2011, pp. 341–347.
- A. Rothkegel and K. Lehnertz. "Multistability, local pattern formation, and global collective firing in a small-world network of non-leaky integrate-and-fire neu- rons". *Chaos* 19 (2009), p. 015109.

1 Introduction

Systems that we denote as complex are usually comprised of a large number of interconnected or interacting parts, and due to their complicated structure or organization, they defy an exact description. Examples are as diverse as ant and bee colonies, living organisms and in particular their nervous system, human economies and social interactions, and the climate system [1]. Due to their ubiquitous appearance in nature, complex systems are a central object of study in all natural sciences. Their study is intimately connected to the study of non-linear dynamics as the absence of the superposition principle hinders us to relate the global dynamics to the dynamics of the constituents. In contrast, as soon as nonlinearity is involved, the global behavior of complex systems is often crucially influenced by their structure, and we can observe emerging features which are not part of the dynamical spectrum of the constituents.

In many cases constituents can be classified into a small number of functionally different units which interact in such a way that the interaction represents a weak disturbance of their intrinsic dynamics. In this case, the complexity lies in the interaction network, while the dynamics of constituents is amenable and often well-understood. We denote such a system as a complex network, the constituents as nodes or vertices of the network, and we depict the interaction structure as connections or edges between nodes. The study of complex networks touches many disciplines involving scientists which tackle different parts of the issue. While experimentalists investigate the topology of natural networks or describe their functional behavior, theorists relate structure to function in controllable and simplified setups [2–5]. Examples of complex networks are contact networks, in which connection means some kind of communication or interaction between humans, technological and infrastructural networks, like the internet, streets and flight routes, and biological networks like food webs, blood vessels, or mammalian brains in which a vast number of neurons is connected by literally billions of synapses. Even if we can determine both nodes and edges of complex networks in large numbers, it is not clear how we should characterize these networks; when a hundred or more nodes are involved graphical representations of networks become unmanageable and do not provide insight. It is an challenge to describe natural networks by properties which are meaningful and possibly relate to dynamical behavior of networks, or to define model

networks which capture some property of natural networks.

A sensible starting point for the investigation of networks, especially if their structure is largely unknown, is to assume that connections or interactions can be described as random. The study of the structure of random networks has a long history in discrete mathematics [6, 7], and much work has been devoted to determine their statistical properties. Much less is known about the emerging dynamics of these networks when they are interpreted as connection structure of an ensemble of dynamical systems. Random networks represent a strong idealization and are defined by a single parameter, the number of connections. As models of natural networks, however, they have several shortcomings: The assumed homogeneity is unreasonable when networks comprise regions with differing conditions. E.g., a infrastructural network which spans over different geographical regions, or a neural network which spans different brain structures is most likely not homogeneous. Moreover, for random networks the distribution of node degrees (which is the numbers of connections of a node) follows a Possonian distribution while natural network show a prevalence towards power-law distributions [8, 9]. A simple consequence is that natural network often contain hubs, i.e., nodes with very many connections, whose existence is very unlikely in random networks.

A third point in which random and natural networks may differ, is that the structure of natural networks often reflects their embedding in space; the probability that two nodes in a natural network are connected depends on their distance and shows a strong preference towards shorter connections. This is to be expected as communication over long distances usually is expensive. For the human brain, it is clear that a large amount of long synapses consumes space and energy. Taking into account the mean number of synapses per neuron and the space they consume, one can easily rule out the assumption of a large amount of long-ranged synapses, as their volume would not fit into human skulls [10]. It is plausible that evolution has provided us with an organization structure which saves biological material. For man-made networks like infrastructure or contact networks, the strong prevalence towards short-ranged connections is also evident; transportation over long distances is time- and resource-consuming. Moreover, even a small number of long-ranged connections can drastically reduce the length of shortest paths between nodes in the network and may be sufficient to guarantee global communication. This observation has led to the notion of *small worlds* which denotes a sparsely connected and large network in which arbitrary nodes can communicate via only a few mediators. Watts and Strogatz defined model networks, which reflect the described observations in spatially embedded social and biological networks and which contain a lattice-like structure which

is disturbed by some amount of random long-ranged connections [11]. The construction rules allow to interpolate continuously between regular lattices and random networks, which both are classical and well-studied organization structures. Although the construction is nearly trivial, their seminal paper has since inspired hundreds of studies aimed at investigating the dynamics of these networks, and characterizing the structure of natural networks to show that they resemble the scheme.

Synchronization means an adjustment of rhythms of oscillatory systems [12]. Among more complicated possibilities, this adjustment can take the form that all systems share a common phase (complete synchrony) or that they display a fixed or approximately fixed phase difference (phase locking). Synchronization can be induced via noise, common to all elements, or via mutual interaction defined by some coupling network. Synchronization phenomena are ubiquitous in nature. Examples in biological systems range from synchronized chirping of crickets, synchronized blinking of fireflies [13, 14], to mammalian physiology [15], including pacemaker cells in hearts [16], insulin secreting cells in the pancreas [17] and brains. Example from physics include Josephson junctions [18] and laser [19]. For networks whose nodes are associated with humans, rhythmic hand-clapping [20], La Ola waves [21] and synchronization of pedestrian motion [22] have been discussed. Also, consensus reaching in so-called agent network has been shown to be strongly linked to synchronization [23] and oscillator models have been considered as a technical means to achieve synchrony in wireless networks [24].

A general observation which can be made across many structural different systems is that synchronization is hindered by the presence of inhomogeneities. Networks consisting of nodes with different dynamics [25, 26] are less likely to synchronize than networks with homogeneous node dynamics. Also, networks with heterogeneous interaction delays [27] or with nodes differing largely in their degrees synchronize less easily than networks with fixed time delays or degrees [28–32]. Correlations between the number of connections of a node and its connected nodes (assortativity) [32, 33] or correlations between the number of incoming and outgoing connections of a node have also been shown to have a significant influence on the network's synchronization propensity [34]. In addition, networks with short path lengths between nodes (like random networks) often synchronize completely, while networks with long path lengths (like lattices) show phase-locking, especially in the presence of transmission delays.

Computational models which are defined by differential equations may describe oscillatory behavior in the form of a closed and attractive curve in state space, a so-called limit cycle. Examples include the FitzHugh-Nagumo neuron,

the van-der-pol oscillator and many others. When we couple these oscillatory systems weakly, so that the trajectories of the coupled systems still are very close to the limit cycle, it is sensible to approximate the systems by phase oscillator whose phase variable is a parametrization of the limit cycle. The coupling for these phase oscillators is given as a phase response as every excitation leads back to the limit cycle. In this way a potentially high dimensional systems is reduced to one dimension and it is clear, that the approximation can only hold for a limited range of coupling strengths. The described approach is called phase reduction and has been discussed even in the presence of noise [35, 36] or for chaotic oscillators like the Roessler or the Lorenz system [37].

In many biological networks (like the heart or the brain) interactions are short-lasting and may be modeled as pulses, which are fired at a given oscillator phase [38, 39]. A classical example is the integrate-and-fire oscillator, which is arguably the simplest neuron model and denotes a simple threshold element which accumulates *charge* which, at some point in time, is released in form of pulses to other oscillators. When these are modeled as some fast decaying function, even all-to-all coupled systems may show a rich dynamical spectrum including asynchronous [40], synchronous or partially synchronous [41] states, quasiperiodicity, and chaos [41–43]. In the limit of vanishing pulse duration, systems interact via δ-pulses which leads to dynamical systems which are nonsmooth and often require one to develop new approaches for numerical methods or analysis tools [43–45]. The size of the δ-pulse depends on the phase of the oscillator which receives it and is usually specified in form of the phase response curve (PRC). It is natural to study in which way the dynamical behavior is influenced by the choice of the PRC.

A central theme of research into complex systems is the study of the emergence of macroscopic properties. We can thus ask the question what types of macroscopic behaviors are generated by synchronization phenomena in complex networks ? Clearly asynchronous motion leads to constant behaviors while synchronous motion leads to oscillatory behavior. Nevertheless, the microscopic scale may show chaotic and highly fluctuating behavior. Similar as for Brownian motion (or many other phenomena studied in the context of equilibrium thermodynamics or excitable media [46]) fluctuations average out when taking a more distant point of view. However, there are exceptions to this rule in which fluctuations and/or chaotic behaviors extend from the microscopic to the macroscopic scale. A prominent example are extreme events which represent rare occurrences (compared to the timescale of the system) of abnormally low or large amplitudes in macroscopic observables. Examples include earthquakes, tornadoes, stock market crashes, harmful algae bloom and epileptic seizures and are

usually associated with disastrous financial and personal consequences [47–49]. The possible dynamical origins and mechanism that lead to such behaviors are only poorly understood, and only few models are capable of supporting such behaviors [50–58].

In this thesis, we study synchronization phenomena in complex networks of oscillators. More concretely, we consider δ-pulse-coupled, excitatory integrate-and-fire oscillators, possibly endowed with refractory periods and time delayed interactions, and describe their dynamics when coupled onto random networks and onto spatial networks with both short- and long-ranged connections.

We demonstrate that in random networks, these oscillators show asynchronous states and a broad range of synchronization phenomena which may lead to completely or partially synchronous states, and to states with irregular macroscopic behavior, which persists after long periods of time and for large networks. To explain these observations, we define different types of continuum models which describe the thermodynamic limit of large networks and provide a macroscopic point of view on the dynamics. For these continuum models, evolution equations for the distribution of oscillator phases are derived. Investigations of such equations have been widely successful in explaining synchronization phenomena of similar systems [26, 39, 42, 59–63].

We show that in spatial networks with short and long-ranged connections, the dynamics is determined by the interplay between pattern formation and synchronization phenomena. In addition to various kinds of wave-dominated states, we report here on so-called chimera states [64–66], in which the networks split into asynchronous and synchronous regions. Depending on oscillator parameters, these regions may, after transients, be fixed in shape and size, or may evolve constantly leading to macroscopic observables which show non-converging and complicated behavior. The latter take, in the simplest cases, the form of asynchronous firing interrupted by short and rare events of synchronous firing, or of a network rhythm in which more and less synchronous behaviors alternate on a timescale well below the eigenfrequency of oscillators. We describe the mechanism that lead to the generation of these non-converging behaviors, which intimately rely on the dual structure of the considered networks.

All our investigations concern phase oscillators whose interactions are defined by phase response curves. In Chapter 2.1, we provide a definition for these notions and show in which way integrate-and-fire oscillators can be described within the framework. In Chapter 3, we give an experimental description of the dynamics of integrate-and-fire oscillators on random networks, before an investigation of different types of continuum models which are able to reproduce

and explain many of the observations. In Chapter 4, we discuss the dynamics of integrate-and-fire oscillators on spatial networks containing both short- and long-ranged connections, in which synchronization phenomena interplay with the formation of spatial pattern. Finally, we conclude our findings in Chapter 5.

2 Pulse-coupled oscillators

Pulse-coupled oscillators (PCOs) are a paradigmatic model for the study of synchronization phenomena [39]. They present a general framework which comprises the small coupling strength limit of limit cycle oscillator and abstract models like IF neurons. We describe a pulse-coupled oscillator by its phase $\phi \in (0, 1]$, which is assumed to increase linearly with $\dot{\phi} = 1$. Whenever the phase of an oscillator reaches 1, it is said to fire, which is the only time when it interacts with and excites other oscillators which are connected to it via some network. We define this excitation with the phase response curve $\Delta(\phi)$, i.e., the phase change that an oscillator receives due to the firing of a connected oscillator. In our model, excitations are δ-pulses leading to a discontinuity of the phase variable of the receiving oscillator. Note that in the literature the term pulse-coupled oscillators is also used when excitations are defined by a pulse of finite duration with a characteristic shape [41, 67, 68]. When oscillators are embedded into a directed network, we will write $n \prec n'$ if oscillator n is connected to n' (i.e. n influences n' on firing). For every firing oscillator, we consider the following update rule which is applied whenever at some time t_f the phase of an oscillator n reaches 1:

$$\forall n' \succ n \quad \phi_{n'}(t_f^+) = \phi_{n'}(t_f) + \Delta\left(\phi_{n'}(t_f)\right). \tag{2.1}$$

Here we denote by $\phi(t^+)$ the right-sided limit of $\phi(t)$. Oscillators have their phase variable restart from 0 after firing; the moment of firing is associated with a phase $\phi = 1$ (instead of $\phi = 0$). To ease notation, we will also use the phase transition curve $R(\phi)$, which is defined as $R(\phi) = \Delta(\phi) + \phi$ and describes the phase of an oscillator after excitation in dependence on its former phase. Phase response curves (PRCs) and phase transition curves (PTCs) are commonly used when describing neurons. They can be calculated even for high-dimensional neuron models as an approximation, which holds for small coupling strengths. The phase oscillator represents for those neurons a one-dimensional approximation which can be verified by phase response curves of real neurons which are measured by experimentalists [69, 70]. Moreover, more abstract models like oscillatory integrate-and-fire neurons can be expressed in terms of pulse-coupled oscillators. In the following, we provide a short explanation of this neuron model and calculate its PRC.

2.1 Integrate-and-fire neurons

The integrate-and-fire neuron (IF neuron) is a one dimensional model, which is defined by an ordinary differential equation (ODE) and an update rule. Its dynamical variable is the membrane potential $x(t)$, which is the potential difference between the interior and exterior of a neuronal cell. For the IF neuron, incoming excitations which arrive at a high rate are approximated by a constant input current I_{in}. Moreover, As the neuron's membrane is not a perfect isolator, a leakage current must be assumed, which is proportional to the membrane potential and a leakage constant l. The following differential equation describes the time evolution of $x(t)$:

$$\dot{x}(t) = -lx(t) + I_{\text{in}}. \tag{2.2}$$

The differential equation for the potential is identical to the one obtained for charging of a capacitor and is solved—given the initial condition $x(0) = 0$—by the following exponential charging function $U(t)$:

$$U(t) = x(t) = \frac{I_{\text{in}}}{l}(1 - e^{-lt}). \tag{2.3}$$

As soon as the membrane potential reaches the firing threshold θ the neuron is said to fire and we reset the membrane potential to 0. Depending on the parameters l, I_{in} and θ, the membrane potential will either saturate below the threshold (at $U = I_{\text{in}}/l$) or the neuron will fire periodically, with a time T between firings. In the latter case, we will speak of an oscillatory IF neuron. For the sake of simplicity and by fixing a scale for the membrane potential, we assume $\theta = 1$. The condition for being oscillatory thus reads $I_{\text{in}} > l$. By fixing a scale for the time, we can also assume that the period of firing T is one. This assumption forces a relationship onto I_{in} and l:

$$x(1) = 1 = \frac{I_{\text{in}}}{l}(1 - e^{-l}), I_{\text{in}} = \frac{l}{1 - e^{-l}}, \tag{2.4}$$

and allows us to eliminate I_{in} from the time dependence of the membrane potential in Eq. (2.3):

$$x(t) = \frac{1 - e^{-lt}}{1 - e^{-l}}. \tag{2.5}$$

Interactions between IF neurons may be realized by a short, decaying pulse which is injected at neuron n' when the presynaptic neuron fires. Throughout this thesis, we will be considering δ-pulses, and increase the membrane potential of excited neurons in a discontinuous way: Whenever neuron n reaches the

firing threshold at time t_f, the membrane potential of all connected neurons n' is increased by the value of some coupling strength c. There are some subtleties in this definition of excitations for IF neurons which influence the synchronization properties and which have no consensus in the literature. We will make the following assumptions: Firstly, we limit excitations to the value which is needed for the receiving neuron to fire immediately; excessive charge is not carried over to the next firing cycle and no excited neuron can *overtake* the exciting neuron. Secondly, we assume that neurons are not excitable in the moment of firing. This has the following consequence; When two bidirectionally coupled neurons have nearly identical membrane potentials, the one with the larger membrane potential will fire first and excite the second neuron. The second neuron will receive an excitation which is sufficient to make it fire immediately. By our first assumption, the second neuron has a membrane potential $x(t)$ of 0 after firing, regardless how far $x(t)$ was pushed beyond the firing threshold. The first neuron now will not be excited by the second neuron due to our second assumption, and both will reenter their charging cycles synchronized. We will denote this situation as an absorption and will say that the second neuron was absorbed by the first. The notion was introduced in the context of all-to-all coupled networks in which an absorbed oscillator is never separated from the absorbing oscillator by the dynamics and both combined can be conceived as a new oscillator which emits excitations of a larger, effective coupling strength [39]. IF models which have been investigated in the context of earthquakes and sand piles usually consider conservation of charge [71, 72]. We formalise both assumption in the following update rule which is applied whenever at some time t_f a neuron n reaches a membrane potential of 1:

$$\forall n' \succ n \quad x_{n'}(t_f^+) = \begin{cases} 0 & x_{n'} = 0, \\ x_{n'}(t_f^+) + c & 0 < x_{n'} < 1 - c, \\ 1 & 1 - c \leqslant x_{n'} \leqslant 1. \end{cases} \tag{2.6}$$

Additionally, the membrane potential of the firing neuron is reset to $x_n(t_f^+) = 0$. Note that for neurons which reach the firing threshold at the same time—due to excitation or due to the intrinsic dynamics as defined in Eq. (2.2)—the time evolution does not depend on the order in which the update rules are applied. In this sense, the definition is thus well-defined.

Standard IF oscillators

As we fixed the frequency of IF-neurons to one (Eq. (2.5)), we can regard the time during one charging cycle as a phase variable. The membrane potential increases monotonously with time, which allows us to map each membrane potential x bijectively to a phase $\phi(x)$ by setting:

$$\phi(x) = -\frac{1}{l}\ln(1 - x(1 - e^{-l})), \quad x(\phi) = \frac{1 - e^{-a\phi}}{1 - e^{-l}}. \tag{2.7}$$

We consider an oscillator which is excited at time t. To obtain the phase $\phi(t^+)$ directly after the excitation, we can express the phase as membrane potential, add the value of the coupling strength c, and re-express as phase. We obtain for the second branch of the case distinction in Eq. (2.6):

$$\phi(t^+) = \phi\left(x(\phi) + c\right) = -\frac{1}{l}\ln\left(e^{-l\phi} - c\left(1 - e^{-l}\right)\right). \tag{2.8}$$

The first and third branch in Eq. (2.6) express that supra-threshold excitations will lead to a membrane potential of $x = 0$ which corresponds to a phase of $\phi = 1$ and thus to a phase response of $1 - \phi$. We can thus express the phase response for all three branches compactly by

$$\Delta(\phi) = \min\left\{-\frac{1}{l}\ln(e^{-l\phi} - c(1 - e^{-l})) - \phi, 1 - \phi\right\}. \tag{2.9}$$

The minimum in Eq. (2.9) bounds the PRC by $1-\phi$ and the phase transition curve $R(\phi)$ becomes non-invertible; a firing oscillator may absorb oscillators with different phases leading to a phase of 1, independently of the former phase. In Figure 2.1 we show the time evolution of the membrane potential and phase response of an IF neuron with exemplary parameters. For the case of non-leaky IF neurons ($l \to 0$), the PRC in Eq. (2.9) can be continuously extended by:

$$\Delta(\phi) = \min\left\{c, 1 - \phi\right\}. \tag{2.10}$$

2.2 Linear IF oscillators

Many properties of IF neurons do not depend much on the exact form of the charging function $U(t)$ as long as it is monotonously increasing and concave-down. As an easier study object, it is possible [39] to obtain an affine linear PRC

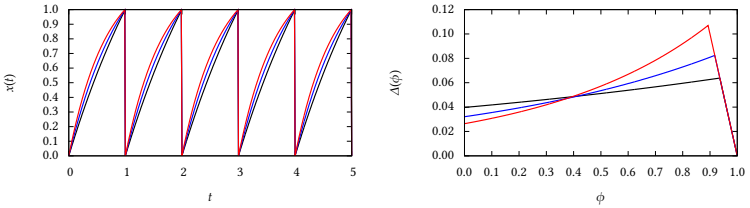

Figure 2.1: Left: Temporal evolution of the membrane potential $x(t)$ of a standard IF oscillator with frequency 1 according to Eq. (2.5) for different parameters (black: $I = 0.5$, blue: $I = 1.0$, red: $I = 1.5$). Right: corresponding phase response curves $\Delta(\phi)$ for this oscillator for $c = 0.05$ according to Eq. (2.9).

if we consider a charging function $U(t)$ of the following form:

$$U(t) = \frac{1}{\beta} \ln(1 + [e^{\beta} - 1]t). \tag{2.11}$$

The parameter β is analogous to I in the definition of the IF neuron's charging functions and determines the curvature of the function. The limit $\beta \to 0$ yields $U(t) = t$, as does $I \to 0$ for integrate-and-fire neurons. The charging function can be generated from the following differential equation:

$$\dot{x}(t) = \frac{1}{\beta}(e^{\beta} - 1)e^{-\beta x}. \tag{2.12}$$

From Eq. (2.11), one obtains with a similar calculation as for the PRC of the standard IF oscillator:

$$\phi(t^+) = \phi\left(x(\phi) + c\right) = \frac{e^{\beta c}}{e^{\beta} - 1}\phi + e^{\beta c} = a\phi + b\beta + \phi. \tag{2.13}$$

Here we used the abbreviations $b = e^{\beta c}$ and $a = \frac{e^{\beta c}}{e^{\beta}-1} - 1$ with which the PRC now takes the simple form:

$$\Delta(\phi) = \min\left\{a + \phi b, 1 - \phi\right\}. \tag{2.14}$$

We will denote an oscillator with this PRC in the following as linear IF oscillator. In Figure 2.2 we show charging functions and phase response curves of such an oscillator. In all our observations, both standard and linear IF oscilla-

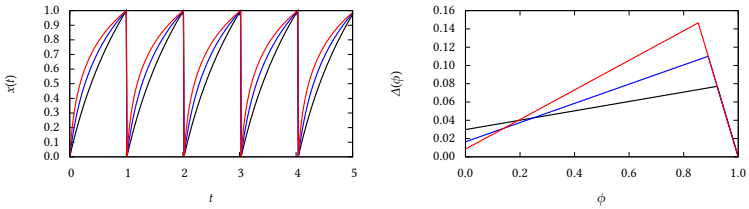

Figure 2.2: Left: Temporal evolution of the membrane potential $x(t)$ of a linear IF oscillator with frequency 1 according to Eq. (2.11) for different parameters (black: $\beta = 1.0$, blue: $\beta = 2.0$, red: $\beta = 3.0$). Right: corresponding phase response curves $\Delta(\phi)$ for this oscillator for a coupling strength $c = 0.05$ according to Eq. (2.14).

tor exhibit qualitatively the same dynamical behaviors. We therefore report our findings in terms of linear IF oscillators, which simplifies many calculations for the continuum models in Chapter 3.4.

Synchronization of two coupled IF neurons

Peskin observed that two bidirectionally coupled excitatory integrate-and-fire neurons synchronize completely [38]. Within the notion of phase oscillators, this is easily verified. For two oscillators which fire shortly after another, the first one is excited shortly after firing, while the second one is excited shortly before firing. The phase difference thus diminishes if $\Delta(\phi)$ has larger values near $\phi = 1$ than near $\phi = 0$. This is certainly the case for the PRCs of standard or linear IF oscillators which are monotonously increasing (see Figure 2.2 and 2.1). Furthermore, if phases are close, the succeeding oscillator is absorbed as indicated by the falling slope near $\phi = 1$. The return map $r(\phi)$ allows us to calculate the synchronization behavior more generally for arbitrary initial phases of two oscillators. $r(\phi)$ maps the phase difference of the two oscillators to the phase difference that is obtained after each oscillator fired and excited the other one once. Given a phase response curve, the return map $r(\phi)$ can be constructed in the following way [39]:

$$\tilde{r}(\phi) := 1 - \phi + \Delta(1 - \phi), \; r(\phi) = \tilde{r}(\tilde{r}(\phi)). \tag{2.15}$$

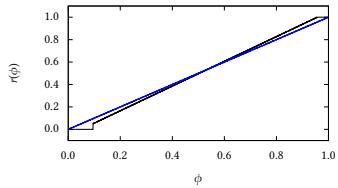

Figure 2.3: Return map $r(\phi)$ according to Eq. (2.15) for linear IF oscillators (see Eq. (2.14)) with $a = b = 0.05$. (black line). Fixed points are given as intersections of $r(\phi)$ with the identity map (blue line). The plot reveals an unstable fixed point out of synchrony (at $\phi \approx 0.6$) and a stable fix point for synchrony at $\phi = 0$. For all initial conditions except the unstable fixed point, complete synchrony is achieved in finitely many firings due to the horizontal curve progression around $\phi = 0$.

Fixed points of this map correspond to stable phase differences. For excitatory IF oscillators the return map has a stable fixed point at $\phi = 0$ and an unstable fixed point at $\phi \approx 0.6$. In Figure 2.3 we show the return map $r(\phi)$ for linear IF oscillators.

2.3 Refractoriness and time delay

The synaptic reception of an action potential in real neurons is not instantaneous. Accordingly, the PCO model has been generalized to include time delayed interactions [73], which change the dynamical behavior greatly. For time-delayed interactions and a small phase difference, both oscillators receive excitations after firing [73]. In this case the oscillator which fires first is excited at a smaller phase than the oscillator that fires last and receives a larger phase advance for increasing PRCs; for two bidirectionally coupled oscillators complete synchrony is repelling for excitatory coupling and attracting for inhibitory coupling. Intriguingly, the latter holds for arbitrary coupling topologies [74]. Another property which is present in real neurons is refractoriness. For a short period after firing, neurons are refractory, meaning that the emission of a second action potential is either impossible or strongly inhibited. The length of the refractory period can vary strongly among different kinds of neurons, but is usually a few times larger than the assumed synaptic time delay. Extensions of IF models which include these effects have been proposed [75,76]. In this thesis,

we will study the influence of both refractoriness and time delay. We will use a trick which allows us to incorporate both time delay and refractoriness into the PRC, thereby keeping a formally undelayed system. This trick can be applied for the case that the time delay is identical on all outgoing connections and its duration is shorter than the refractory period. We start with defining a transformation which introduces a refractory period of length ϑ. For phases at which the oscillator is refractory, the phase response vanishes. We introduce an interval $\phi \in (0, \vartheta]$ into the PRC and rescale the original PRC Δ to fit the remaining phase interval $(\vartheta, 1]$. The transformed PRC Δ_ϑ is defined as:

$$\Delta_\vartheta = \begin{cases} 0 & 0 < \phi < \vartheta \\ \Delta\left(\frac{\phi-\vartheta}{1-\vartheta}\right) & \vartheta \leqslant \phi < 1. \end{cases} \tag{2.16}$$

Let τ denote the time delay of oscillator interactions, such that all excitations which are emitted due to the firing of an oscillator at time t_f, will arrive at connected oscillators at time $t_\mathrm{f} + \tau$. If the oscillator is not refractory after firing, we cannot know which phase it has when its excitations arrive, even multiple excitations could be emitted before the arrival of the first. However, if the oscillator is refractory for a period which is larger than its time delay, its phase will increase only due to the intrinsic dynamics and will be τ on arrival of its excitations. This allows us to replace the oscillator and its delayed connections by an undelayed oscillator without changing the dynamics. The replacement is done by reinterpreting the phase and shifting the PRC in such a way that excitations are again received at $\phi = 1$. The new oscillator thus fires when the phase of the old oscillator is τ and the transformed PRC $\Delta_{\tau,\vartheta}$ is given by

$$\Delta_{\tau,\vartheta} = \Delta_\vartheta(\phi - \tau). \tag{2.17}$$

For linear IF oscillators, the resulting PRC with both additions can be described in the following form.

$$\Delta_{\tau,\vartheta}(\phi) = \begin{cases} 0 & 0 < \phi \leqslant \vartheta - \tau \\ a(\phi - \vartheta + \tau) + b & \vartheta - \tau < \phi \leqslant \phi_\mathrm{ab} \\ 1 - \phi & \phi_\mathrm{ab} < \phi \leqslant 1 - \tau \\ 0 & 1 - \tau < \phi \leqslant 1. \end{cases} \tag{2.18}$$

Here ϕ_ab is the smallest phase at which an absorption occurs which is given by $\phi_\mathrm{ab} = \frac{1-b-\vartheta}{1+a} + \vartheta - \tau$. In Figure 2.4 we show the time evolution of the phase difference for the PRC of linear IF oscillators with and without both transfor-

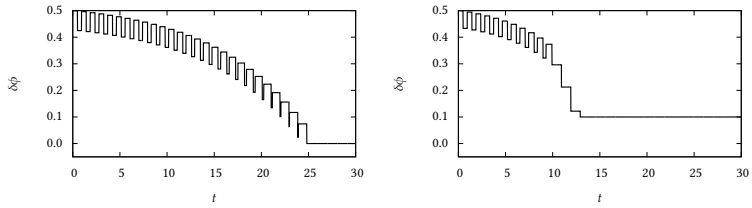

Figure 2.4: Time evolution of the phase difference $\delta\phi = \phi_2 - \phi_1$ between two bidirectionally coupled excitatory linear IF oscillators ($a = b = 0.05$). Oscillators are undelayed and have no refractory periods in the left plot, oscillators are endowed with time delays $\tau = 0.1$ and refractory periods $\vartheta = 0.4$ in the right plot.

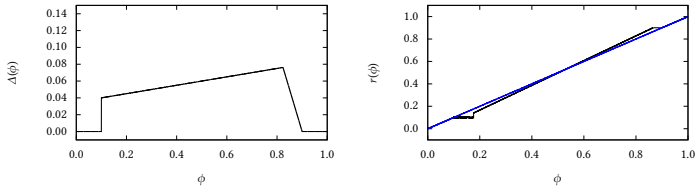

Figure 2.5: Left: PRC for linear IF oscillators with time delay $\tau = 0.1$, and refractory period $\vartheta = 0.2$ and $a = b = 0.05$ according to Eq. (2.18). Right: return map for this PRC (black line) together with the identity map (blue line).

mations. For larger phase differences, the evolution is similar. For the refractory oscillator and starting from a phase difference of $d \approx 0.2$, the preceding oscillator is refractory when the excitations from the succeeding oscillator arrive. The attraction towards the synchronized state is increased at this point. The phase difference does not vanish completely but attains a value between 0 and τ depending on the initial condition. The return maps $r(\phi)$ confirm our observations (see Figure 2.5 right). Due to refractoriness and time delay, the fixed point corresponding to synchrony is replaced by a fixed interval with marginal stability. The horizontal evolution of $R(\phi)$ near this interval implies that attraction to this fixed interval is achieved after a finite number of excitations. In networks in which nodes are connected by long paths only, this inexact phase adjustment

may play an increased role as it adds up along the path. The time delay determines the level of phase adjustment for coupled oscillators. The behavior of two coupled oscillators may give an impression for behavior of larger networks as it provides a model for each pair of connected oscillators which, however, is disturbed by other connections. Therefore, it is plausible that in the dynamical system we study (similarly as in many other dynamical systems), a large time delay hinders synchronization, while a large refractory period promotes synchrony in complex networks.

Measuring synchrony

A main focus of this thesis, is to investigate synchronization phenomena of IF oscillators in complex networks. In particular, we are interested in such phenomena, which do not lead to a certain amount of synchrony in the network, but which show continuous changes. In this case, we cannot assign an amount of order to the network, instead we have to investigate the amount of synchrony in the network as dependent on the time. To measure synchrony for a large number of oscillators, we use the standard order parameter for phase oscillators which is obtained by taking the vector sum of all phases of oscillators in the network:

$$z(t) = 1/N \sum_n e^{2\pi i \phi_n(t)}, \quad r(t) = |z(t)|\,. \tag{2.19}$$

The argument of $z(t)$ specifies the mean phase in the network, while its absolute value $r(t)$ specifies their synchrony. In a way $z(t)$ carries information comparable to both the mean and variance of the distribution of phases [77]. The order parameter $r(t)$ takes a value of 1 for complete synchrony, i.e., identical phases for all oscillators in the network, and $r(t)$ takes small values for a balanced distribution of phases. Note that a small value of $r(t)$ may be obtained by either an asynchronous state with distributed phases or for example by a splay state consisting of a small number of equi-distant phase clusters, in which oscillators belonging to the same cluster are synchronized. Apart from these more or less trivial exceptions, $r(t)$ may show non-converging and complicated behavior for dynamical systems coupled onto complex networks.

Stability of complete synchrony

In their seminal work, Mirollo and Strogatz showed that a network of all-to-all coupled excitatory oscillators with monotonously increasing and concave-down charging function synchronizes completely for nearly all initial conditions [39].

For oscillators coupled on complex networks, however, multistability and irregular behavior can be observed (e.g. [74, 78]). Even regular configurations, like lattices with nearest neighbor coupling show (for two ore more spatial dimensions) configurations which do not lead to synchrony [71,79]. Often it is possible to decide whether the completely synchronized state is stable, which clearly is a much weaker claim than global convergence. For excitatory IF oscillators this is the case for strongly connected networks, i.e., networks in which there is a path in each direction for every pair of nodes. Stability means in our case, that if we take a perturbation of the completely synchronized state $\{\phi_n | n \in N\}$ which has a small size $\delta := \max_n \phi_n - \min_n \phi_n$ then the size δ will converge to 0 with time. If we consider perturbations whose size is smaller than the range of phases $\phi < 1$ at which absorption occurs (the phases of the slope of -1 of $\Delta(\phi)$), then a single excitation will lead to an absorption. As the network is strongly connected, the oscillator with the largest phase will start an avalanche which covers the whole network leading to complete synchrony in finite time and after a single excitation. For inhibitory IF oscillators with delayed interactions, the synchronized state is also stable (assuming that coupling strengths are normalized by the mean degree). This has been shown for arbitrarily connected networks [74]. In contrast, both delayed excitatory IF oscillators and undelayed inhibitory oscillators usually have repelling synchronized states. We will now investigate the stability of synchrony of a network of excitatory oscillators which are endowed with both refractory periods ϑ and time delay $\tau < \vartheta$ [53]. Let $\{\phi_n | n \in N\}$ with size $\delta := \max_n \phi_n - \min_n \phi_n$ again be a perturbation from the synchronized state and let $n_>$ ($n_<$) denote an oscillator with maximal (minimal) phase. For small perturbations with $\delta_0 < \vartheta - \tau$, each oscillator will fire and will then stay refractory until every other oscillator has fired once. We can thus define the size of the perturbation $\delta_1 = \max_n \phi_n(t_1) - \min_n \phi_n(t_1)$ for some time t_1 at which each oscillator has fired exactly once. We define $\delta_2, \delta_3, \ldots$ analogously. The oscillator $n_>$ will not be excited at all and it is not possible for an excited oscillator to overtake the oscillator which emitted the excitation (as we limit our PRC by $1 - \phi$). For purely positive PRCs, we can thus conclude $\delta_1 \leqslant \delta_0$, or $\delta_{i+1} \leqslant \delta_i$ per induction. Moreover, we can give an upper bound for $\delta_\infty := \lim_{i\to\infty} \delta_i$. Since our PRCs do not contain arbitrary small phase changes except near $\phi = 1$ where an excitation immediately leads to absorption, phase-locking of two oscillators is always achieved in a finite number of oscillations. For a finite number of oscillators, we can choose a time t_i' after which all excitations are received in the refractory state. The length of the shortest path between $n_>$ to $n_<$ measured at time t_i' is bounded by the diameter D of the graph (the longest shortest path). As excitations are received when oscillators are refractory, the difference in phase

for every pair of oscillators along such a path is smaller than or equal to τ, and therefore $\delta_\infty = \phi_{n_>} - \phi_{n_<} \leqslant d\tau$. This implies that with time delay and refractory periods, we still have attracting states in the state space with large synchrony and $r(t) \approx 1$. However, a single synchronous state is replaced with a region of *almost* synchronous states, whose spread of phases is smaller than $d\tau$ and which are marginally stable. These states are surrounded by an attracting region in state space (assuming $d\tau < \vartheta - \tau$). It is plausible that an increased size of the attracting region around the stable states (larger ϑ, smaller τ) promotes synchronization phenomena.

2.4 Numerical treatment

We have presented two distinct representation for integrate-and-fire neurons in which the oscillator states are either described by a phase variable or by the membrane potential. Both allow for a numerical treatment of the dynamics. The representation via a membrane potential allows for clock-driven algorithms like the Runge-Kutta schemes when a handling of firing oscillators is included between stepping. Firing times, are in this way limited to the time grid on which the algorithm is based. Moreover, as the intrinsic dynamics of oscillators has analytic solutions, approximate numerical solvers may be overly resource demanding. The representation via a phase variable allows for an event driven approach, which performs better for networks of small mean degree [44, 80]. In this approach, oscillators are registered in a priority queue which is ordered by the time of the next firing. Repeatedly, the first element in this queue is removed, reinserted at the bottom and excitations to other oscillators are handled. Instead of a dense time grid, only firing times are considered in the event based approach. The implementation of the priority queue must allow for an update of priority of selected elements to account for excitations. The performance for large networks depends crucially on the scaling of the required operations, which are: selection of the element with the highest priority, removing of this element, insertion of an element into the queue, increase of priority (for excitatory oscillators), and/or decrease of priority (for inhibitory oscillators). With a so-called calendar queue [81], all of these operations can be achieved in finite time if a parameter (the bucket size) is chosen in a sensible way. However, this queue has a large overhead and relies on distributed firing times. For synchronous oscillators the queue is slow. Tree structures do not share these disadvantages [82], they have however $O(N)$ scaling for decrease of priorities. They thus present a good choice for the excitatory oscillators which we are consider-

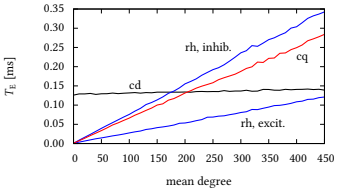

Figure 2.6: Execution times per firing neuron T_E in dependence on the mean degree for random networks of 10000 integrate-and-fire neurons. Values were obtained using event-driven approaches implemented in Conedy with a calendar queue ("cq", red), with a relaxed heap ("rh", blue) and with a clock-driven approach ("cd", black; Runge-Kutta-Fehlberg with step size control and an absolute error of 10^{-5}). The calculation was done for both inhibitory and excitatory neurons. While the relaxed heap implementation is much faster for excitatory neurons ("rh, excit."), both types of neurons are integrated equally fast with the calendar queue and the clock-driven integrator. Tests were performed on a PC with 1.5 GFLOPS (2.4 GHz). (Lines are for eye-guidance only).

ing here. To allow for an efficient numerical treatment of these oscillators, we developed a computational tool (Conedy), which is written in C++ and combines both event-driven and clock-driven approaches. The software has been published [83] under the GNU license and is available under www.conedy.org and www.github.com/Conedy. In Figure 2.6 we present a comparison of execution times for the different integration schemes for pulse-coupled oscillators implemented in Conedy.

3 Dynamics on random networks

The study of the structural properties of random networks has a long history [6, 7]. The dynamics which emerges when nodes of the network are associated with dynamical systems, however, has only been a topic for a few decades. Random networks are a popular choice for modeling purposes in cases in which the knowledge about the organization structure of the system under investigation is limited. In the following, we will introduce the different types of random networks that we study. Let $\mathcal{N} = (V, \prec)$ be a network, which is in our notation an index set $V \subset \mathbb{N}$ together with a binary relation such that for two nodes $v_1 \prec v_2$ indicates that there is a directed connection from v_1 to v_2. Given such a network, we define dynamics of PCOs according to Eq. 2.1. We fix a vertex set V of size $N = |V|$ and a mean degree m. Using these parameters, we connect V according to the following construction rule:

directed Erdős-Rényi network We add directed connections between randomly chosen nodes $v_1 \neq v_2$ which are still unconnected until the network has a mean number m of ingoing and outgoing connections per node.

Note that undirected networks can easily be described by this general framework if we require that for each v_1 and v_2 with $v_1 \prec v_2$ we also have a connection in the opposite direction ($v_2 \prec v_1$):

undirected Erdős-Rényi network We add directed connections in both directions between randomly chosen nodes $v_1 \neq v_2$ which are still unconnected until the network has a mean number m of connections per node.

Networks resulting from this construction are denoted as random graphs by mathematicians and are usually attributed to Erdős and Rényi. Note that very similar networks can be constructed by choosing a uniform connection probability p for every pair of nodes, as was proposed by Gilbert [6] independently from the work of Erdős and Rényi. While a uniform connection probability also follows from the described construction, the total number of connections N_E in the network is fixed whereas N_E follows a binomial distribution for random networks defined via p. However, for larger network sizes, N_E is distributed sharply around its mean $N_\mathrm{E} = pN^2$, which allows us to consider both constructions schemes of random networks as essentially the same. When considering

the dynamics of pulse-coupled systems a third type of network model has been investigated (see e.g. [67, 84]). In this model, we consider a collection of N oscillators which are coupled all-to-all, but whose connections do not function reliably. Instead only a fraction of excitations are processed by these connections. Similar as for Erdős-Rényi networks, we can equally specify the probability that a connection transmits an excitation or we can specify the number of transmitted connections for every firing oscillator. We chose the latter and define the following dynamical rule for such a network:

synaptic failure network Whenever an oscillator v_1 in the network fires, we excite m randomly chosen oscillators in the network.

Note that we use the symbol m here to denote the number of excitations per firing oscillator, whereas we used m for the mean degree of Erdős-Rényi networks, which specifies the mean number of excitations per firing oscillator in these networks. The term synaptic failure network is motivated by the observation that synapses in neuronal networks do not reliably transmit excitations to post-synaptic neurons [85]. The activation of a neuron following a synaptic excitation is dependent on the release of neurotransmitter which are contained in a number of so-called synaptic vesicle. Excitation is thus delivered in quants which are given by the size of these vesicles. The strength of synapses is commonly described as stochastic and is determined by the probability that vesicles are released and the number of available vesicles [86]. Release probabilities vary largely even in the same brain structure and can be as low as 1%. We interpret excitations as the release of a vesicle instead of as a post synaptic excitation. Under this assumption synaptic failure networks represent an idealization of this dynamics for a well-connected neuronal network. For various kinds of oscillator dynamics, comparable network dynamics can be observed for all three kinds of random networks. Nevertheless, they may produce different dynamics even for large networks. It can be argued that synaptic failure networks are simpler objects than Erdős-Rényi networks as the network is symmetric with respect to interchange of every pair of nodes. In fact, for given parameters N and m, there is only one synaptic failure network whereas constructed directed or undirected Erdős-Rényi networks with the same parameters differ. While the construction of those is also symmetric with respect to nodes, constructed networks are most likely not. In particular, nodes in the network have different number of connections which usually has a significant influence on their dynamical behavior. The distinction between Erdős-Rényi networks and synaptic failure networks is comparable to quenched and annealed disorder in condensed matter. While Erdős-Rényi networks have quenched disorder which is frozen at

time of generation, the synaptic failure network defines interaction by making use of a random influence which changes with time. In this chapter, we will describe and compare the dynamics which arises from the three notions of random networks when endowed at each node within the network with the dynamics of linear IF oscillators (Eq. (2.14)). Note that for all-to-all coupling convergence to complete synchrony has been shown for nearly all initial conditions [39]. In contrast, we observe—in dependence on oscillator parameters—asynchronous states, (partially) synchronous states, and irregular behavior with self-generated changes between randomness and order. The dynamics in all of these states can be characterized as chaotic. Because of the discrete nature of the system under study, an analysis of Lyapunov spectra is not straightforward. We will show how these complications can be tackled and will provide an estimation of the largest Lyapuonv exponent λ for dynamical states which are stationary. Finally, we investigate continuum models which capture the thermodynamic limit and allow us to characterize asynchronous states and their loss of stability in terms of bifurcations.

3.1 Asynchronous states

We start with a discussion of asynchronous states than can be observed for larger networks in all three types of random networks, and we first consider the case of linear IF oscillators without time delays and refractory periods. When not stated differently, we will use uniformly distributied initial phases as initial conditions for networks. Complete synchrony in Erdős-Rényi networks is stable (see Chapter 2.2). For synaptic failure networks, it is in principle possible that a perturbation may lead away from complete synchrony. As all excitations in these networks are distributed randomly, we cannot even exclude situations in which some oscillators receive no excitations at all during some observation time. Nevertheless, once a highly synchronous state is achieved (in synaptic failure networks) a return to asynchronous dynamics is highly unlikely. For all three types of random networks and for network sizes above a few hundred oscillators, we were able to find oscillator and network parameters such that synchrony is not reached during the observation times we can consider due to computational constraints. Choosing such parameters and starting from homogeneously distributed phases in $[0, 1]$, we observe after a short transient small values of the order parameter r with minor fluctuations only. In Figure 3.1 we show the temporal evolution of r for linear IF oscillators of exemplary parameters in directed, sparse random networks of different sizes. Note that we do not claim that the

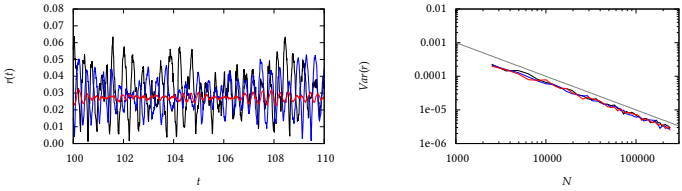

Figure 3.1: Left: Temporal evolution of the order parameter r for synaptic failure networks of linear IF oscillators (see Eq. (2.14)) with a fixed mean degree of 15.0 and for different networks sizes N. Black: $N = 2500$, blue: $N = 10000$, red: $N = 250000$. Measurements with directed and undirected Erdős-Rényi networks give similar results. Right: Variance of r in $t \in [100, 200]$ for synaptic failure networks (black), directed Erdős-Rényi networks (blue), and undirected Erdős-Rényi networks (red) in dependence on the network size N. The variance of r shows a $1/x$ scaling (black line). Oscillator parameters: $a = 0.01, b = 0.04$.

behavior as depicted in Figure 3.1 is stable, in the sense that no transition to complete synchrony is possible. For synaptic failure networks a realization of the stochastic influences can easily be constructed such that networks synchronize. However, such a realization is so unlikely that we cannot observe transitions. For Erdős-Rényi networks, it seems likely that the asynchronous behavior is equally unstable, but has an very large live time. We discuss this point further in Chapter 3.3 where we describe transients to synchrony. The question of the stability of the asynchronous behavior is not important for the network dynamics. For all practical purposes it is stable, as its live time is so long that we cannot observe transitions. During the asynchronous behavior, r shows small oscillations, which decrease in amplitude for larger networks and converges to some small value larger than zero. The variance of r scales with the network size as $1/N$. Such scaling is often encountered in systems which are far from critical transitions. Note that if we consider N as a number of independent measurements, then the average over these measurements will have variance which scales as $1/N$ [87]. This is just the formula for the statistical error. In some sense, the scaling is thus an indication for the independence of the dynamics at different positions in the system [88]. Note that small values of r can also result from, e.g., balanced groups of phase clusters which are distributed evenly on the phase circle. This is, however, not the case for the oscillator and network parameters

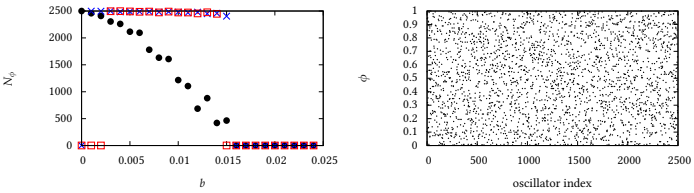

Figure 3.2: Left: Number of different phases N_ϕ after preiteration (at $t = 100$) of a directed Erdős-Rényi network ($m = 50$) of 2500 linear IF oscillators in dependence on b and for $a = 0$ (black), $a = 0.001$ (blue), $b = 0.002$ (red). Oscillators synchronize completely for $b > 0.015$ leading to $N_\phi = 1$. Smaller value of b may lead to asynchronous behavior with values of N_ϕ in the same order of magnitude as N. Measurements with undirected random or synaptic failure networks gave comparable results. Right: phases of a directed Erdős-Rényi network of 2500 oscillators ($a = 0.0, b = 0.015, m = 50$).

of Figure 3.1. To verify that phases are not concentrated, we measured the number N_ϕ of oscillators in the network which have pairwise different phases at a given point of time. In Figure 3.2 we show N_ϕ in dependence on the oscillator parameters. With the exception of the non-leaky case ($a = 0$), we observe no accumulation of oscillators at a distinct phase in the asynchronous behavior. Even then the number of different phases remains of the same order of magnitude as the number of oscillators in the network. Although the oscillators we consider adapt their phases completely when a supra-threshold excitation is received, we observe that at any point in time nearly all oscillators in the network have different phases. Therefore, it is possible to describe the distribution of phases in the network at any point in time t by a distribution function $\rho(\phi)$ which deviates significantly from a uniform distribution. The distribution function itself is smooth and shows only minor fluctuations in time. The order parameter can be expressed by $r = \int \rho(\phi) e^{2\pi i \phi} d\phi$. It is clear that we cannot expect $r = 0$ for distributions which are not uniform. In fact the order parameter can be quite large depending on network and oscillator parameters. Guided by this observation, we will not use small values of r as criterium for asynchronous behavior. Instead we characterize the dynamics of networks as being in an *asynchronous state*, if the network exhibits constant macroscopic observables and if the oscillator phases in the network can be described by a phase distribution $\rho(\phi)$ which shows small fluctuations over time only. Given this definition asynchronous

states are asynchronous as synchrony or partial synchrony will lead in some way to oscillations in $\rho(\phi)$. Furthermore, we associate the network behavior at different times to the same asynchronous state, as we cannot (per definition) distinguish between them macroscopically. For synaptic failure networks every excitation is deposited at a random target node. The phase of an excited oscillator is thus also described by $\rho(\phi)$. For Erdős-Rényi networks, however, it is conceivable that oscillators which are connected to oscillators with a certain phase ψ have a distribution $\rho_\psi(\phi)$ which differs from $\rho(\phi)$ and that this distribution $\rho_\psi(\phi)$ depends non-trivially on ψ. This can mean for example that connected oscillators in the network have a different expected phase difference than unconnected oscillators. For an Erdős-Rényi network in an asynchronous state, it is plausible that for oscillators which tend to synchronize, the expected phase difference is smaller for connected than for unconnected oscillators. As excited oscillators in an Erdős-Rényi network are those, which are connected to a firing oscillator with $\phi = 1$, the distribution of phases of excited oscillators is given by $\rho_1(\phi)$. In Figure 3.3 and Figure 3.4, we show $\rho(\phi)$ and $\rho_1(\phi)$ for all three considered notions of random networks. As expected, $\rho(\phi)$ and $\rho_1(\phi)$ coincide for synaptic failure networks, while they differ for Erdős-Rényi networks. We can also consider $\rho_\psi(\phi)$ as a function $\varrho(\psi, \phi) := \rho_\psi(\phi)$ which depends on two variables and which can be interpreted as the distribution of edges whose source node has phase ψ and whose target node has phase ϕ. Correlation of the phases of connected oscillators then means that $\varrho(\psi, \phi)$ cannot be produced by a simple product of the phase distributions ($\rho(\psi)\rho(\phi) \neq \varrho(\psi, \phi)$). In Figure 3.5, we show a measurement of ϱ for directed and undirected Erdős-Rényi networks in asynchronous states. The two networks show clear differences in this distribution although their macroscopic dynamics is similar. Although synaptic failure and Erdős-Rényi networks often have similar dynamics, Erdős-Rényi networks can be considered as much more complicated mathematical objects; after the construction of the network, different nodes are not exchangeable. A prominent difference between nodes in a Erdős-Rényi network is the degree of incoming connections d_i. For excitatory systems, we can expect that the sub-population of nodes with larger d_i will move faster around the phase circle and fire more often than those nodes with a smaller d_i. The network can thus be conceived as a collection of oscillators with different frequencies. In Figure 3.6, we show the correlation between this frequency and d_i and the phase distribution for sub-populations of nodes with a fixed d_i. Each of these phase distributions in Figure 3.6 left, resembles the phase distribution of synaptic failure networks for $m = d_\mathrm{i}$. In the following chapter, we investigate the dynamics of the asynchronous states microscopically and study their sensitivity to initial conditions.

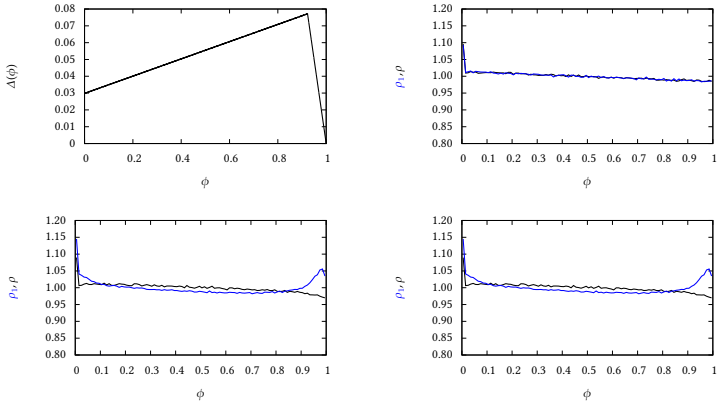

Figure 3.3: Asynchronous states in networks of 100000 linear IF oscillators with $a = 0.002, b = 0.01, m = 15.0$. Top left shows the PRC $\Delta(\phi)$. The other three plots show the distribution $\rho(\phi)$ (black) of all phases in the network measured in the interval $t \in [100, 150]$ every $\delta t = 0.2$, and the distribution of phases $\rho_1(\phi)$ (blue) of excited oscillators. Distributions were measured for oscillators coupled on synaptic failure networks (top right), directed Erdős-Rényi networks (bottom left), and undirected Erdős-Rényi networks (bottom right).

3.2 Chaoticity

The largest Lyapunov exponent is a well-established measure, which allows one to characterize sensitivity to initial conditions and to give indications for chaos in smooth dynamical systems [89]. Due to the discontinuities in integrate-and-fire systems, the standard notion is not directly applicable. However, several approaches have been undertaken to generalize the standard definition to non-smooth systems [45, 78, 90, 91]. In the following, we will discuss the arising difficulties, and show how the largest Lyapunov exponent λ can be defined in our system. Furthermore, we provide an estimation for dynamical states of which we know the distribution of phases of excited oscillators. We use superscript indices to denote different trajectories from some network, while subscript indices are as before used to specify nodes in the network. When neurons are defined by the membrane potential, the reset after firing transports the state discontinuously to another region in state space. Let us track the time evolution of a

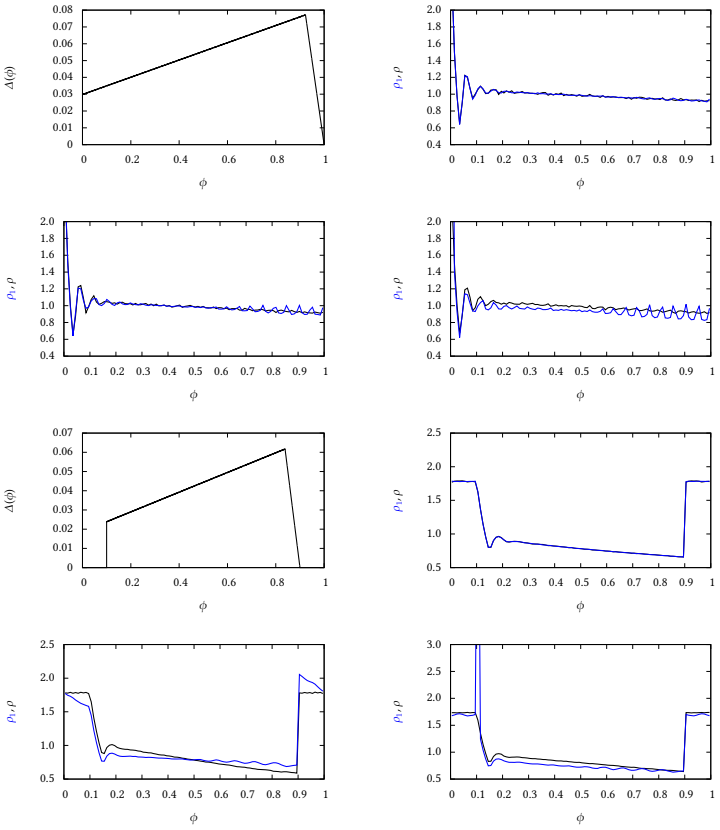

Figure 3.4: Top four plots: same as Figure 3.3 but for linear IF oscillators with $a = 0.01, b = 0.04$ and a mean degree $m = 15.0$. Bottom four plots: same as Figure 3.3 but for linear IF oscillators ($a = b = 0.05$) with time delay $\tau = 0.01$ and refractory periods $\vartheta = 0.02$.

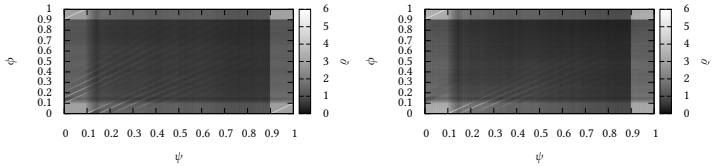

Figure 3.5: The distribution of edges $\varrho(\psi, \phi)$ whose source node has phase ψ and whose target nodes has phase ϕ for an undirected Erdős-Rényi network (left) and a directed Erdős-Rényi network (right). Edges were measured in the interval $t \in [50, 150]$ every $\delta t = 0.01$. The dynamics shows asynchronous states in networks of 500,000 linear IF oscillators with $(a, b, \tau, \vartheta) = (0.05, 0.05, 0.1, 0.2)$ and $m = 10$.

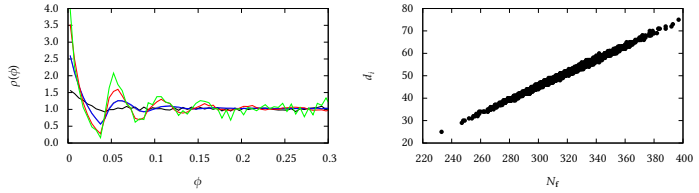

Figure 3.6: Asynchronous states in a directed Erdős-Rényi network ($N = 10000, m = 15.0$) of linear IF oscillators $(a, b, \tau, \vartheta) = 0.01, 0.04, 0.0, 0.0)$. Left: Phase distribution $\rho(\phi)$ for the sub-population with a fixed degree d_i of incoming connections of 5 (black), 15 (blue), 25 (red), and 30 (green). The distribution of the total population is in this plot indistinguishable from the distribution for $d_i = 15$. Right: Number of firings N_f in time interval $[0, 300]$ in dependence on the indegree d_i.

single oscillatory integrate-and-fire neuron starting from two initial membrane potentials $x^1(0) > x^2(0)$, and let us consider two trajectories $x^1(t)$ and $x^2(t)$ and in particular their distance at some time $\left|x^1(t) - x^2(t)\right|$. The firing and reset of the first neuron will separate the trajectories. However, after firing of the second neuron, the distance shrinks back to the order of magnitude as before. Clearly, it is not desirable to measure or account for this short-lasting large distance between trajectories. Note that this problem does not appear if we consider the phase representation of neurons and define distances in such a way that phases which correspond to shortly before firing and to shortly after firing are close. As Lyapunov exponents are invariant under variable transformations [92], we obtain the same contributions for the continuous part of the dynamics for both the phase and the membrane potential representations. The excitations in pulse-coupled systems lead to a similar problem: consider the state space of two connected neurons (and two sets of nearby initial conditions) and assume that one neuron receives an excitation from the other at time t ($t+\delta$) for the first (second) set of initial condition. The distance between both trajectories then is large in the time interval $(t, t+\delta)$ as here the excitation did only occur in the first set of initial conditions. To characterize the influence of the excitation on the distance of trajectories, it is thus advisable to compare the distance before t and after $t+\delta$ when the excitation was received in both sets of initial conditions. Nevertheless, the distance is enlarged by a finite value as consequence of the excitation. As the times between excitations contribute to the dynamics in a trivial way, it is sensible to transform the system into a map by restricting the time variable to the times of firing neurons [40, 67, 93]. Lyapunov exponents can then be defined as for other time-discrete dynamical systems. The approach we choose to describe sensitivity to initial conditions will guarantee that two trajectories stay at constant distance between excitations whereas excitations may decrease or increase the distance discontinuously. For large networks and many excitations, we observe an exponential dependence of the distance d between two trajectories which evolve from nearby initial conditions. The slope of the exponential dependence d corresponds in a natural way to the largest Lyapunov exponent λ. We will use λ to characterize the different dynamical behaviors that we describe in this thesis. Moreover, to gain a better understanding of the chaoticity of the asynchronous states in Erdős-Rényi networks, we define in this chapter a stochastic model, which allows us to relate the measured values λ to the PRC of oscillators, when the distribution of phases of excited oscillators is known. We consider the state space $\mathscr{V}$ which is spanned by all phases of oscillators in the network. An arbitrary vector in $\mathscr{V}$ thus is of the form $\Phi = (\phi_1, ..., \phi_N)$, with $\phi_1, \dots, \phi_N \in [0, 1]$. We endow the phase circle with a metric which takes the

cyclicity of phases into account

$$\|\phi_i^1 - \phi_i^2\| = \min\{\left|\phi_i^1 - \phi_i^2\right|, 1 - \left|\phi_i^1 - \phi_i^2\right|\} \tag{3.1}$$

and sum quadratically over different components of state space vectors to obtain a metric $d(\Phi^1, \Phi^2)$ for state space vectors:

$$d\left(\Phi^1, \Phi^2\right) = \frac{1}{N}\sqrt{\sum_{i=1}^{N}\left\|\phi_i^1 - \phi_i^2\right\|^2}. \tag{3.2}$$

Note that $\mathscr{V}$ endowed with this metric is compact which excludes the case of diverging trajectories in which we have positive Lyapunov exponents without chaos. When we consider a PRC with $\Delta(0^+) \neq \Delta(1)$, an arbitrary small distance between two trajectories can lead to a finite separation after a single excitation. For this to occur, we need two connected oscillators, which have similar phases, such that their order of firing is different in both trajectories. However, the probability P of this situation vanishes, when we consider two trajectories, which are very close. Suppose the phases are distributed according to some distribution $\rho(\phi)$, we can estimate the probability for a pair of oscillators to have a phase difference smaller than ϵ by the following integral:

$$P \sim \int_0^1 d\phi_1 \int_{\phi_1-\epsilon}^{\phi_1+\epsilon} d\phi_2 \rho(\phi_1)\rho(\phi_2) \approx 2\epsilon \int_0^1 d\phi_1 \rho^2(\phi_1). \tag{3.3}$$

The integral vanishes for small ϵ and phase distributions without concentration. Therefore, discontinuities in the PRC do not influence the divergence of trajectories at small distances. We can estimate the probability at other discontinuities of the PRC with similar arguments.

To characterize divergence of trajectories for a network of N oscillators, we consider two state space vectors $\Phi^1 = (\phi_1^1, \dots, \phi_N^1)$ and $\Phi^2 = (\phi_1^2, \dots, \phi_N^2)$ which are seperated by a vector of differences $\mathscr{E} := \Phi^2 - \Phi^1 = (\epsilon_1, \dots, \epsilon_N)$. The networks that we consider are homogeneous in the sense that we have, at least on the level of construction, nodes which are interchangable. Therefore, it is sensible to consider the distribution of the components of $\mathscr{E}$. Note that a fixed point in the state space $\mathscr{V}$ is not conceivable in our system. This would mean that no oscillators are firing anymore and phases would increase due to the intrinsic dynamics of oscillators. The most trivial dynamics we can expect is a limit cycle, i.e., a so-called splay state in which all oscillators have different phases and pass the firing

threshold without overtaking one another. Such states have been observed for oscillators with decreasing PRCs [68, 94]. State space vectors at different times of a splay state will obviously not converge towards each other. The largest Lyapunov exponent in such a state is therefore 0. We can, however, characterize the convergence towards the limit cycles by the first non-vanishing Lyapunov exponent, which for the splay state is negative. Even when such a splay state is an attractor of the dynamics for some network of PCOs, transients can be very long for larger networks, and their mean duration has been shown to scale exponentially with the network size. Similar as for turbulent systems, attractors may play no role for the emerging behavior when transients become so long that it is not possible to observe their ending. Moreover the behavior of single oscillators during this transients may be highly irregular and fluctuating, and can be described as chaotic in the original meaning of the word. This unexpected observation has lead to the term stable chaos, which describes the co-occurence of non-negative Lyapunov exponents and seemingly chaotic behavior that can be observed in high dimensional systems [95]. Note that two state space vectors which mainly differ by an offset in all phases are probably badly chosen to characterize the distance between the trajectories they belong to, as in first approximation phases increase. For weakly coupled oscillators, the state space vector with the smaller phases will move closer with time because the intrinsic dynamics increases the phases of all oscillators in the network. We can always evolve the vector with smaller phases until $\mathscr{E}$ is approximately zero. Therefore, we can assume that the mean value of $\mathscr{E} = (\epsilon_1, ..., \epsilon_N)$ vanishes. For difference vectors $\mathscr{E}$ with zero mean, the sample variance of the components of $\mathscr{E}$ is (due to our definition in Eq. (3.2)) given by the state space metric: $\mathrm{Var}(\mathscr{E}) = N/(N-1)d^2(\Phi^1, \Phi^2)$. To estimate the largest Lyapunov exponent, we use the standard algorithm [96]; we evolve two sets of initial conditions Φ_1 and Φ_2 whose distance $\mathrm{Var}(\mathscr{E})$ is of the order of 10^{-10}. We start with uniformly distributed components of $\mathscr{E}$. However, the starting distribution has little influence on the final results because it quickly converges to some broad stable distribution which is not Gaussian. In Figure (3.7) we show the time evolution of this distribution for a directed Erdős-Rényi network of oscillators. After the distance has either grown or shrunk by a predefined amount, we rescale one phase vector such that the distance is again 10^{-10}. For diverging trajectories, this rate of growth of the distance corresponds to the largest Lyapunov exponent. However, for the case that we have only one vanishing Lyapunov exponent, we can characterize this convergence by the largest non-vanshing Lyapunov exponent. To allow us to characterize a possible convergence towards a limit cycle in $\mathscr{V}$, we introduce the necessary time offset δ in one system as to eliminate the mean of $\mathscr{E}$ at every rescaling. For small coupling

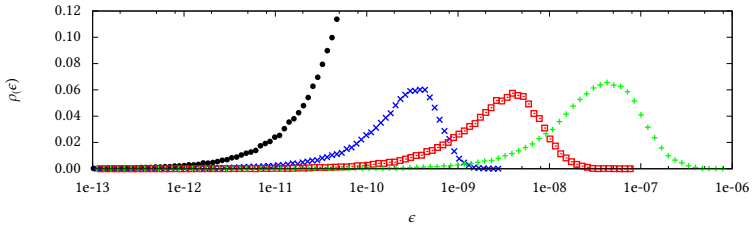

Figure 3.7: Divergence of trajectories in a directed Erdős-Rényi network ($N = 100000, m = 15$) of linear IF oscillators with $a = 0.02, b = 0.03, \tau = \vartheta = 0$ starting from uniformly distributed phases (black). The plot contains histograms of the logarithm of components of the difference vector $\mathscr{E}$ measured at time $t = 0$ (black), 3 (blue), 6 (red), and 9 (green).

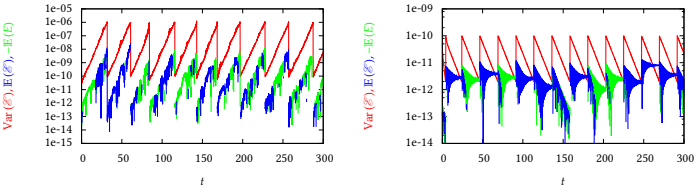

Figure 3.8: Time evolution of the distance between trajectories $\mathrm{Var}(\mathscr{E})$ (red) for Erdős-Rényi networks ($N = 1000, m = 100$) and for different PRCs. The mean phase shift $\mathbb{E}(\mathscr{E})$ is plotted in green and blue for positive and negative values, respectively. Left: $\Delta(\phi) = 0.01(1 - \cos(2\pi\phi))$, right: $\Delta(\phi) = 0.01(e^{-10\phi})$. The distance was rescaled to 10^{-10} when it exceeded 10^{-6} or 10^{-10}.

strengths, the addition of an time offset will reasonably correspond to a removal of contributions to the zero Lyapunov exponent. To minimize the influence of numerical artefacts, all computations were done with 128 bit double precision. In Figure (3.8), we show the time evolution of the distance between trajectories from two measurements of the largest Lyapunov exponent, which were obtained for asynchronous states of directed Erdős-Rényi networks with different PRCs. Using this measurement, the network of inhibitory oscillators shows convergence of the distance of trajectories while the asynchronous state of the network

of excitatory oscillators has a positive Lyapunov exponent. As a preliminary attempt, we present the following argument to explain the difference in convergence behavior for both PRCs. The derivative of the phase transition curve is given by $R'(\phi) = \Delta'(\phi) + 1$. Therefore, $R(\phi)$ is a contraction for phases ϕ at which the PRC has negative slope and an expansion for positive slope. An excitation of an oscillator with phase ϕ will increase the distance between trajectories only if the PRC has positive slope at this ϕ. It can therefore be expected that trajectories converge for the PRC which was used in Figure 3.8 right as the PRC contains a phase jump at $\phi = 0$ and is otherwise monotonously decreasing. The same is the case for the PRC of inhibitory integrate-and-fire neurons for which stable chaos and a non-positive Lyapunov spectrum has been reported [90, 91]. PRCs which are derived from limit cycle oscillators, however, often are continiuous and have both increasing and decreasing parts (see Figure 3.8 left). The behavior remains unexplained using this simple argument and depends specifically on the phases of the excited oscillators. The PRC of excitatory integrate-and-fire oscillators, contains a jump to larger values at $\phi = 0$. The integral over the part of the PRC with negative slope is thus larger than over the part with positive slope. Still, we observe divergence of trajectories (similar as in Figure 3.8 left). This is because the falling edge with slope of -1 near $\phi = 1$ does not effectively reduce the distance between trajectories, as our preliminary argument did not account for the uncertainty of the firing oscillator. When an oscillator with some index e and phase near 1 is excited, its phase after excitation ($\phi = 1$) is insensitive to the phase before. However its phase after the excitation depends on the time at which it received the excitation from some firing oscillator with index f. For two close trajecties, the phase difference ϵ_f of the firing oscillator f is carried over, such that the phase difference of e is $-\epsilon_e$ afterwards. We will, in the following, present a stochastic model which accounts for the uncertainty of firing oscillators and which allows us to estimate the largest Lyapunov exponent, thereby relating it to the PRC and the distribution of excited oscillator phases. The latter is assumed to be a characteristic of some stationary dynamical behavior, which can be the aforedescribed asynchronous state, or some (partially) synchronous state.

We consider a single excitation and compute its influence on the distance of two trajectories we compare. Assume that an oscillator f fires at some time t_f and has a connection towards an excited oscillator e. For the second state space vector with nearby phases, the oscillators have phases $\phi_f + \epsilon_f$ and $\phi_e + \epsilon_e$, respectively. Oscillator f will thus fire at time $t_\mathrm{f} - \epsilon_f$. We compare the phases for both space state vectors at some time after oscillator f has fired in both

trajectories and calculate the new phase difference ϵ'_e as:

$$\begin{aligned}\epsilon'_e &= \Big[(\phi_e + \epsilon_e) + \Delta(\phi_e(t_\mathrm{f} - \epsilon_f) + \epsilon_e)\Big] - \Big[\phi_e + \Delta(\phi_e(t_\mathrm{f}))\Big] \\ &= \epsilon_e + \Delta(\phi_e(t_\mathrm{f}) + \epsilon_e - \epsilon_f) - \Delta(\phi_e(t_\mathrm{f})) \approx \epsilon_e + \Delta'(\phi_e)(\epsilon_e - \epsilon_f) \qquad (3.4)\end{aligned}$$

.

The excitation will affect only the e-th entry in $\mathscr{E}$ according to Eq. (3.4). Note that ϵ_e and ϵ_f may have different signs and thus compensate each other. We define the following stochastic process to model the divergence of trajectories and the evolution of the difference vector $\mathscr{E}$, which is facilitated by a large amount of such excitations. The model depends on the distribution of phases of excited oscillators $\rho_1(\phi)$ and on their PRC $\Delta(\phi)$. We repeat that this distribution differs for Erdős-Rényi networks from the distribution of oscillator phases in the network (see Figures 3.3 and 3.4).

- We start with a vector ($\mathscr{E} = (\epsilon_i | i = 1, ..., N)$) which represents at index i the phase difference of oscillator i between two trajectories.
- Recursively, we define the vector $\mathscr{E}^{(M)} = (\epsilon_i^{(M)} | i = 1, ..., N)$ which represents the phase differences after M excitations.
- For every iteration step we chose a source node index f and a target node index e randomly from $1, ..., N$. Additionally, we draw a random phase ϕ from the distribution function $\rho_1(\phi)$.
- By recursion, we define $\mathscr{E}^{(M+1)}$ to be identical to $\mathscr{E}^{(M)}$ in all components other than e. The e-th component is defined as

$$\epsilon_e^{(M+1)} = \epsilon_e^{(M)}(1 + \Delta'(\phi) - \epsilon_f^{(M)}\Delta'(\phi)). \qquad (3.5)$$

In Figure 3.9 we show different realizations of this stochastic process for different N. Note that the evolution of the difference vector $\mathscr{E}$ in the stochastic model relies on the assumption that the components in the difference vector of oscillators are uncorrelated to their phase. For Erdős-Rényi networks both source and target nodes are not chosen randomly, and it is conceivable that difference components ϵ_i and ϵ_j are correlated differently for connected or unconnected oscillators. For synaptic failure networks (and for the stochastic model), the excited oscillator is chosen randomly. The firing oscillator, however, is not random but given by the oscillator with the largest phase. Also, we change ϵ_e and ϵ_f after each firing, while in synaptic failure networks, we excite multiple oscillators

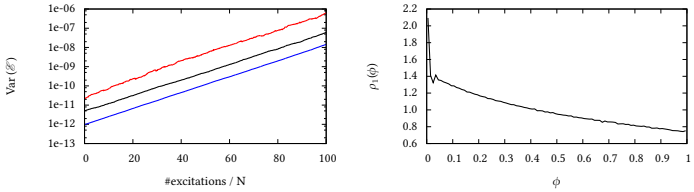

Figure 3.9: Left: Variance of the difference vector $\mathscr{E}$ as generated by the stochastic process for $N = 100$ (red), $N = 1000$ (black) and $N = 10000$ (blue). The chosen distribution of excited phases $\rho_1(\phi)$ (right) was measured from asynchronous states of a directed Erdős-Rényi networks ($N = 10000, m = 15$) of linear IF oscillators with $(a, b, \tau, \theta) = (0.045, 0.02, 0.0, 0.0)$.

depending on the mean degree. In sum, when estimating the divergence of trajectories in random or synaptic networks by the evolution of $\mathscr{E}$ for the stochastic model, we make the approximation that for every excitation the index of excited and firing oscillator, and the phase of the excited oscillator are independent.

In the following, we will calculate the drift of the stochastic process, i.e. the expected increase of $\mathrm{Var}(\mathscr{E})$ per iteration step M. To account for and quantify the possible compensation in the terms of Eq. (3.5), we consider the ensemble $\mathscr{S}$ of all possible evolutions starting from all initial vectors $\mathscr{E}$ in which each component is distributed independently and equally with variance $v^{(0)}$. In our calculation the distribution itself has no influence on the trend. We leave the exact form thus open. Regarding this ensemble $\mathscr{S}$ we consider the distribution $\zeta_i^{(M)}$ of the phase difference $\epsilon_i^{(M)}$ in some component i after M iterations and investigate the influence of a single excitation. Due to the symmetry in the construction, it is clear that the distributions $\zeta_i^{(M)}$ are identically distributed for all $i \in N$. We will denote the common variance of these distributions by $v := \mathbb{E}\left(\zeta_i^{(M)}\zeta_i^{(M)}\right)$ were we use $\mathbb{E}$ as symbol for the expectation value defined for the ensemble $\mathscr{S}$. Although we chose initial conditions without correlations between components, the iterations introduce some level of correlations between ζ_i and ζ_j for $i \neq j$ which we will quantify. Again we assume that the correlation between two arbitrary components $i \neq j$ is identical due to the symmetry of the problem. We denote it with $\gamma := \mathbb{E}\left(\zeta_i^{(M)}\zeta_j^{(M)}\right)$. Let us calculate for some M the value of $\gamma' := \mathbb{E}\left((\zeta_i^{(M+1)}\zeta_j^{(M+1)})\right)$ after a single excitation in dependence on $\gamma = \mathbb{E}\left(\zeta_i^{(M)}\zeta_j^{(M)}\right)$ before the excitation. Using Eq. (3.5) we first average over the indices of firing and excited oscillators.

The average over the phase distribution will be performed afterwards. Assuming uniformly distributed indices, we have $(N-1)^2$ cases in which γ does not change at all as neither oscillator i nor oscillator j is excited. For $2(N-1)$ cases, oscillator i is excited and j is not the firing oscillator (or vice versa). In this case we obtain with

$$\gamma' = \mathbb{E}\left(\zeta_i^{(M)}\zeta_j^{(M)}\right)\left(1+\Delta'(\phi)\right) - \mathbb{E}\left(\zeta_i^{(M)}\zeta_f^{(M)}\right)\Delta'(\phi) = \gamma\left(1+\Delta'(\phi)\right) - \Delta'(\phi) = \gamma \quad (3.6)$$

also no change in correlation. Finally, we have two cases in which i is excited and j is the firing oscillator (or vice versa). We obtain

$$\gamma' = \mathbb{E}\left(\zeta_i^{(M)}\zeta_j^{(M)}\right)\left(1+\Delta'(\phi)\right) - \Delta'(\phi)\mathbb{E}\left(\zeta_j^{(M)}\zeta_j^{(M)}\right) = \gamma\left(1+\Delta'(\phi)\right) - \Delta'(\phi)v \quad (3.7)$$

averaging over i and j, we obtain

$$\begin{array}{rl} \gamma' = & \frac{1}{N^2}\left((N-1)(N-1)\gamma + 2(N-1)\gamma + \gamma(1+\Delta'(\phi)) - \Delta'(\phi)v\right) \\ & \gamma + \frac{2}{N^2}\Delta'(\phi)(\gamma - v). \end{array} \quad (3.8)$$

Similarly, we calculate the change in variance $v' := \mathbb{E}\left(\zeta_i^{(M+1)}\zeta_i^{(M+1)}\right)$ due to a single excitation. We have no influence if an oscillator other than i is excited. If, however, i is excited, we obtain using Eq. (3.5)

$$\begin{array}{rcl} v' & = & \mathbb{E}\left(\zeta_i^{(M)}(1+\Delta'(\phi)) - \zeta_f^{(M)}\Delta'(\phi)\right)^2 = \\ & = & (1+\Delta'(\phi))^2\mathbb{E}\left(\zeta_i^{(M)}\zeta_i^{(M)}\right) + \Delta'^2(\phi)\mathbb{E}\left(\zeta_f^{(M)}\zeta_f\right) - 2(1+\Delta'(\phi))\Delta'(\phi)\mathbb{E}\left(\zeta_i^{(M)}\zeta_f^{(M)}\right) \\ & = & v(1+2\Delta'(\phi)+2\Delta'^2(\phi)) - 2(\Delta'^2(\phi)+\Delta'(\phi))\gamma. \end{array} \quad (3.9)$$

Averaging over i, the change in variance is given by

$$v' = v + \frac{2}{N}\left(\Delta'(\phi) + \Delta'^2(\phi)\right)\left(v-\gamma\right). \quad (3.10)$$

Averaging over the phase ϕ of the excited oscillator and using the abbreviations

$$\alpha = \frac{2}{N}\int_0^1 \left(\Delta'(\phi) + \Delta'^2(\phi)\right)\rho_1(\phi)d\phi, \quad \beta = \frac{2}{N^2}\int_0^1 \Delta'(\phi)\rho_1(\phi)d\phi \quad (3.11)$$

we can represent Eqs. (3.10) and Eq. (3.8) as the following linear equation:

$$\begin{pmatrix} v' \\ \gamma' \end{pmatrix} = \begin{pmatrix} 1+\alpha & -\alpha \\ -\beta & 1+\beta \end{pmatrix}\begin{pmatrix} v \\ \gamma \end{pmatrix} \quad (3.12)$$

The matrix has an eigenvalue of 1 and of $1+\alpha+\beta$. For the case that α and β are

positive, which is the case for the excitatory IF oscillator we study, contributions to the smaller eigenvalue will vanish after some excitations and the vector gets aligned to the eigenvector $(\alpha, \beta)^T$ associated with the eigenvalue $1 + \alpha + \beta$. As β scales with $1/N^2$ and α scales with $1/N$, correlations play no role in the limit $N \to \infty$ and we have in this case $v' = v(1 + \alpha)$ for the growth of the variance. If we assume that $\mathscr{E}^{(M)}$, as generated by the stochastic model, estimates the vector of phase differences between two trajectories, we can calculate the mean (taken over realizations) of the distance after M excitations as:

$$\mathbb{E}\left(d^2(\Phi^{(M)}, \Phi^{(M)} + \mathscr{E}^{(M)})\right) = \frac{1}{N}\sum_i \mathbb{E}\left(\zeta_i \zeta_i\right) = v^{(M)} = v^{(0)}(1+\alpha)^M. \tag{3.13}$$

Considering a mean firing rate of ν, we have at time t an expected number of νtmN excitations and thus:

$$v(t) = v^{(\nu mtN)} = v^{(0)} \prod_{i=1}^{\nu mtN} \left[1 + \frac{2}{N}\int_0^1 \left(\Delta'(\phi) + \Delta'^2(\phi)\right)\rho_1(\phi)d\phi\right]. \tag{3.14}$$

Using a well-known formula for the exponential function, we get for large N:

$$v(t) \approx v^{(0)} \prod_{i=1}^{\nu mt} e^{2\int\left(\Delta'(\phi)+\Delta'^2(\phi)\right)\rho_1(\phi)d\phi} = v^{(0)} e^{\nu mt \int\left(\Delta'(\phi)+\Delta'^2(\phi)\right)\rho_1(\phi)d\phi} \tag{3.15}$$

We denote the estimation of the largest non-vanishing Lyapuonv exponent which we obtain from the drift of the stochastic process by λ_{SM} and obtain

$$\lambda_{\mathrm{SM}} = \ln\left(\sqrt{\frac{v(1)}{v(0)}}\right) = \nu m \int_0^1 (\Delta'(\phi) + \Delta'^2(\phi))\rho_1(\phi)d\phi. \tag{3.16}$$

Given that the assumptions of the stochastic model are justified, we can estimate the largest Lyapunov exponent by Eq. (3.16) for different stationary dynamical behaviors in dependence on their distribution of excited oscillator phases $\rho_1(\phi)$. Recall that the term quadratic in $\Delta'(\phi)$ originates from the influence of the uncertainty of the firing oscillator. As we see from Eq. (3.16), we have negative contributions to λ for excitations to oscillators with phases ϕ for which $-1 < \Delta'(\phi) < 0$. Let's consider again absorption of oscillators, which happens if an oscillator is excited near a phase of 1. The PRC then has a slope of –1. According to Eq. (3.16), such an excitation has no influence on the largest Lyapunov exponent, which is sensible: The phase of the oscillator before excitation has no influence on the

phase afterwards (which is 1). However, the uncertainty of the firing oscillator is carried over to the excited oscillator. Therefore, only one value of the distance vector is exchanged by another, which does not change the distance of trajectories on average. Note that for complete synchrony, all excitations are received by oscillators with phase $\phi = 1$. We therefore have $\rho_1(\phi) = \delta(\phi - 1)$ and, as expected, $\lambda_{\mathrm{SM}} = 0$. For excitatory, linear IF oscillators, excitations which do not lead to absorption yield a positive contribution to λ_{SM}. This means that λ_{SM} is positive for all stationary dynamical behaviors characterized by $\rho_1(\phi)$ for which $\rho_1(\phi)$ takes non-vanishing values outside the slope of -1 near $\phi = 1$. We therefore expect stationary network behaviors which are asynchronous or partially synchronous to be chaotic. For low-dimensional systems, if we chose two nearby initial conditions on a chaotic attractor, their difference vector may have contributions from other Lyapunov exponents. Therefore, one usually evolves both initial conditions to ensure that contributions to all but the largest Lyapunov exponent die out. For the stochastic process, however, we do not have degrees of freedom changing the speed of divergence/convergence. The distribution of the components of ϵ may change with time (see Figure 3.7). Its shape, however, does not influence λ_{SM}.

In Figure 3.10, the numerically estimated largest Lyapunov exponent is compared to λ_{SM} as determined by Eq. (3.16) with measured distributions $\rho_1(\phi)$ and firing rates ν for asynchronous states of Erdős-Rényi networks. For the considered parameters, Eq. (3.16) presents a reasonable approximation to the largest Lyapunov exponent, and we find no significant correlation between ϵ_e, ϵ_r and ϕ_r. However, for large mean degrees and strongly varying PRCs, the phases of oscillators and their component of the difference vector become correlated. We demonstrate this effect for linear IF oscillators with refractory periods ϑ and time delays τ. In Figure 3.11 we show a similar measurement as presented in Figure 3.10 for oscillators with τ and ϑ. When an oscillator r is refractory, its component in $\mathscr{E}$ cannot increase. As other components do increase, r in its refractory period has on average smaller a smaller ϵ_r than oscillators which are not refractory; the assumption that ϕ_r and ϵ_r are independent is just an approximation (see Figure 3.11 top right) which is better for smaller Lyapunov exponents as then the short time a oscillator is in its refractory period is not enough to introduce large differences in ϵ_r compared to other oscillators.

In Figure 3.11, we measure λ_{SM} for different dynamical behaviors, including complete synchrony ($\tau \in [0, 0.05]$), partially synchronous states ($\tau \in [0.05, 0.08]$, $\tau \in [0.14, 0.15]$) and asynchronous states (for the remaining range of τ). We give a detailed description of the dynamics of these states in Chapter 3.3. Note, that the value of τ does not influence the shape of the distribution of excited phases

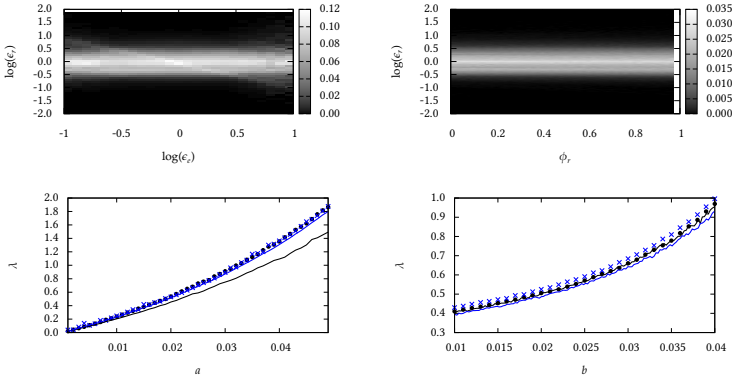

Figure 3.10: Top: two dimensional histogram of the observed pairs (ϵ_e, ϵ_r) and (ϕ_r, ϵ_r) when tracking the divergence of two nearby trajectories in asynchronous states of Erdős-Rényi networks ($N = 5000, m = 15$) of linear IF oscillators $(a, b, \tau, \vartheta) = (0.02, 0.03, 0.0, 0.0)$. The histograms are normalized column-wise. For every excitation, ϵ_e and ϵ_r denote the component of the difference vector of the emitting and receiving oscillator, respectively. ϕ_r denotes the phase of the excited oscillator. Both histograms point to that ϵ_e, ϵ_r and ϕ_r show no significant correlations for the chosen parameters. Bottom: Largest Lyapunov exponent for asynchronous states of networks ($N = 5000, m = 15$) of linear IF oscillators in dependence on their parameters. Numerical values are shown as data points, lines represent calculated values obtained from Eq. (3.16) with measured distributions of excited oscillators $\rho_1(\phi)$ and firing rates ν. Both were done for directed Erdős-Rényi networks (black) and undirected Erdős-Rényi networks (blue). The bottom left (right) plot shows the influence of a (b) for $b = 0.02$ ($a = 0.02$).

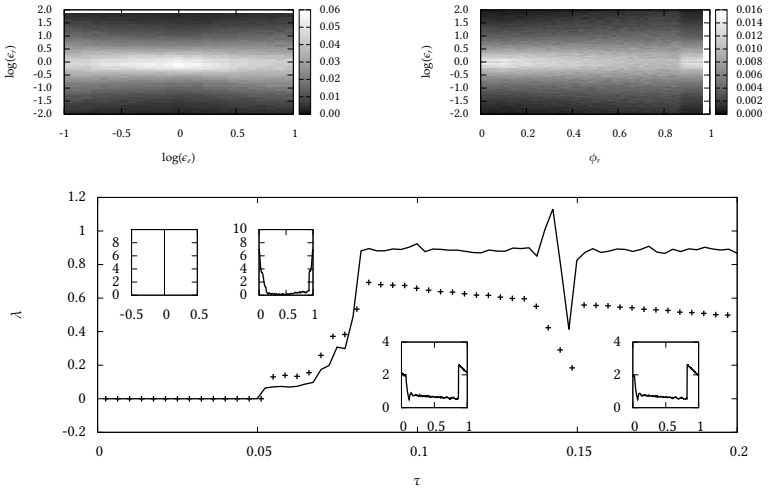

Figure 3.11: Top: two dimensional histogram of the observed pairs (ϵ_e, ϵ_r) and (ϕ_r, ϵ_r) when tracking the divergence of two nearby trajectories in asynchronous states of directed Erdős-Rényi networks ($N = 10000, m = 15$) of linear IF oscillators $(a, b, \tau, \vartheta) = (0.05, 0.05, 0.012, 0.2)$. The histograms are normalized column-wise. For every excitation, ϵ_e and ϵ_r denote the component of the difference vector of the emitting and receiving oscillator, respectively. ϕ_r denotes the phase of the excited oscillator. The top right histogram show a slightly tendency towards smaller values of ϵ_r for ϕ values in the refractory period. Bottom: Largest Lyapunov exponent for asynchronous states of networks ($N = 10000, m = 15$) of linear IF oscillators in dependence on their parameters. Numerical values are shown as data points, lines represent calculated values obtained from Eq. 3.16 with measured distributions of excited oscillators $\rho_1(\phi)$ and firing rates ν. Inset shows $\rho_1(\phi)$ for different τ. From left to right $\tau \in [0.0, 0.05]$, $\tau = 0.072371$, $\tau = 0.132371$, $\tau = 0.174871$. Note that simple relationships between τ and ϑ can lead to artifacts and were therefore avoided.

in asynchronous states, instead ρ_1 is merely shifted by τ. We provide more justification for this observation in our discussion of the continuum models, which allow us to describe $\rho_1(\phi)$ in terms of differential equations. As both $\rho_1(\phi)$ and $\Delta(\phi)$ are merely shifted for different τ in asynchronous states, it is clear that λ_{SM} takes the same value and is constant in $\tau \in [0.08, 0.2]$. However, λ_{SM} as approximation to the Lyapunov exponent of the network dynamics becomes worse with increasing τ (see Figure 3.11), as here ϵ_e becomes more and more dependent on ϵ_r. The expected absolute value of ϵ_e is smaller than those of ϵ_r, as firing oscillators are refractory before firing for $\phi \in [1-\tau, 1]$, while the excited oscillator is and ϵ_r is likely to have increased by other excitations during this time. With this observation in mind, we can specify when the approximation in Eq. (3.16) is reasonable, namely when λ itself is small, such that the component of an oscillator in $\mathscr{E}$ changes little during its transportation on the phase circle.

We have described that linear IF oscillators coupled on Erdős-Rényi networks can give rise to asynchronous states with nearly constant order parameters and distribution of phases. We also characterized the microscopic dynamics to be chaotic. Now, we will discuss synchronous states and transients towards them.

3.3 (Partially) synchronous states

The asynchronous states that we described can only be observed for larger networks. If we choose some set of parameters (for which the oscillators exhibit asynchronous ehavior) and decrease the network size, we will eventually observe transitions to synchrony. In Figure 3.12 we show the influence of the network size on the mean transient durations for small networks. All three kinds of random networks that we consider show exponential scaling. While we cannot measure these transient durations for the network sizes we are interested in, we have no reason to assume that the scaling is different for larger networks or that transition become impossible at some critical network size. However, the exponential scaling certainly means that transitions become unobservable for even medium-sized networks. We note the analogy to turbulent fluids [97, 98], where even for moderate volumes, the observable dynamics consists of transients and is unrelated to the attractor. Moreover, we remark the analogy to stable chaos, where transient and fluctuating behavior eventually leads to limit cycle behavior [68]. In our case, transient and fluctuationg behavior eventually leads to synchrony [78, 99]. In both cases even medium sized networks may exhibit transient durations which are orders of magnitude above the timescales which can be observed with numerical simulations. The dependence of the tran-

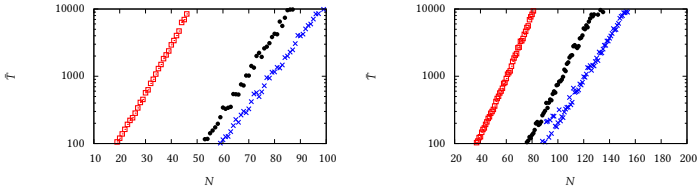

Figure 3.12: Mean transient duration $\bar{T}$ for random networks ($m = 15$) of linear IF oscillators in dependence on the network size N. Blue: synaptic failure networks, black: directed Erdős-Rényi networks, red: undirected Erdős-Rényi networks. Left: $a = 0.02, b = 0.02$, right: $a = 0.02, b = 0.028$

sient duration on oscillator parameters shows a smooth transition for small networks which sharpens to a critical transition for large networks. We will discuss in the following the behavior for reasonably large networks in which the notion of asynchronous states as defined in Chapter 3.1 is practical, and discuss the loss of stability of these states in dependence on oscillator parameters. We start with a discussion of the behavior in Erdős-Rényi networks of linear IF oscillators without refractory periods and time delays.

Linear IF oscillator

Depending on network and oscillator parameters, asynchronous states loose stability and we observe different kinds of transients which lead to synchronous states when starting from distributed phases in $[0, 1]$. Surprisingly, the parameter region in the (a, b)-plane which we associate with asynchronous states, does not contain small values of b, such that we observe with increasing b, first synchronous, then asynchronous and again synchronous states. In Figure 3.13, we show the average order parameter $\langle r \rangle$ in dependence on the parameters a and b of linear IF oscillators coupled onto directed and undirected Erdős-Rényi networks. We can distinguish the parameter region with asynchronous states and small values of $\langle r \rangle$ from the region in which oscillators in the network synchronize completely after a few collective oscillations leading to $\langle r \rangle = 1$. Note that complete synchrony is stable for arbitrary a and b (see Chapter 2.2). For the black regions shown in Figure 3.13, the networks may show both synchronous and asynchronous behavior depending on the intial condition. We observe two boundaries of the parameter region with asynchronous states, which intersect

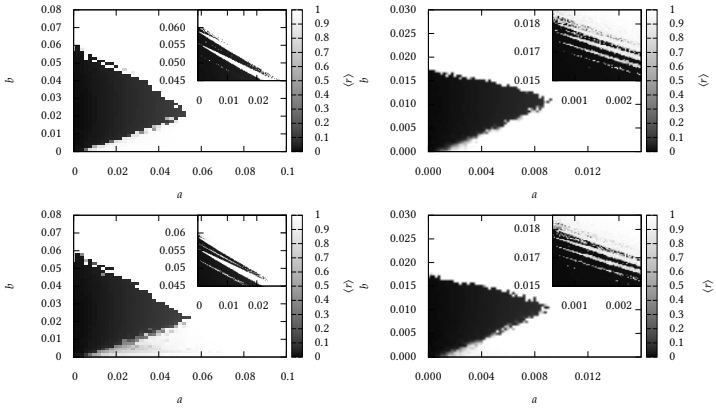

Figure 3.13: Average order parameter $\langle r \rangle$ in $t \in [100, 200]$ for directed linear IF oscillator networks (see Eq. 2.18) in dependence on oscillator parameters a and b. Random networks have 10000 oscillators and a mean degree of 15 (left) and 50 (right) and are directed (top) or undirected (bottom). The inset shows a closer view which reveils a fine structure near the upper boundary of the parameter region with asynchronous states.

with discontinuous slope. Both boundaries give rise to different transients to synchrony when starting from homogeneously distributed phases. We will denote the boundary which lies at larger(smaller) values of b in the following as upper(lower) boundary. The dynamical behavior near and above the upper boundary is similar for directed and undirected Erdős-Rényi networks. For parameters above the boundary, we observe a quick convergence to complete synchrony within a few oscillations. Near the boundary, this convergence may set in after periods of seemingly stationary behavior which may vary considerably in duration (see Figure 3.14 top). At the lower boundary, we observe irregular global behavior which seems stable for undirected Erdős-Rényi networks and leads to complete synchrony for directed Erdős-Rényi networks (see Figure 3.14 bottom). Macroscopically, we established in Chapter 3.1 that asynchronous states can be described by a distribution of phases, which possibly represents some kind of stable equilibrium. We will make this notion more concrete when discussing the continumm models in Chapter 3.4, and regard it as a intuitive notion for the moment. For finite networks, such a distribution can only be approximated

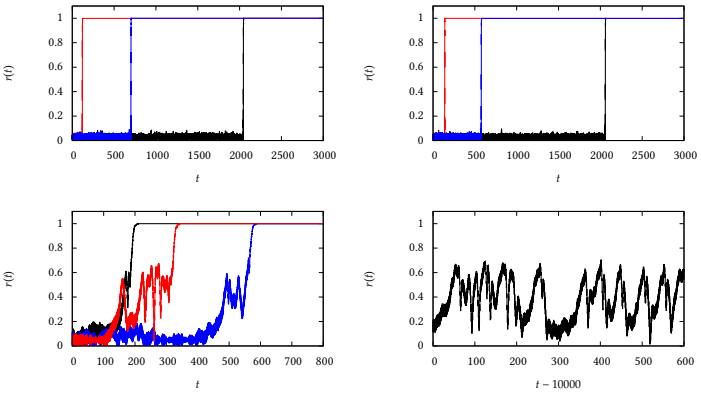

Figure 3.14: Exemplary time evolutions of the order parameter $r(t)$ of directed Erdős-Rényi networks (left) and undirected Erdős-Rényi networks (right) of linear IF oscillators. Colors represent differeent sets of uniformly distributed initial phases. Networks parameters: ($m = 15, N = 10000$). Different color-coded curves correspond to different uniformly distributed phases as initial conditions. Top: oscillator parameters ($a = 0.02, b = 0.053$) were chosen from the upper boundary of the regime with asynchronous behavior (cf. Figure 3.13 left). Bottom: oscillator parameters were chosen near the lower boundary ($a = 0.02, b = 0.0075$). At the lower boundary, directed Erdős-Rényi networks show complicated transients to complete synchrony, while undirected Erdős-Rényi networks show stable, irregular behavior.

which automatically introduces finite-size fluctuations. If the basin of attraction of these equilibrium solutions is small, it is conceivable that it can be left due to these fluctuations. The expected life time thus increases with the network size because finite-size fluctuations diminish. Additionally, we can change the equilibrium and its basin by changing model parameters, which also influences the transient durations, or turns the equilibrium solution unstable.

In Figure 3.15, we show the dependence of the mean transient duration $\bar{T}$ on oscillator parameter b for different network sizes. For a fixed set of parameters near the upper boundary, we observe exponentially distributed durations of transients. Moreover, transient durations of directed and undirected Erdős-Rényi networks show similar distributions. For large network sizes the param-

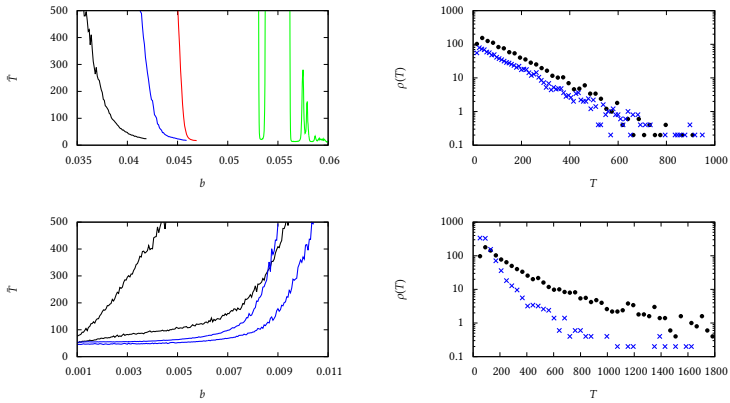

Figure 3.15: Statistical properties of transients to synchrony observed for parameters near the boundaries of the regime of asynchronous states for directed Erdős-Rényi networks (cf. Figure 3.13). Top left: mean transient duration $\bar{T}$ near the upper boundary in dependence on b and for a fixed value of $a = 0.02$ for different network sizes $N = 500$ (black), 1000 (blue), 2000 (red), 10000 (green). Right: frequency distribution $\rho(T)$ of transient durations near the upper boundary $a = 0.02, b = 0.0375$ for directed Erdős-Rényi networks (blue) and undirected Erdős-Rényi networks (black) with $N = 500$ and $m = 15$. Bottom left: mean transient duration $\bar{T}$ near the lower boundary in dependence on b and with $a = 0.02$ for $N = 500$ (black) and $N = 1000$ (blue). Values for both undirected (blue) and directed (black) Erdős-Rényi networks. Bottom right: distribution of transient durations $\rho(T)$ for networks of $N = 500, b = 0.0085$ for directed (blue) and undirected (black) Erdős-Rényi networks.

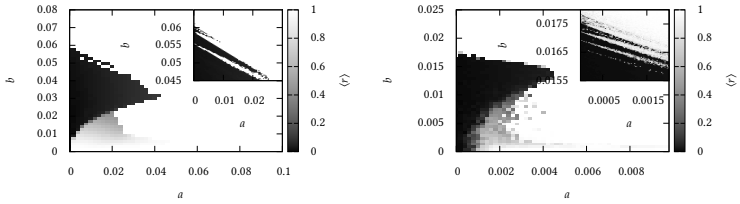

Figure 3.16: Average order parameter $\langle r \rangle$ in $t \in [100, 200]$ for linear IF oscillator coupled onto synaptic failure networks in dependence on PRC parameters a and b. Networks have 10000 oscillators and a mean degree of 15 (left) and 50 (right). The inset shows a closer view which reveals a fine structure near the upper boundary of the parameter region with asynchronous states.

eter dependence shows a fine structure with multiple changes between more stable and less stable states. This fine structure can also be observed in the two-dimensional measurements presented in Figure 3.13. The dynamical origins of the fine structure require further investigations. It is conceivable that it is influenced by the initial condition which is far from the system's equilibrium in this parameter regime. The boundary and its fine structure progress similarly for directed and undirected Erdős-Rényi networks. Near the lower boundary, we observe large differences in the distributions of transient durations, even for small networks (see Figure 3.15 bottom). Moreover, the transient durations are not well described by an exponential function, which reflects the irregular and complicated dynamics during the transients (Figure 3.14 bottom left).

We will now discuss the dynamical behavior of synaptic failure networks, which show comparable dynamics near the upper boundary (see Figure 3.16) and a similar progression of the latter as for Erdős-Rényi networks. Near the lower boundary, however, syanptic failure networks show additional dynamical behaviors. To describe these, we assess the firing rate $\nu(t)$ by counting the number of firing oscillators given some temporal discretization grid. The grid size has to be chosen in a trade-off which guarantees enough firing oscillators in each bin and sufficient resolution of the temporal changes of $\nu(t)$. In Figure 3.17 we show $\nu(t)$ and the order parameter $r(t)$ for such a partially synchronous state near the boundary at which stability of asynchronous solutions is lost. After a few oscillations $\nu(t)$, $r(t)$ and $\rho(\phi, t)$ show a simple periodic behavior. The phase density shows a *deviation* from the equilibrium solution which is localized in ϕ and is periodically shifted in direction of larger phase values. The continuum

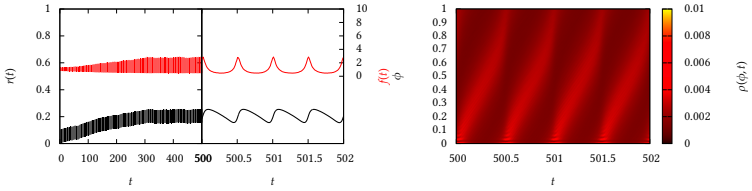

Figure 3.17: Left: Temporal evolutions of order parameter $r(t)$ and firing rate $\nu(t)$ of a synaptic failure network ($N = 10^6, m = 15$) of linear IF oscillators starting from homogeneously distributed phases. Right: distribution of phases $\rho(\phi, t)$ in the network in dependence on time after the transient. Oscillator parameters $a = 0.02, b = 0.023$. After the transient, the dynamics shows a periodic behavior.

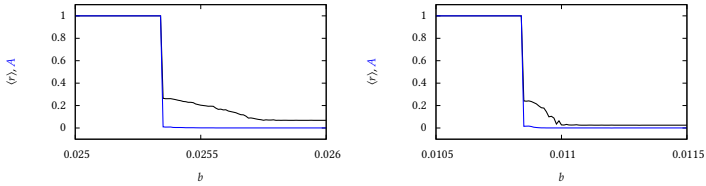

Figure 3.18: Average order parameter $\langle r \rangle$ and largest avalanche size A in the interval $t \in [100, 200]$ for linear IF oscillators coupled onto synaptic failure networks ($N = 10^6$) in dependence on b and for $a = 0.027, m = 15$ (left), and $a = 0.003, m = 50$ (right). The networks exhibit synchronous states for larger values of b. Smaller values of b lead to limit cycles with a periodic behavior of $r(t)$ and eventually to complete synchrony at the appearance of avalanches (cf. Figure 3.19 top).

model which we present in the next chapter provides evidence that the described solutions are–in the limit of large networks–indeed periodic and can be considered as limit cycles which emerge from supercritical Andronov-Hopf bifurcation points which lie on the boundary of the region with asynchronous states. These limit cycles are observable at the full length of the lower boundary. When we choose parameters which are farer away from the parameter region with asyn-

chronous states, e.g. by choosing lower values of b, the size of the deviation increases as does the range of assumed values of the firing rate $\nu(t)$. Beyond some critical parameter value for b, we observe, when starting from uniformly distributed phases, the deviation to increase until the firing rate $\nu(t)$ diverges. We explain the latter as follows: When a suprathreshold excitation is received, the excited oscillator adapts its phase towards the firing oscillator and fires itself at the same instant. A large number of oscillators with phases near 1 may lead to a kind of chain reaction in which every firing oscillator makes on average another oscillator fire. If this happens, an amount of oscillators which is of the same order of magnitude as the network size fires simultaneously. The discretization grid we use to assess $\nu(t)$ limits the values we can detect from above. To assess infinite values of $\nu(t)$ and thus avalanches, we computed for every firing oscillator, the number of oscillators which fired at exactly the same time. We will denote an simultaneous firing as an avalanche, and measure its size A by the fraction of the network that fires simultaneously. Avalanches can also be observed in the asynchronous states but they rarely exceeds a few oscillators and thus have no influence on the collective dynamics for large networks.

An avalanche represents a spontaneous adaptation of a large part of the oscillators to a common phase. It is therefore not surprising that the appearance of avalanches may lead to complete synchrony after a few collective firings as we observe for larger values of a (see Figures 3.18 and 3.19 top). For smaller values of a, however, we observe partially synchronous states with recurring avalanches, which are observable in a large parameter region (grey regions in Figure 3.16) Depending on oscillator and network parameters, these states can appear seemingly periodic (similar as the limit cycles near the lower boundary of the asynchronous parameter regime) but with an avalanche of a fixed size as part of the periodic behavior. However, we also observe more complicated states in which the sizes of avalanches appear completely irregular. In those states, avalanches have a desynchronizing influence on the dynamics. In the middle part of Figure 3.19, we show a transient to a (seemingly) periodic state with recurring avalanches. Due to the large number of excitations which are emitted from oscillators in the avalanche, the whole distribution of phases is changed discontinuously. After the avalanche the firing oscillators have a phase of 0 and represent—in the notion of the phase density—a δ-peak. Due to the intrinsic dynamics of oscillators, the peak travels to larger phase values, and due to excitations which arrive at its contributing oscillators, it decays rapidly. As every oscillator will receive on average m excitations during one firing cycle, very few oscillators will remain at the δ-peak when it reaches $\phi = 1$. Excitations to oscillators from the δ-peak arrive at different times and lead to different

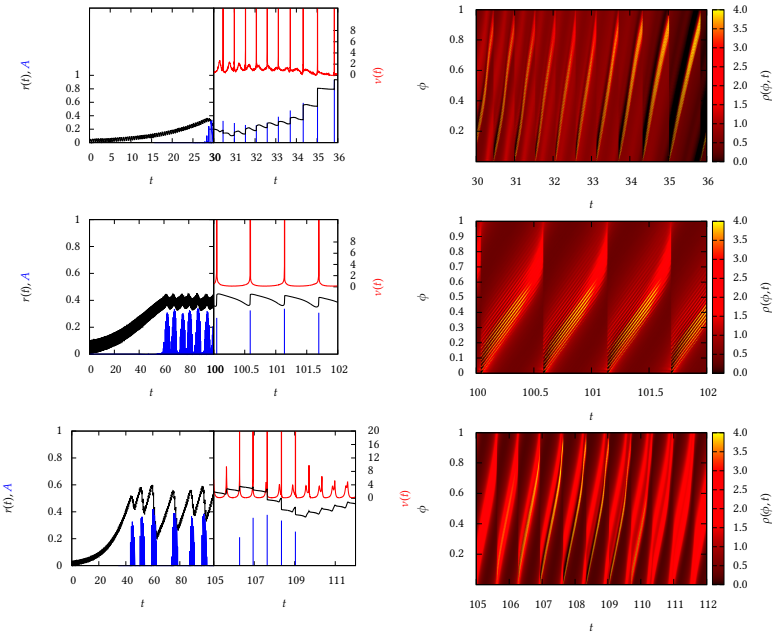

Figure 3.19: Left: Temporal evolutions of order parameter $r(t)$ (black) and firing rate $\nu(t)$ (red) of a synaptic failure network of 10^6 linear IF oscillators starting from homogeneously distributed phases. Avalanche sizes A are marked in blue. Right: distribution of phases in the network $\rho(\phi, t)$ in dependence on time after the transient. Top: avalanches lead to a fast convergence to complete synchrony ($a = 0.003, b = 0.009, m = 50$). Middle: seemingly periodic time evolution with a recurring avalanche of a fixed size ($a = 0.02, b = 0.022, m = 15$). Bottom: irregular behavior with recurring avalanches ($a = 0.002, b = 0.006, m = 50$).

phase responses (provided $a \neq 0$). Therefore, no additional phase concentrations are generated. Instead, at a phase distance given by the phase response curve, a local maximum is generated which consists of oscillators which were part of the avalanche and received one excitation. Analogously, local maxima are generated with oscillators which received more than one excitation. This leads to the characteristic structure in the phase distribution shown in the middle part of Figure 3.19. As oscillators with a certain phase are influenced by random excitations, their phases will differ after some time. This leads to a smoothing of the structure when it is transported to larger phase values. The resulting shape of the structure when it reaches $\phi = 1$ then determines the next avalanche. Although the described state seems periodic, some variability remains even for large network sizes. With our simulations it is not possible to decide if this variability is due to finite size effects or if it has some dynamical origin.

For larger mean degrees, the global dynamics becomes irregular (see Figure 3.19 bottom). Here, the phase distribution shows oscillations with increasing amplitude until avalanches appear. These have a desynchronizing influence, which can be explained in the following way: When the oscillators of the avalanche fire, their excitations shift $\rho(\phi)$ to larger phase values. However, oscillators are not excitable at the instant of their firing, which leads to a gap in the phase distribution (see Figure 3.19 bottom right) between the oscillators which fired before the avalanche (with finite firing rates) and the oscillators of the avalanche. Both parts are transported to larger phase values and are again smoothed out to a single increase of lower amplitude with finite firing rates. The gap can also be seen in the firing rate $\nu(t)$ which shows a bimodal behavior at the falling slopes of $r(t)$. Intriguingly, the described mechanism does not necessarily lead to a periodic behavior but to an irregular behavior which depends sensitively on initial conditions and which persists for long periods of time. However, it is not clear how strongly finite size fluctuations influence the observed irregularity. We compared simulations with networks up to sizes of 10^7 oscillators and found no loss of irregularity in observables like $r(t)$ for the parameters of Figure 3.19 bottom. The introduced gap is more pronounced for smaller coupling strengths and larger mean degrees, as here the smoothing back to a single increase is slow and possibly takes many oscillations. It is therefore plausible that we observe irregular behavior for $m = 50$, while smaller mean degrees lead to the seemingly periodic behavior like in Figure 3.19 middle in which the gap is smoothed and vanishes during its transport towards $\phi = 1$ during a single oscillation.

Note that partially synchronous states as those described in Figure 3.17 lead to a periodic behavior of $r(t)$. The range of assumed value for $r(t)$ is therefore no advisable characteristic for irregularity. To characterize the deviation from simple

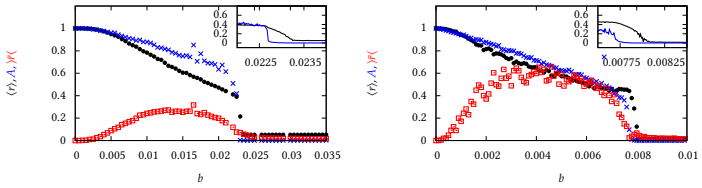

Figure 3.20: Average order parameter $\langle r \rangle$ (black), largest avalanche size A (blue), and range $\rangle \bar{r} \langle$ of the series of local maxima of r (red). All three characteristics were determined for the interval $t \in [1000, 2000]$ and for linear IF oscillators coupled onto synaptic failure networks ($N = 10^6$) in dependence on b and for $a = 0.02, m = 15$ (left) and $a = 0.0015, m = 50$ (right). The networks show for larger b asynchronous states. Smaller values of b lead to limit cycles with a periodic behavior in $r(t)$ and eventually to irregular states with recurring avalanches (see Fig 3.19 bottom and middle) . The insets show a closer view on $\langle r \rangle$ and A near the loss of stability.

limit cycles in global observables, we calculate the series of local maxima $\bar{r}(t)$ of $r(t)$. Both asynchronous states and limit cycles will lead to constant values of $\bar{r}(t)$, while more complicated time evolutions can be assessed by a statistical property of $\bar{r}(t)$ which characterizes fluctuation. In Figure 3.20 we show cuts through the (a, b)-plane in direction of b for both $m = 15$ and $m = 50$. We observe from larger to smaller values of b first asynchronous states, then a small region with periodic solutions as in Figure 3.17, and finally irregular behavior as in Figure 3.19 middle and bottom. The irregular behavior can be observed for a large range of parameters below the lower boundary. Note that the irregular behavior that emerges in undirected Erdős-Rényi networks is also accompanied by avalanches (Figure 3.14). In Figure 3.21, we show a time evolution for a larger networks for which we detected avalanches in the same way as we did for Figure 3.19. It seems likely that the dynamics here is comparable for what we described for synaptic failure network. However, this point needs further investigations, inparticular regarding the absence of irregular behaviors in directed Erdős-Rényi networks.

Linear IF oscillator with refractory periods and time delay

We will now discuss the dynamics of oscillators with time delays and refractory periods. Interestingly, we observe for these large differences in the dynamical

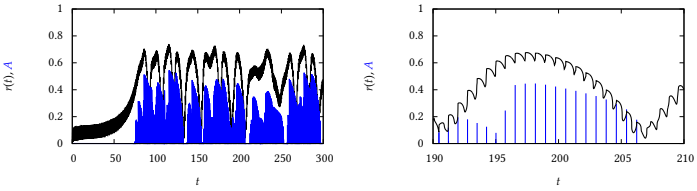

Figure 3.21: Time evolution of the order parameter for an undirected Erdős-Rényi network ($N = 250000, m = 50$) for parameters below the lower boundary ($a = 0.004, b = 0.008$). Avalanche are indicated as blue lines with a height A which reflects the fraction of concurrently firing oscillators. The right plot shows a closer view.

behavior of random and synaptic failure networks. While Erdős-Rényi networks show asynchronous states similarly as before (see Figure 3.23 left), synaptic failure networks synchronize completely for arbitrary small coupling strengths (see Figure 3.22). We explain the observed differences as follows. By adding a refractory period, the attraction of two oscillators which are already synchronized is increased, as the oscillator which precedes is refractory (cf. Figure 2.5) when the excitation from the succeeding oscillator arrives. Note oscillators in a synaptic failure network are stochastic and it is thus possible to separate both oscillators if one receives more excitations than the other. However, they receive on average the same amount of excitations. This is in contrast to Erdős-Rényi networks in which oscillators have different numbers of incoming connections. Refractory periods thus promote synchrony to a much smaller degree in those networks. In contrast to the simpler oscillators, we observe no fine structure near the upper boundary of the regime with asynchronous solutions and no partially synchronous states near the lower boundary for both directed undirected Erdős-Rényi networks. The transition durations show near both boundaries exponential behavior for larger transient durations.

In the following chapter, we will provide descriptions of the dynamics in the thermodynamic limit of $N \to \infty$. We represent the population of oscillators in the network by a density function $\rho(\phi, t)$ and derive evolution equations for $\rho(\phi, t)$ for different conditions on the networks we want to desribe. We provide three descriptions which are tailored to dense networks, to sparse synaptic failure networks and to sparse Erdős-Rényi networks. The evolution equations will be formulated for PCOs of arbitrary PRC, whereafter we return to linear

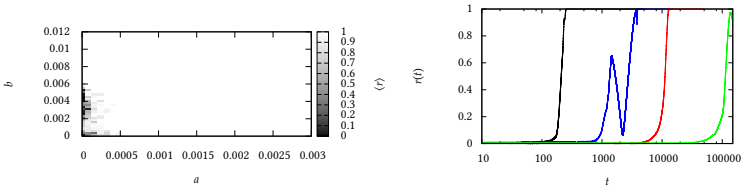

Figure 3.22: Left: Average order parameter $\langle r \rangle$ for synaptic failure networks ($N = 10000, m = 50$) of linear IF oscillator networks in dependence on PRC parameters a and b. Oscillators are endowed with time delay $\tau = 0.01$ and refractory periods $\vartheta = 0.05$ (see Eq. 2.18). $\langle r \rangle$ was averaged over $t \in [100, 200]$. Right: Time evolution of the order parameter $r(t)$ for synaptic failure networks of linear IF oscillators with $\tau = 0.01, \vartheta = 0.05, a = 0.0$ and $b = 10^{-3}$ (black), $b = 10^{-4}$ (blue), and $b = 10^{-5}$ (red), and $b = 10^{-6}$ (green)

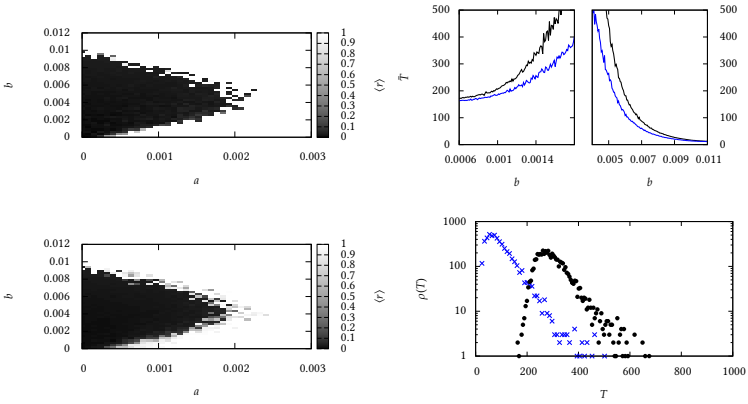

Figure 3.23: Left: Average order parameter $\langle r \rangle$ for directed Erdős-Rényi networks (top) and undirected Erdős-Rényi networks (bottom) of linear IF oscillators in dependence on PRC parameters a and b. Oscillators are endowed with time delay $\tau = 0.01$ and refractory periods $\vartheta = 0.05$ (see Eq. 2.18). $\langle r \rangle$ was averaged over $t \in [100, 200]$. Network parameter: $N = 10000, m = 50$. Right top: Mean transient duration $\bar{T}$ in dependence on b and for a fixed value of $a = 0.001$ for directed Erdős-Rényi networks (black) and undirected Erdős-Rényi networks (blue). Right bottom: distribution of transient durations of directed Erdős-Rényi networks $N = 10000$ near the lower boundary (black, $b = 0.001$) and near the upper boundary (blue, $b = 0.009$).

IF oscillators to illustrate the equations. This approach allows us to provide an explanation for many of the behaviors that we described before.

3.4 Continuum models

Let us consider a sequence of networks $(\mathcal{N}_i | i \in \mathbb{N})$ such that their number of nodes diverges $|\mathcal{N}_i| = N_i \to \infty$. If we associate each network's nodes with a dynamical system, we can define and investigate macroscopic observables. For the right conditions on the networks in the sequence, these observables may show similar behavior for large i as we are considering systems which are less and less influenced by finite-size effects. We can ask the question if it is possible to define a limiting dynamics, i.e., differential equations which describe the dynamics in the thermodynamic limit of infinitely large networks. As candidates for such conditions, we consider that either the mean degree m_i or the connection probability p_i converges for $i \to \infty$. Given that m_i and p_i are parameters of our network construction, we can expect that they are parameters of the evolution equation in the thermodynamic limit. As we have $m_i = N_i p_i$, the convergence behavior of one of the two variables will determine the other. A converging connection probability implies that the number of connections per oscillator diverges which is why we denote the respective limit as limit of dense networks. In contrast, for converging mean degrees, the number of links in the networks becomes small compared to the number of possible links in the networks wherefore we denote the respective limit as limit of sparse networks.

sparse limit $m_i \to m, N_i \to \infty, p_i \to 0$

dense limit $m_i \to \infty, N_i \to \infty, p_i \to p$

Note that for a given m, we can define very different sparse networks (e.g. Erdős-Rényi networks or lattices) with different dynamical behaviors even for large network sizes. Therefore, we cannot expect a unique limiting dynamics for sparse limits. Although denseness seems to be a much stronger restriction for a network, we are not aware of any result which has been obtained that dense networks can be expected to have similar dynamics for large sizes, although it seems plausible. In the following, we assume that the networks in limits are either Erdős-Rényi networks or synaptic failure networks and discuss all four possibilities that arise when combining these network notions with one of our two limits.

Let us consider a single oscillator and its equations of motion in a large network. If we know all fire times t_j of its connected oscillators, we can describe its

phase as

$$\dot{\phi}(t) = 1 + \sum_j \delta(t - t_j)\Delta(\phi(t_j)). \tag{3.17}$$

For a Erdős-Rényi network, the excitation times are correlated in a complicated way (depending on the network) and this formula is not directly useful. For synaptic failure networks, however, it can be argued that the sum of δ-pulses can be expressed as a Poisson process. Note that the Poisson process can be uniquely characterized as being memoryless and ordered [100, 101]. Memorylessness means that the excitation times in a specific interval do not depend on the history up to this point. This is clearly the case for synaptic failure networks in which all excitations are distributed independently and the rate of arriving excitations depends only on the firing rate, not on the patterns of excitations so far. In contrast, memorylessness is violated for Erdős-Rényi networks; when an oscillator has received many excitations in the near past, the probability to receive more is small, as many connected oscillators just fired and are thus likely to have small phases. This remains true even if the global firing rate is time independent. Orderliness means that excitations do not arrive simultaneously. This property is violated in partially synchronous states, in which a macroscopic amount of oscillators fires simultaneously as we described in Figure 3.19. Then again, whenever oscillator phases are distributed such that we can describe them by a normalized distribution function $\rho(\phi, t)$, orderliness is fulfilled. Although the arrival rate at oscillators in Erdős-Rényi networks is not memoryless, the assumption of a Poissonian process may still provide a sensible approximation, which is better when we have many connections and asynchronous oscillators. We thus make this assumption —aiming at both random and synaptic failure networks—and denote with $\eta_{\lambda(t,\phi)}(t)$ an inhomogeneous Poisson process with time and phase-dependent rate $\lambda(t, \phi)$. The firing rate $\nu(t)$ in the network is given by the fraction of oscillators which cross $\phi = 1$ in some small time interval, i.e., the probability flux $J(\phi, t)$ at $\phi = 1$:

$$\nu(t) = J(1, t). \tag{3.18}$$

For deterministic dynamics, $J(\phi, t)$ can be expressed as the product of density and velocity of oscillators at $\phi = 1$. For finite coupling strengths, however, the situation is more complicated, as even oscillators with $\phi(t) < 1$ can cross $\phi = 1$ at time t if they receive an excitation. We will defer the exact definition of the flux to the corresponding chapters for synaptic failure and Erdős-Rényi networks. For a specific oscillator in a synaptic failure network, the probability that it receives an excitation when another oscillator fires is given by m/N, independently on its phase. The arrival rate, i.e. the rate of incoming excitations is thus independent

on the oscillator phase or network size and reads $\lambda(t,\phi) = \lambda(t) = m\nu(t)$. Using this, we can express the equation of motions of a single oscillator in the limit of sparse synaptic failure networks as:

sparse limit synaptic failure network

$$\dot{\phi}(t) = 1 + \eta_{\lambda(t)}(t)\Delta(\phi(t)), \quad \lambda(t) = mJ(1,t). \tag{3.19}$$

Note that this equation only contains m as network parameter which we assumed to be finite in the sparse limit. For Erdős-Rényi networks, we described in the last chapter (see Figures 3.3 and 3.4) that the distribution of excited phases does not coincide with the distribution of phases in the network. To account for this, we do need the dependence of the excitation rate $\lambda(t,\phi)$ on the phase ϕ. We defer the definition of $\lambda(t,\phi)$ to the chapter for the continuum model for Erdős-Rényi networks and define

sparse limit Erdős-Rényi network

$$\dot{\phi}(t) = 1 + \eta_{\lambda(t,\phi)}(t)\Delta(\phi(t)). \tag{3.20}$$

For the dynamics in the limit of dense networks, the arrival rate diverges. In order to retain a finite effective phase velocity, we rescale the coupling strength to account for the diverging number of incoming connections m for each node. More exactly, we assume that the product of PRC and mean degree m converges to a limiting PRC, which we denote with $F(\phi)$ to avoid confusion with the PRC of single excitations:

$$\Delta_i(\phi)m_i \to F(\phi). \tag{3.21}$$

$F(\phi)$ can be interpreted as the phase change per time interval and per firing rate that an oscillator in the network receives due to excitations. For the firing rate, we assume no dependence on the phase for both synaptic failure networks and Erdős-Rényi networks as we observe the distribution of phases $\rho(\phi)$ and the distribution of excited phases $\rho_1(\phi)$ to approximate each other for Erdős-Rényi networks of large mean degrees m. Moreover, the evolution equations for Erdős-Rényi networks that we describe in Chapter 3.4.3, predicts a difference between $\rho(\phi)$ and $\rho_1(\phi)$ which declines for larger m. Assuming a phase independent rate, we can express the phase change $d\phi$ in a small time interval dt by the number of excitations which arrive during dt. The latter follows a Poisson distribution and is for large rates well approximated by a Gaussian distribution with mean and variance $\lambda(t)$:

$$\dot{\phi}(t) \approx 1 + (m_i J(1,t) + \sqrt{m_i J(1,t)}\xi(t))\Delta_i(\phi(t)). \tag{3.22}$$

Here we used $\xi(t)$ to denote Gaussian white noise with zero mean and unit variance. For the limit of dense networks, $m_i\Delta_i$ stays finite an therefore $\sqrt{m_i}\Delta_i$ vanishes such that we end up with a purely deterministic equation for single oscillators:

dense limit random and synaptic failure network

$$\dot{\phi}(t) = 1 + J(1,t)F(\phi). \tag{3.23}$$

Again, the equation does not depend on parameters which diverge in the limit of dense networks (like m or N). In the following chapters, we will revisit the limits as described in Eqs.(3.19), (3.20), and (3.23) and investigate the corresponding master equations.

3.4.1 Sparse synaptic failure networks

We intent to derive a master equation for Eq. (3.19). In the same way, as for finite networks, the point process of incomming excitations of a single oscillator approximates Eq. (3.19), the macroscopic dynamics of finite networks will approximate the dynamics as given by the master equation. Note that the synaptic failure networks can be regarded as Mont-Carlo simluations to the dynamics of the master equation [102]. Monte-Carlo simulations are often used as a numerical validation of complex problems when solutions are hard to obtain. Here, our description is different; we investigated the dynamics of finite networks and consider the continuum model as a limit of those. The master equation will be given in form of a continuity equation

$$\partial_t \rho(\phi,t) + \partial_\phi J(\phi,t) = 0. \tag{3.24}$$

The (probability) flux $J(\phi,t)$ is meant to describe the fraction of oscillators which pass a imaginary membrane at phase ϕ per time interval. However, as we expect phase densities which are discontinuouos in ϕ, we have to be careful how $\rho(\phi)$ should be defined and interpreted. Consider a distribution of objects in the unit interval with identified end points, such that we have two different densities ρ_1 and ρ_2 for $\phi < 0.5$ and $\phi > 0.5$. The densities $\rho(\phi)d\phi$ at $\phi = 0.5$ and $\phi = 1.0$ are in this situation no well-defined quantity. For many applications it would not be necessary to define $\rho(0.5)$ and $\rho(1.0)$ at all. However, for our dynamical system, the number of oscillators with phase $\phi = 1$ corresponds to the firing rate and directly influences the dynamics and we thus need to define $\rho(1.0)$ in some way, at least in the sense of some limit.

We will use a different approach here, and define $\rho(\phi)$ as the density of particles, in a small interval whose left boundary is fixed at ϕ. In this sense we restrict the notion of infinitesimal phase intervals $d\phi$ in expressions like $\rho(\phi)d\phi$. This defines $\rho(0.5) = \rho_2$ and $\rho(1.0) = \rho_1$ and makes the density function continuous for left-sided limites. Note that the choice to fix the right boundary is arbitrary, we could equally well have required a fixed left boundary. Naturally, the definition of $\rho(\phi)$ also influences the probability flux. Integrationg over Eq. (3.24) and using the fundamental theorem of calculus, we obtain

$$\partial_t \int_{\phi_0}^{\phi_0+\epsilon} \rho(\phi, t) = -J(\phi_0) + J(\phi_0 + \epsilon). \tag{3.25}$$

The change of particles in the interval $[\phi_0, \phi_0 + \epsilon]$ is given by the flux through the interval boundaries at a and $a + \epsilon$. Due to the nature of excitations in our system, we have to discuss the influence of oscillators which are moved exactly to ϕ_0 by an excitation and in particular if they pass the imaginary surface with which we define $J(\phi)$. As oscillators with phase $\phi < \phi_0$ do not contribute to $\rho(\phi_0)$ and oscillators with phase $\phi = \phi_0$ do, an oscillator passes the membrane if its phase is ϕ_0 and was smaller before the excitation. However, oscillators with phases $\phi > \phi_0$ do contribute to $\rho(\phi_0)$ as do oscillators with phase ϕ. Therefore, an oscillator does not pass the membrane if its phase is ϕ_0 and was larger before the excitation. The flux which follows from our interpretation of $\rho(\phi)$ can thus be defined as the density of oscillators which pass a membrane which is infinitely close to ϕ and below ϕ. When we consider ρ and J at $\phi = 0$, the expressions are meant as a short notation of the right-sided limit (e.g. $\rho(0, t) := \lim_{\varphi \to 0} \rho(\varphi, t)$). We assume $J(\phi, t)$ to depend continuously on ϕ. In particular we assume $J(1, t) = J(0, t)$ as all firing oscillators are injected after firing. Integration on both sides over ϕ in (3.24) immediately yields that the integral of ρ does not change with time, which allow us to interpret ρ as a probability density.

In the following, we will provide some heuristic considerations, which allow us to infer the continuity equation, before we derive in a more axiomatic approach both differential equation and boundary condition from a general definition of the flux. We start by considering non-interacting oscillators. An arbitrary initial phase distribution $\rho_0(\phi)$ for such oscillators, will be shifted unchanged to larger values with constant velocity 1. The solution in this case is given by $\rho(\phi, t) = \rho_0(\phi - t)$, which is a solution of the one-dimensional, first order convection equation:

$$\partial_t \rho(\phi, t) = -\partial_\phi J(\phi, t), \quad J(\phi, t) = \rho(\phi, t). \tag{3.26}$$

Requiring continuity for the flux immediately gives us the boundary condition:

$$\rho(0,t) = \rho(1,t). \tag{3.27}$$

We will now consider the influence of excitations. We can expect for a given phase ϕ two terms which determine the change of the density $\rho(\phi)$. One term corresponding to oscillators, which are excited and disappear at ϕ and one term corresponding to oscillators with other phases which are excited and arrive at ϕ (see Figure 3.24). We will denote the possible origin phases for which oscillator wills – after excitation – arrive at ϕ by $R_i^{-1}(\phi)$. More formally, we define for a given phase ϕ and an appropriate index set I_ϕ the reverse images of the phase transition curve R under ϕ as $\{R_i^{-1}(\phi)|i \in I_\phi\}$. The master equation for $\rho(\phi)$ contains a term for each of these inverse images, reflecting the oscillators which are originating from $R_i^{-1}(\phi)$ and arrive at ϕ due to an excitation. Consider oscillators which are concentrated in a small interval of size $d\phi$ around $R_i^{-1}(\phi)$, namely $[R_i^{-1}(\phi), R_i^{-1}(\phi) + d\phi]$. Given the probability distribution ρ, the fraction of oscillators in this interval is $\rho(R_i^{-1}(\phi), t)d\phi$. For a rate $\lambda(t)$ per time interval dt we expect a decrease in the density by $\rho(R_i^{-1}(\phi, t)\lambda(t)$. Oscillators are–after excitation–contained in $[R(R_i^{-1}(\phi)), R(R_i^{-1}(\phi) + d\phi)]$, which is an interval of size $d\phi R'(R_i^{-1}(\phi))$. We have to account for the different sizes of the origin and target intervals, which reflects the fact that R may expand or contract the distance between pairs of phases. If we interpret for a chosen discretization grid $d\phi$ $\rho(\phi, t)d\phi$ as the number of oscillators contained in $d\phi$, and if we use the same tightness around ϕ and $R_i^{-1}(\phi)$, we obtain an increase of the density $\rho(\phi)$ by $\lambda(t)\rho(R_i^{-1}(\phi))/R'(R_i^{-1}(\phi))$. Repeating this argument for every root and including the convection term at the right hand side of Eq. (3.26) we get:

$$\partial_t \rho(\phi, t) = -\partial_\phi \rho(\phi, t) - \lambda(t)\rho(\phi, t) + \lambda(t) \sum_{i \in I_\phi} \frac{\rho(R_i^{-1}(\phi), t)}{1 + \Delta'(R_i^{-1}(\phi))}. \tag{3.28}$$

Note that $\lambda(t) = mJ(1,t) = m\rho(\phi, t)$ depends for $m \neq 0$ on $\rho(\phi, t)$ and Eq. (3.28) is thus non-linear. If we have $|\Delta'| < 1$ for all phases, the phase transition curve $R(\phi)$ is strictly monotonous and we have exactly one reverse image of $R(\phi)$ for every phase ϕ. This is usually the case for PRCs which are derived from limit cycle oscillators [103]. In this case we can express the probability flux for which

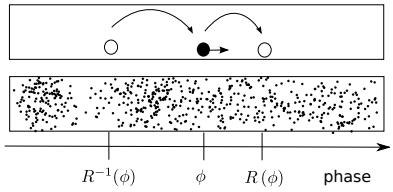

Figure 3.24: Schematic of the different terms in the equation (Eq. (3.28)) describing the evolution of the phase density $\rho(\phi, t)$. $\rho(\phi, t)$ is transported to larger phases due to the intrinsic dynamics of oscillators. Additonally, it is decreased due to oscillators with phase ϕ which are excited and disappear at ϕ and increased due to oscillators with phase $R^{-1}(\phi)$ which are excited and appear at ϕ.

the continuity equation takes the form of Eq. (3.28) by:

$$J(\phi, t) = \rho(\phi, t) + \lambda(t) \int_{R^{-1}(\phi)}^{\phi} d\tilde{\phi} \rho(\tilde{\phi}, t). \tag{3.29}$$

However, we are interested in the case that entire intervals are mapped by R to a single value, as we have for absorbing oscillators. In this case, the expressions (3.28) and (3.29) are ill-defined. Additionally, Eq. (3.28) does not allow us to deduce a formula for the firing rate which we defined in form of the flux. Therefore, we define a generalization of Eq. (3.29) which is expressed only in terms of $R(\phi)$ and not in terms of its reverse image. To this end, we define $I_{\rightarrow}(\phi)$ as the set of all phases smaller than ϕ which are mapped by the PTC $R(\phi)$ to a phase larger than ϕ. Oscillators with phases in $I_{\rightarrow}(\phi)$ contribute to the flux $J(\phi, t)$ as an excitation will move them past ϕ. Analogously we define $I_{\leftarrow}(\phi)$ at the set of phases larger than ϕ which are mapped to smaller value of ϕ by $R(\phi)$:

$$I_{\rightarrow}(\phi) = \{\tilde{\phi} < \phi | R(\tilde{\phi}) \geqslant \phi\}, \quad I_{\leftarrow}(\phi) = \{\tilde{\phi} > \phi | R(\tilde{\phi}) < \phi\}. \tag{3.30}$$

Using this notation, the general definition of the flux is given as:

$$J(\phi, t) = \rho(\phi, t) + \lambda \int_{I_{\rightarrow}(\phi)} \rho(\tilde{\phi}, t) d\tilde{\phi} - \int_{I_{\leftarrow}(\phi)} \rho(\tilde{\phi}, t) d\tilde{\phi}. \tag{3.31}$$

The first term in Eq. (3.31) corresponds to the flux induced by the intrinsic dynamics of oscillators. The second (third) term corresponds to excitations which move oscillators past an imaginary membrane at ϕ in direction of larger (smaller) values. Let us first argue, that Eq. (3.31) indeed reproduces Eq. (3.28) if R has at most countably many reverse images for some φ. We write the sets $I_{\rightarrow}(\phi)$ and $I_{\leftarrow}(\phi)$ in the form of Heaviside functions and differentiate the flux in Eq. (3.31):

$$\partial_\phi J(\phi,t) = \partial_\phi \rho(\phi,t) + \lambda \int \rho(\tilde{\phi},t) d\tilde{\phi} \partial_\phi \left[\theta(\phi-\tilde{\phi})\theta(R(\tilde{\phi})-\phi) - \theta(\tilde{\phi}-\phi)\theta(\phi-R(\tilde{\phi}))\right]. \tag{3.32}$$

The derivative of the integrals can then be calculated, using the product rule and assuming that differentiating Heaviside functions yields δ-distributions:

$$\begin{aligned} &= \partial_\phi \left[\theta(\phi-\tilde{\phi})\theta(R(\tilde{\phi})-\phi) - \theta(\tilde{\phi}-\phi)\theta(\phi-R(\tilde{\phi}))\right] \\ &= \delta(\phi-\tilde{\phi})\left[\theta(R(\tilde{\phi})-\phi) + \theta(\phi-R(\tilde{\phi}))\right] + \delta(R(\tilde{\phi})-\phi)\left[\theta(\phi-\tilde{\phi}) + \theta(\tilde{\phi}-\phi)\right] \\ &= \delta(\phi-\tilde{\phi}) + \delta(R(\tilde{\phi})-\phi). \end{aligned} \tag{3.33}$$

Using the rule of substitution, we can evaluate the remaining δ-distribution as long as $R(\phi)$ has at most countably many reverse images. Together with the convection term of Eq. (3.31), we immediately obtain Eq. (3.28).

Eq. (3.31) has the advantage that we can derive boundary conditions from it. Assume we have a PRC Δ which has an interval B in which Δ has a slope of -1 pointing to some phase φ (as is the case for the PRC of IF oscillators for $\varphi = 1$). Then the function $I_{\rightarrow}(\phi)$ which maps phases to sets is discontinuous in the following sense: $I_{\rightarrow}(\varphi)$ will contain A while $I_{\rightarrow}(\varphi^+)$ may well be empty. We can and should in this case still assume a continuous flux $J(\varphi,t)$ (as defined in Eq. (3.31)) which, however, forces a discontinuous boundary condition on the phase distribution $\rho(\phi,t)$:

$$\underbrace{\rho(\varphi,t) + \lambda \int_{I_{\rightarrow}(\varphi)} \rho(\tilde{\phi},t) d\tilde{\phi} - \lambda \int_{I_{\leftarrow}(\varphi)} \rho(\tilde{\phi},t) d\tilde{\phi}}_{J(\varphi)} =$$

$$\underbrace{\rho(\varphi^+,t) + \lambda \int_{I_{\rightarrow}(\varphi^+)} \rho(\tilde{\phi},t) d\tilde{\phi} - \lambda \int_{I_{\leftarrow}(\varphi^+)} \rho(\tilde{\phi},t) d\tilde{\phi}}_{J(\varphi^+)}. \tag{3.34}$$

If we have many oscillators with phases slightly below the firing threshold, it may be the case that an oscillator that fires at time t will excite and make other oscillators fire at the same time t. The firing of these other oscillators then may further increase the firing rate $\nu(t)$ similar as in an avalanche. Our definitions so far account for these avalanches. If we insert our formula for the arrival rate $\lambda(t) = mJ(1,\phi)$ in Eq. (3.31) and set $\phi = 1$, we obtain:

$$\lambda = mJ(1,t) = m\rho(1,t) + m\lambda \int\limits_{I_{\rightarrow}(1)} \rho(\tilde{\phi},t)d\tilde{\phi} + m \int\limits_{I_{\leftarrow}(1)} \rho(\varphi,t)d\varphi). \tag{3.35}$$

We can solve this equation with respect to λ to obtain an expression solely in terms of the phase distribution:

$$\lambda = m\rho(1,t)/(1 - m \int\limits_{I_{\rightarrow}(1)} \rho(\tilde{\phi},t)d\tilde{\phi} + m \int\limits_{I_{\leftarrow}(1)} \rho(\varphi,t)d\varphi). \tag{3.36}$$

The last term in the denominator corresponds to oscillators which receive an inhibitory excitation and traverse the firing threshold in the *wrong* direction. Such oscillators decrease the firing rate as they are counted as negative flux across $\phi = 1$. This is clearly not desirable. We avoid this situation by considering only PRCs which are bounded by $-\phi$ from below. In this way, an inhibitory excitation can at most set the phase of the excited oscillator to 0 and no threshold crossing is possible.

The denominator of Eq. (3.36) may vanish, which leads to a diverging firing rate. Although numerical solvers which base on some finite difference scheme will fail at this point, the behavior of finite synaptic failure networks remains meaningful. We observe an avalanche effect in those simulations. When every firing oscillator absorbs–on average–at least one other oscillator, a macroscopic amount of oscillators (of the order of the network size) will fire at the same time instant. Avalanches appear, when the degree is large and when the phase distribution contains large values in the interval $I_{\rightarrow}(1)$, which are phases at which oscillators are moved past the firing threshold by a single excitation. At the avalanche the noise which is injected into each oscillator due to the mutual interaction (see Eq. (3.19)) is no longer ordered; oscillators may receive multiple excitations at the same time and the phase distribution in the finite network is changed discontinuously. After the avalanche, a phase cluster containing a macroscopic amount of oscillators is injected at $\phi = 0$. While this situation often leads to complete synchrony (in fact every transient to complete synchrony contains such avalanches after some time), it does not have to; In Chapter 3.3,

we reported on limit cycles with partial synchrony in which avalanches occur periodically. In the notion of the continuity equation, we have a δ-peak which is injected at $\phi = 0$ at the time of the avalanche. However, the continuum dynamics and the framework introduced so far cannot account for this behavior, especially when the firing rate as defined by Eq. (3.36) turns negative.

To summarize: Given a PTC $R(\phi)$ and a mean degree m, we consider the unit interval $[0, 1)$ in which 1 is identified with 0, and define on this interval a continuous conserved probability flux as in Eq. (3.31). This definition determines a continuum model of oscillators which can be interpreted as the limiting dynamics of sparse synaptic failure networks. We infer from this definition the differential equation

$$\partial_t \rho(\phi, t) = -\partial_\phi \rho(\phi, t) - \lambda(t)\rho(\phi, t) + \lambda(t) \sum_{i \in I_\phi} \frac{\rho(R_i^{-1}(\phi), t)}{1 + \Delta'(R_i^{-1}(\phi))} \tag{3.37}$$

where the excitation rate is given by

$$\lambda = m\rho(1)/(1 - m \int_{I_\rightarrow(1)} \rho(\tilde{\phi}, t) d\tilde{\phi} + m \int_{I_\leftarrow(1)} \rho(\varphi, t) d\varphi). \tag{3.38}$$

Additionally, we infer for phases φ at which $R^{-1}(\phi)$ has uncountably many reverse images, the following boundary condition:

$$\rho(\phi, t) + \lambda \int_{I_\rightarrow(\varphi)} \rho(\tilde{\phi}, t) d\tilde{\phi} = \rho(\varphi^-) - \lambda \int_{I_\leftarrow(\varphi^-)} \rho(\tilde{\phi}, t) d\tilde{\phi} \tag{3.39}$$

Due to the non-linearity of the system (which is explicit in both the boundary conditions and in the differential equation), solutions of different mass $\int_0^1 \rho(\phi) d\phi$ have different shape, although the time evolution does not change mass. If we investigate solutions with a different mass, the firing and excitation rates are interpreted wrongly as they both are entities relative to the size of the population. To ensure that the firing rates are interpreted as expected, we additionally require for the initial conditions that solutions are normalized to 1:

$$\int_0^1 \rho(\phi, 0) d\phi = 1 \tag{3.40}$$

In the following, we will provide a analysis of the equations for linear IF oscillators.

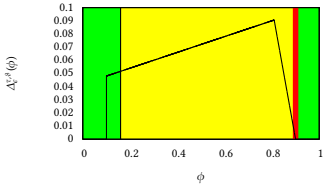

Figure 3.25: Phase response curve of linear IF oscillators (see Eq. (2.18)) for exemplary parameters $(a, b, \tau, \vartheta) = (0.06, 0.06, 0.1, 0.2)$. Phase intervals are colored depending on the number of reverse images of the PTC. Green for no reverse image, yellow for one reverse image. The phase $1 - \tau$, at which we have uncountably many reverse images, is marked in red.

Linear IF oscillator

We consider the phase response curve of linear IF oscillators with time delay τ and a refractory period ϑ as given in Eq (2.18). To evaluate the differential equation Eq. (3.37), we investigate the inverse images of the phase transition curve (see Fig 3.25). For the interval $[0, b]$, we have no reverse images and thus no term reflecting arriving oscillators. For the interval $[b, 1]$, we have exactly one reverse image at $R^{-1}(\phi) = \frac{\phi - b}{1+a}$. For $\phi = 1 - \tau$, we have uncountably many reverse images reflecting the fact that all excited oscillators with phases in the interval $[\phi_{\text{ab}}, 1]$ have a phase of 1 after excitation. In the intervals $[0, \vartheta - \tau]$ and $[1 - \tau, 1]$, the PTC is the identity and the two excitation terms in Eq. (3.37) cancel each other out. The differential equation reads

$$\begin{aligned}
\partial_t \rho(\phi, t) &= -\partial_\phi \rho(\phi, t) && 0 < \phi < \vartheta - \tau \\
\partial_t \rho(\phi, t) &= -\partial_\phi \rho(\phi, t) - \lambda(t)\rho(\phi, t) && \vartheta - \tau < \phi < b + \vartheta - \tau \\
\partial_t \rho(\phi, t) &= -\partial_\phi \rho(\phi, t) - \lambda(t)\rho(\phi, t) + \tfrac{\lambda(t)}{1+a}\rho(\tfrac{\phi - b}{1+a}, t) && b + \vartheta < \phi < 1 - \tau \\
\partial_t \rho(\phi, t) &= -\partial_\phi \rho(\phi, t) && 1 - \tau < \phi < 1.
\end{aligned} \tag{3.41}$$

From Eq. (3.39) we obtain the following boundary condition for $\phi = 1 - \tau$:

$$\rho((1-\tau)^-, t) = \rho(1 - \tau, t) + \lambda \int_{\phi_{\text{ab}}}^{1-\tau} \rho(\tilde{\phi}, t) d\tilde{\phi}. \tag{3.42}$$

For other boundaries between the case distinctions in Eq. (3.41), we assume con-

tinuity of ρ. For the case without time delay ($\tau = 0$), the boundary condition concerns the firing threshold and we have according to Eq. (3.38):

$$\lambda = m \frac{\rho(1,t)}{1 - m \int_{\phi_{\mathrm{ab}}}^{1} \rho(\tilde{\phi},t) d\tilde{\phi}}. \tag{3.43}$$

Otherwise, the rate is given by $\lambda = mJ(1,t) = m\rho(1,t)$.

Stationary solutions

We continue with a description of the stationary equilibrium solutions. Let $\rho_0(\phi)$ be such a solution, i.e., a normalized solution of Eqs. (3.41)–(3.43) with $\partial_t \rho_0(\phi,t) = 0$. The differential equation can be described in the following way:

$$\begin{array}{ll} \partial_\phi \rho(\phi,t) = 0 & 0 < \phi < \vartheta - \tau, \\ \partial_\phi \rho(\phi,t) = -\lambda \rho(\phi,t) & \vartheta - \tau < \phi < b + \vartheta - \tau, \\ \partial_\phi \rho(\phi,t) = -\lambda \rho(\phi,t) + \frac{\lambda}{1+a} \rho(\frac{\phi-b}{1+a},t) & b + \vartheta - \tau < \phi < 1 - \tau, \\ \partial_\phi \rho(\phi,t) = 0 & 1 - \tau < \phi < 1. \end{array} \tag{3.44}$$

We start with some easy conclusions which we can draw from this equation: The shape of stationary solutions does not depend on the time delay τ since it only influences the boundaries of the case distinction by an offset. Therefore, solutions with the same parameters apart from τ can be obtained from each other by shifting the phase variable. Furthermore, solutions are constant during the refractory periods of oscillators and decay exponentially in the interval $[\vartheta - \tau, b + \vartheta - \tau]$. Despite the seemingly simple form, the delay term in Eq. (3.44) destroys all hope for analytic solutions in the interval $[b + \vartheta - \tau, 1 - \tau]$.

In the following, we will describe a shooting approach, which can be used to obtain numerical solutions. For excitatory oscillators, which we consider, the differential equation (3.44) depends for some phase ϕ only on smaller phases. If we thus interpret ϕ as a time variable, we have a delay differential equation with state-dependent delays which is causal and can be solved by some stepping algorithm which evolves some initial state $\rho(\phi = 0)$ incrementally to $\rho(\phi = 1)$. The solution obtained in this way depends on the initial value $u_0 := \rho(\phi = 0, t = 0)$ and on the rate λ, and we will denote it by $\rho(\phi; u_0, \lambda)$. For the findings presented in this chapter, we used the DDESOLVER to obtain such solutions, a code which implements continuously embedded sixth-order Runge-Kutta methods [104]. Note, for given fixed λ Eq. (3.44) represents a linear initial value problem, although the full boundary value problem, which describes the stationary solutions is non-linear. If we chose u_0 and λ positive, the solution $\rho(\phi; u_0, \lambda)$ will

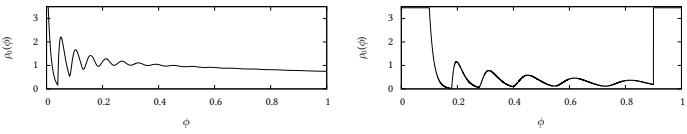

Figure 3.26: Stationary solutions of the continuum model with sparse connectivity ($m = 15$) for IF oscillators determined numerically by shooting. Left: $(a, b, \tau, \vartheta) = (0.04, 0.04, 0.0, 0.0)$, right: $(a, b, \tau, \vartheta) = (0.2, 0.1, 0.1, 0.2)$.

also be positive as the only negative term in Eq. (3.44) scales with $\rho(\phi, t)$. The continuity equation in the stationary case states that the flux is constant in ϕ and we have $J(0) = J(1)$ for $\rho(\phi; u_0, \lambda)$. As our main assumption for deriving boundary conditions is continuity of the flux, it is thus also clear that the solution $\rho(\phi; u_0, \lambda)$ fulfills the boundary condition at the firing threshold. As all firing oscillators are reinjected at phase $\phi = 0$, we have $J(0) = J(1) = \lambda/m$. As we do not consider excitations past the firing threshold, we have $\rho(0) = J(0)$.We can thus conclude that if we choose initial state u_0 and excitation rate λ such that $u_0 m = \lambda$, then solutions will fulfill our assumptions for the firing rate Eq. (3.38). We are left with one degree of freedom given by λ which has to be chosen in such a way that the solution $\rho(\phi; \lambda/m, \lambda)$ is normalized. We will use the following definition:

$$I(\lambda) = \int_0^1 \rho(\phi; \frac{\lambda}{m}, \lambda) d\phi \tag{3.45}$$

The shooting approach now consists of starting with some initial value, and calculating $I(\lambda)$ in a iterative fashion with the goal to determine the value at which $I(\lambda)$ takes a value of 1. The approach thus depends highly on a continuous dependence on parameters of the solution $\rho(\phi; \lambda/m, \lambda)$, which is provided for delay differential equations as ours which are defined by Lipschitz continuous functions [105]. In Figure 3.26 we show solutions which we obtained with the described shooting approach for different parameters.

Uniqueness and Existence of stationary solutions can be related to properties of the function $I(\lambda)$. Monotonicity of $I(\lambda)$ is a sufficient requirement for stationary solutions to be unique. Moreover, any $\lambda' > 0$ with $I(\lambda') > 1$ means that a solution of $I(\lambda) = 1$ exists as $I(0) = 0$ and as $I(\lambda)$ depends continuously on λ.

Let us first consider $\lim_{\lambda \to \infty} I(\lambda)$. For large excitation rates λ an oscillator with phase ϕ will be excited immediately without any time for convections. Its phase value will thus instantly jump to $R(\phi), R(R(\phi))$, etc. until it leaves the unit inter-

val. Consider now that a flux λ/m injected at $\phi = 0$. The oscillators will traverse the interval $[0, \vartheta-\tau]$ with velocity 1 as the phase response vanishes here. Starting from $\phi = \vartheta-\tau$ oscillators receive excitations and the fraction of oscillators which received no excitation decays as the following function $f(\phi;\lambda) := \lambda/me^{-\lambda(\phi-\vartheta+\tau)}$. Note that the integral of $f(\phi;\lambda)$ is $1/m$, independently of λ and $f(\phi;\lambda)$ concentrates to $\phi = \vartheta-\tau$ for large λ. In other words $f(\phi;\lambda)$ converges to $1/m\delta(\phi-\vartheta+\tau)$. Analogously, we obtain δ-peaks at phases which correspond to $1, 2, \ldots$ excitations, until the oscillators reach $\phi = 1-\tau$. Every of these phases gives a contribution of $1/m$ to $I(\lambda)$. For large λ we can thus describe $I(\lambda)$ by counting the number of iterations of $R(\phi)$ that fit into $[\vartheta-\tau, 1-\tau]$ and add the constant behavior during the refractory periods:

$$I(\lambda) \approx \frac{\max_i \left\{R^{(i)}(\vartheta-\tau) < 1-\tau\right\}}{m} + \vartheta\frac{\lambda}{m}. \tag{3.46}$$

This expression diverges for $\vartheta > 0$, which implies that stationary solutions exist for this case. However, for $\vartheta = 0$ the expression converges to

$$I(\infty) = \frac{\max_i \left\{R^{(i)}(0) < 1\right\}}{m}, \tag{3.47}$$

which depending on m may be below 1 such that we have no guaranee for a solution in this case. Note, that we have stationary solutions for every value of λ because $\rho(\phi;\lambda/m,\lambda)$ can always be interpreted as a stationary solution if we choose the right value for m. Assume, we have $\rho(\phi;\lambda_1/m,\lambda_1)$ with some value for $I(\lambda_1)$. We can choose as parameter $m' := mI(\lambda_1)$ and $\rho(\phi;\lambda_1/',\lambda_1)$ and $\rho(\phi;\lambda_1,\lambda_1)$ will only differ in their normalization because ρ are solutions of a linear initial value problem and are thus also linear in their initial value, which we specified as second argument in the notation $\rho(\phi;u_0,\lambda)$. Moreover, we easily see that $\rho(\phi;\lambda_1/m',\lambda_1)$ is normalized to 1:

$$\int_0^1 \rho(\phi;\frac{\lambda}{m'},\lambda)d\phi = \frac{1}{I(\lambda_1)}\int_0^1 \rho(\phi;\frac{\lambda}{m},\lambda)d\phi = 1. \tag{3.48}$$

In Figure 3.27 we show stationary solutions with increasing mean degrees and firing rates which more and more approximate the menitoned sequence of δ-peaks that corresponds to $\lambda \to \infty$.

Using the stationary solution for diverging firing rate, we can argue that a unique solution cannot be expected for arbitrary phase response curves: For infinite excitation rate λ, $\rho(\phi;\infty/m,\infty)$ depends only on those values of Δ where

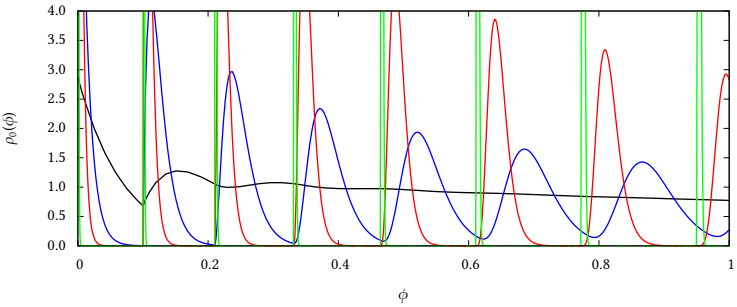

Figure 3.27: Stationary solutions of the continuum model with sparse connectivity for IF oscillators ($a = 0.1, b = 0.1$) and for $m = 5$ (black), $m = 7$ (blue), $m = 7.5$ (red), and $m = 8.0$ (green) as determined numerically by shooting.

$\rho(\phi; \infty/m, \infty)$ has δ-peaks. Even if we take large but finite values of λ, the solution will only depend on the values of $\Delta(\phi)$ in a finite number of regions around these δ-peaks which we can make arbitrary small. If we now consider any of stationary solutions (e.g. those in Figure 3.26), we can increase the PRC near $\phi = 0$ in a region which is so small that the stationary solution is nearly unchanged. Moreover, we can make the increase so drastic that a single excitation will remove an excited oscillator from the unit interval. In this case, the firing rate λ_0 and the norm $I(\lambda_0) = 1$ of the stationary solution are not changed, while in the limit $\lambda \to \infty$ only a single δ-peak at $\phi = 0$ remains and we thus have $\lim_{\lambda\to\infty} I(\lambda) = 1/m$. Also, we have $I(0) = 0$ such that we can chose λ_1 and λ_2 with $I(\lambda_1) = I(\lambda_2)$ by the intermediate value theorem. As before λ_1 and λ_2 correspond to stationary solutions for the right value of m such we have indeed more than one stationary solution for such a PRC. Altough the situation here is somewhat obscure, it is conceivable that multistability plays a role for less artificial PRCs which oscillate such that the frequency is slightly larger than the amplitude. In this case, the oscillations in solutions have a similar frequency as those in the PRC. Moreover as convection times also influence oscillations in solutions, we can tune the frequency in some range by changing the firing rate (see Figure 3.27).

Uniqueness

In the following, we will show that stationary solutions are unique for linear IF oscillators with arbitrary parameters $a, b > 0$ and $\tau < \vartheta < 1$. More generally, we will demonstrate that $I(\lambda)$ is monotoneously increasing for PRCs with $\Delta'(\phi) \geqslant -1$.

As the first step, we relate $I(\lambda)$ defined for some PRC to an exit time problem for the stochastic dynamics of single oscillators in Eq. (3.19). To this end, we consider the interval $(0, 1)$ to be open and with no oscillator in it at time t. If we now inject a constant flux $J(0)$, oscillators will traverse the interval and exit at $\phi = 1$ after some time which varies due to the stochastic nature of Eq. (3.19). We consider the distribution $P(t)$ of these exit times. The flux $J(1, t)$ will increase from $J(1, 0) = 0$ and eventually approach the injected amount $J(0)$, at which time the same amount of oscillators leave and exit the interval. If we inject $J(0) = \lambda/m$, then the number of oscillators which are in the interval at a large time t, is given by $I(\lambda)$ as defined in Eq. (3.45) and can be expressed by integrating over the difference of incoming and outgoing fluxes:

$$I(\lambda) = \int_0^\infty J(0) - J(1, t)dt = \int_0^\infty \frac{\lambda}{m} - J(1, t)dt. \tag{3.49}$$

Given the distribution of exit times $P(t)$, we can express the outgoing flux by integrating over the time t_0 at which the oscillators were injected into the interval

$$I(\lambda) = \lim_{\kappa\to\infty} \int_0^\kappa \frac{\lambda}{m} - J(1, t)dt = \lim_{\kappa\to\infty} \int_0^\infty dt \int_0^t dt_0 \left[\frac{\lambda}{m} - P(t - t_0)\frac{\lambda}{m}\right]. \tag{3.50}$$

The domain of the second integral is the area of the quadrant $(t_0, t) \in [0, \infty] \times [0, \infty]$ which lies above the diagonal. If we parameterize this domain by $u := t - t_0$ and t_0, we obtain, using substitution for multiple variables,

$$I(\lambda) = \lim_{\kappa\to\infty} \int_0^\infty du \int_0^{\kappa-u} dt_0 \left[\frac{\lambda}{m}(1 - P(u))\right] = \frac{\lambda}{m} \int_0^\infty du \left[1 - (1 - u)P(u)\right]. \tag{3.51}$$

As every oscillator eventually reaches $\phi = 1$, we have $\int_0^\infty P(u)du = 1$, and we obtain a surprisingly simple relationship, which says that the norm of $I(\lambda)$ is given by the product of the injected flux and the mean exit time.

$$I(\lambda) = \frac{\lambda}{m} \int_0^\infty uP(u)du \tag{3.52}$$

For inhibitory PRCs, the mean exit time obviously increases with λ and $I(\lambda)$ is

monotonously increasing as desired. Let us compare the exit times of the oscillators subject to Poissonian noise with the naive approximation in which we consider an effective velocity of $v(\phi) = 1 + \lambda\Delta(\phi)$. The resulting approximation is $I(\lambda) \approx \lambda/m \int_0^1 1/v(\phi)d\phi$. Compared to the exit times as described by Eq. (3.54), the approximation does not account for the fact that when $\Delta(\phi)$ has large values for some phase, silghtly larger phases are likely to be jumped over by oscillators. The effective velocity $v(\phi)$ does not account for the probability that an oscillator which starts at $\phi = 0$ actually reaches phase ϕ. Note that the probability for an oscillator to reach a certain phase ϕ again is proportional to the stationary solutions (see Figure 3.26) and may show large fluctuations.

Let us represent Eq. (3.52) by an integral equation. We define $M(\varphi)$ as the mean time an oscillator with phase $1 - \varphi$ driven by its intrinsic dynamics and Poissonian excitations (Eq. (3.19)) remains in the unit interval before it reaches $\phi = 1$. The mean exit time for the entire interval then is $M(1)$, while we define $M(\varphi) = 0$ for $\varphi < 0$. $M(\varphi)$ can now be expressed by an average over the time of its next excitation. Assuming an exponential distribution $w(t) := \lambda e^{-\lambda t}$ for the times between excitations, we can relate these times to probabilities. For the case that the oscillator receives an exitation at time $1 - \varphi'$, it has a phase of $1 - \varphi + t + \Delta(t)$ afterwards. The mean time the oscillator needs to travers the remaining phase distance (from $1 - \varphi + t + \Delta(t)$ to 1) can again be expressed by $M(\varphi)$ which results in the following integral equation for $M(\varphi)$:

$$M(\varphi) = (1 - \int_0^\varphi w(t)dt)\varphi + \int_0^\varphi w(\varphi - t)\Big[(\varphi - t) + M(t - \Delta(1 - t))\Big]dt. \tag{3.53}$$

Here the first term corresponds to the situation, that the oscillator does not receive another excitation before leaving the unit interval. Inserting $w(t)$, we obtain:

$$M(\varphi) = \frac{1 - e^{-\lambda\varphi}}{\lambda} + \int_0^\varphi \lambda e^{-\lambda(\varphi - t)} M(t - \Delta(1 - t))dt. \tag{3.54}$$

Multiplying Eq. (3.54) by λ/m, we obtain for $I(\lambda, \varphi) := \int_0^\varphi \rho(\phi; \lambda/m, \lambda)$ a similar equation which we define as generalization of $I(\lambda)$ such that $I(\lambda, 1) = I(\lambda)$:

$$I(\lambda, \varphi) = \frac{1 - e^{-\lambda\varphi}}{m} + \int_0^\varphi \lambda e^{-\lambda(\varphi - t)} I(\lambda, t - \Delta(1 - t))dt. \tag{3.55}$$

The equation is a Volterra integral equation of second kind. Its solution depends on the boundary condition that $I(\lambda, \varphi) = 0$ for $\varphi < 0$ which means that oscillators which are already past the boundary at $\phi = 1$ have no contribution to the mean

exit time. As the kernel $\lambda e^{-\lambda(\varphi-t)}$ is conitunuous, so is the solution $I(\lambda,\varphi)$ in the second argument. Note that for constant phase responses (non-leaky oscillators), Eq. (3.55) can be solved analytically using the Laplace transform.

Finally, we can demonstrate that $I(\lambda)$ is strictly increasing in λ for PRCs with $\partial_\phi \Delta(\phi) \geqslant -1$. For convenience, we will use the abbreviations $G(\lambda,\varphi) := (1 - e^{-\lambda\varphi})/m$, $H(\lambda,u) := \lambda e^{-\lambda u}$, and $z(\varphi,u) := \varphi + u - \Delta(1-\varphi-u)$. $G(\lambda,\varphi)$ is strictly increasing in both arguments. Using our assumption about the PRC, we see that $z(\varphi,u)$ is increasing in both arguments but not necessarily strictly increasing. Eq. (3.55) takes the following form:

$$I(\lambda,\varphi) = G(\lambda,\varphi) + \int_0^\infty H(\lambda,u) I(\lambda, z(\varphi,-u)) du. \tag{3.56}$$

Note that we have extended the integral from φ to ∞ using $I(\lambda,\varphi) = 0$ for $\varphi < 0$.

We will first argue that $I(\lambda,\varphi)$ is monotoneously increasing in its 2nd argument for every $\lambda > 0$. Assume this were not the case. As $I(\lambda,\varphi)$ is continuous in its 2nd argument, we can choose φ_0 such that $I(\lambda,\varphi)$ is increasing up to φ_0 and such that φ_0 is the largest number with this property. Moreover, we choose $\varphi_1 > \varphi_0$ silghtly larger, such that $I(\lambda,\varphi_0)$ decreases in $[\varphi_0,\varphi_1]$ and such that the falling slope in $[\varphi_0,\varphi_1]$ has arbitrary small integral. Let us compare $I(\lambda,\varphi_0)$ and $I(\lambda,\varphi_1)$ as determined by the R.H.S. of Eq. (3.56). $G(\lambda,\varphi)$ is strictly increasing in φ. $I(\lambda, z(\varphi,-u))$ as function of φ is a composition of two increasing functions and therefore itself increasing up to φ_0. Moreover, the interval $[\rho_0,\rho_1]$ yields an arbitrary small contribution to the integral. We can deduce that $I(\lambda,\varphi_1) > I(\lambda,\varphi_0)$ which is in contradiction to the assumed maximality of ρ_0. Therefore, $I(\lambda,\varphi)$ must be increasing in its 2nd argument. Using Eq. (3.56), we calculate the derivative of $I(\lambda,\varphi)$:

$$\partial_\lambda I(\lambda,\varphi) = \partial_\lambda G(\lambda,\varphi) + \int_0^\infty I(\lambda, z(\varphi,-u)) \partial_\lambda H(\lambda,u) + \int_0^\infty H(\lambda,u) \partial_\lambda I(\lambda, z(\varphi,-u)) du. \tag{3.57}$$

The first term of the R.H.S. of Eq. (3.57) is positive as $G(\lambda,\varphi)$ is increasing in its first argument. For the second term, we use the functional form of $H(\lambda,u)$. Using $\partial_\lambda H(\lambda,u) = \partial_\lambda \lambda e^{-\lambda u} = \partial_u (u e^{-\lambda u})$ and integrating by parts, we obtain a positive contribution for the second term as I and z are increasing in their 2nd arguments. We now fix λ and show analogous as before that $\partial_\lambda I(\lambda,\varphi)$ is increasing in φ. As $\partial_\lambda(I(\lambda,0)) = 0$, we can thus conclude that $\partial_\lambda I(\lambda,1) > 0$ as desired.

As the PRC of linear IF oscillators with time delay τ and refractory periods ϑ satisfies the assumption that we made ($\Delta'(\phi) \geqslant -1$), we have unique stationary

solutions for the case we are interested in. We continue with a discussion of the existence of these stationary solutions.

Existence

As $I(\lambda)$ is strictly increasing for linear IF oscillators, we only have to investigate the limit of large excitations rates $I(\infty)$ to determine existence of solutions. Solutions exist if $I(\infty)$ exceeds 1. If $I(\infty)$ is below 1, then $I(\lambda)$ stays below 1 for arbitrary excitation rates $\lambda \in [0, \infty)$. We already characterized $I(\infty)$. For oscillators with refractory periods, $I(\infty)$ diverges and we thus have stationary solutions for every set of the other parameters $a, b, m > 0$ and $\tau < \vartheta$. For oscillators without refractory periods, we use the formula in Eq. (3.31) and obtain the following condition:

$$1 < \frac{\max_i\{R^{(i)}(0) < 1\}}{m}. \tag{3.58}$$

In Figure 3.28, we show the firing rate of solutions in dependence on parameters a, b and m of linear IF oscillators obtained by shooting. For large coupling strengths (above the red lines given by $I(\infty) = 1$), no solutions could be obtained. If we approach the boundary at which stationary solutions become impossible, the firing rate diverges. In Figure 3.29, we show firing rates for those oscillators. In contrast to the case without time delay, we observe that solutions have a bounded firing rate, which is in agreement with the observation that oscillators with refractory periods ϑ have a maximum fire frequency of $1/\vartheta$.

Time-dependent Solutions

To obtain numerical solutions for the time-dependent case, the partial differential equation (PDE) for the continuum model with sparse connectivity (Eq. (3.37)) can be approximated by a system of ordinary differential equations, which then can be solved with standard algorithms. Due to the non-linear and complicated boundary condition, it is difficult to apply spectral methods, in which the solution is expressed in some function space basis. Such methods would rely on a function basis which fulfills the boundary condition.

Instead we pursue a finite difference approach in which the continuous phase variable ϕ is replaced by a grid with a constant tightness of $\Delta x = 1/B$. We intent to obtain approximations for $\rho(\phi, t)$ at the phases of the B grid points. The evolution equations for $\{\rho_i | i = 1, \dots, B\}$ will form a coupled system of ordinary differential equations. We define $A_i := [i/B, (i+1)/B]$ and interpret ρ_i as an ap-

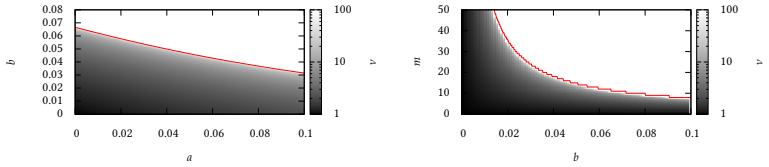

Figure 3.28: Firing rate of normalized stationary solutions of Eqs. (3.41)–(3.43) for $\tau = \vartheta = 0$ as determined by shooting. White points indicate parameter combinations for which no normalized stationary solution could be obtained. Left: dependence on oscillator parameters a and b for $m = 15$. Right: dependence on the mean degree m and on b, for $a = b$. The red line indicates the boundary up to which solutions can be obtained, given by Eq. (3.58).

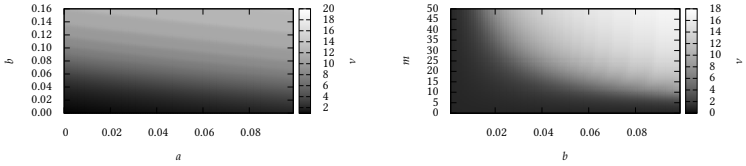

Figure 3.29: Same as Figure 3.28 but for oscillators with time delays and refractory periods ($\tau = 0.01, \vartheta = 0.05$).

proximation of the values of ρ in the interval A_i:

$$\rho_i(t) \approx \int_{A_i} \rho(\phi, t) dt. \tag{3.59}$$

The discretization of the terms in the partial differential equation in Eq. (3.37) is standard with the exception of the state-dependent non-local term. In fact, we are not aware of any study in which such terms have been discretize. The 2nd term on the r.h.s. of Eq. (3.37) is easily aprroximated by $\lambda(t)\rho_i$. There are different possibilities, in which way the derivatives of the first term can be estimated, which differ in the numerical stability of the resulting ODE system. Approximations are denoted as first-order if the differential equation for some bin depends only on two bin counts, of its own bin or of neighboring bins. Under

this restriction, we still have different possibilities to estimate the slope of $\rho(\phi)$ locally:

forward/downwind $\partial_\phi \rho(\phi) \approx (\rho_{i+1} - \rho_i)/\Delta x$,

backward/upwind $\partial_\phi \rho(\phi) \approx (\rho_i - \rho_{i-1})/\Delta x$,

centered $\partial_\phi \rho(\phi) \approx (\rho_{i+1} - \rho_{i-1})/2\Delta x$.

The convection term transport a wave train to larger phases without change to the shape. Intuitively, the time evolution at some bin ρ_i thus must depend on ρ_{i-1} rather than on ρ_{i+1}, as the same amplitude of the wave first appears in ρ_{i-1} and then in ρ_i. Therefore, the upwind scheme in which $\partial_t \rho_i$ depends on ρ_i and ρ_{i-1} seems a good choice. In fact both the forward and the centered scheme are unconditionally unstable for explicit integration methods, i.e. the integration diverges for arbitrary small step sizes. They can, however, be applied when using implicit integration algorithms. To allow for a fast numerical integration with explicit methods, we used backward schemes for all our computations. Two main influences of error are introduced due to discretization. For one, discretized systems may show numerical dispersion and spurious oscillations. Additionally, discretized systems show some amount of diffusion even if no diffusion was present in the continuous system [106]. As our primary interest is synchronization, we have to be aware of this influence as it is plausible that asynchronous solutions are stabilized by this diffusion term. However, both errors can be controlled by increasing the tightness of the discretization grid.

For the third term on the r.h.s. of Eq. (3.37), we aim – with a view on a bifurcation analysis –at an discretization such that the time derivative of each bin ρ_i depends continuously on both parameters a and b. It is therefore not sufficient to round and associate the oscillators in an entire bins with oscillators in an origin bin. Instead, we have to account for the case that the oscillators of some origin bin are distributed along various destination bins. We will account for this in the following computation in which we denote with $\partial_t \rho_i^D(t)$ the contribution to $\partial_t \rho_i$ of the delay term. Denoting with X_A the function which takes a value of 1 for phases in A and 0 otherwise, we can define an orthogonal finite basis with $a_i(\phi) = X_{A_i}/B$. Using this basis, we can express Eq. (3.59) as a projection: $\rho_i = \langle a_i, \rho \rangle$. We obtain for the contribution of the non-local term in Eq. (3.37)

$$\partial_t \rho_i^D(t) = \lambda(t) \left\langle \sum_{j \in I_\phi} \frac{\rho(R_i^{-1}(\phi), t)}{1 + \Delta'(R_i^{-1}(\phi))}, a_i \right\rangle = \frac{\lambda(t)}{B} \sum_{j \in I_\phi} \int_{A_i} \frac{\rho(R^{-1}(\phi))}{R'(R^{-1}(\phi))} d\phi \tag{3.60}$$

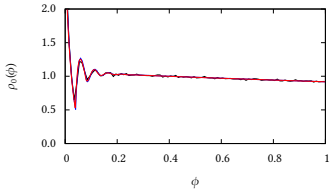

Figure 3.30: Stationary solution $\rho_0(\phi)$ for sparse networks ($m = 15$) of linear IF oscillators ($a = 0.01, b = 0.04$) obtained by shooting (blau), together with the obtained distribution after transients of finite difference approximations to 1000 dimensions (red) and of synaptic failure networks of 10^6 oscillators (black).

Applying the rule of substitution and approximating $X_{R^{-1}}(A_i)$ in the basis a_i we obtain

$$\begin{aligned} \partial_t \rho_i^D(t) &\approx \frac{\lambda(t)}{B} \sum_{j\in I_\phi} \int_{R^{-1}(A_i)} \rho(\phi) d\phi = \frac{\lambda(t)}{B} \sum_{j\in I_\phi} \int \rho(\phi) \chi_{R^{-1}(A_i)} d\phi \\ &= \sum_{j\in I_\phi} \frac{\lambda(t)}{B} \int \rho(\phi) \sum_k \left\langle a_k, \chi_{R^{-1}(A_i)} \right\rangle a_k(\phi) d\phi \\ &= \sum_{j\in I_\phi} \sum_k \rho_k \frac{\lambda(t)}{B^2} \mu(A_k \cap R^{-1}(A_i)). \end{aligned} \tag{3.61}$$

Here, we have denoted with μ a one-dimensional volume measure. For linear IF oscillators, the term leads to many case distinctions. However, the term depends continuously on the model parameters a and b as required. The treatment of the integrals in the firing rate and in the non-linear boundary condition is straightforward. To validate the discretization, we choose oscillator parameters for which stationary solutions are stable. We can then compare the distribution after transients, with results we obtain from the shooting approach (Chapter 3.4.1) or with the dynamics of synaptic failure networks (Chapter 3), which can be regarded as Monte-Carlo simulations. In Figure 3.30, we show such an comparison.

Stability

The finite difference approach allows us to probe the stability of the asynchronous solutions numerically. When we start with a phase distribution which differs from some asynchronous solution by a small localized perturbation, it may be the case that this perturbation either declines or increases with time. In the

latter case the asynchronous solutions are unstable and not observable. Stability can be studied in dependence of model parameters, and the critical parameters at which stability is lost can be characterized in terms of bifurcations, which allows one to explain and predict the dynamical behavior near the loss of stability. Bifurcation analysis is usually performed for finite dimensional systems of ordinary differential equations (ODE). One way to compute bifurcations of PDEs is to choose a discretization which approximates the PDE by a finite dimensional ODE (e.g. by a finite difference approach), which can then be analyzed with established numerical tools. In order for the results to be trustworthy, the bifurcation diagram has to *converge*, showing small differences only between higher dimensional discretizations. The asynchronous solution of the continuum model corresponds to a fixed point in the discretized ODE system. We can investigate the change of position of this fixed point in state space if we change model parameters, and more importantly, we can track the loss of stability. To assess the type of bifurcation the spectrum of the Jacobi matrix has to be computed. The Jacobi matrix is singular at the bifurcation point and the way in which one or more of its eigenvalues change sign at the bifurcation point determines the type of bifurcation. For details, we refer to reader to standard textbooks [107].

The prototypical bifurcation in the context of synchronization is the supercritical Andronov-Hopf bifurcation (AHB). The typical behavior at this bifurcation is that stability is lost, and near the bifurcation limit cycles are created which increase in amplitude with the distance to the bifurcation. Compared to, e.g., the saddle-node bifurcation, these limit cycles have arbitrary small amplitude near the bifurcation. This is the behavior that we observe for the discretizations and for synaptic failure networks with parameters near the lower boundary of the parameter region with asynchronous states (see Figures 3.31 and 3.17). As mentioned, discretization introduces numerical diffusion which can be expected to spuriously stabilize solutions and to enlarge the parameter regions which lead to asynchronous solutions. In contrast, finite size fluctuations of synaptic failure networks may allow the system to leave the basin of attraction of the asynchronous solution and thus diminish the parameter region in which they are prevalent.

To explain the loss of stability from an intuitive point of view, we consider a small perturbation localized in ϕ of the stationary solution. The phase of an oscillator represented by this perturbation is shifted to larger phase values due to its intrinsic dynamics and due to excitations, according to the stochastic differential equation given in Eq. (3.19). The uncertainty of the oscillator's phase after some time leads to a broadening of the perturbation and increases with the strength of excitations and thus with $|b|$ (and to some degree with a). When

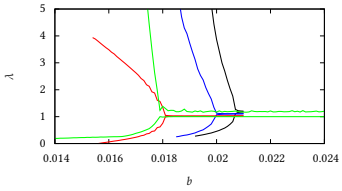

Figure 3.31: Largest and smallest value of the firing rate λ in the interval $t \in [100, 200]$ for the sparse continuum model ($m = 15$) of linear IF oscillators in dependence on the oscillator parameter b and for $a = 0.01$. Values were obtained by a finite difference approximations to 50 dimensions (red), to 100 dimensions (blue), to 1000 dimensions (black) and for synaptic failure networks (green) of 10^6 oscillators.

oscillators which are represented by the perturbation fire, positive values of a lead to a sharpening of the perturbation as oscillators receive larger excitations if they are close to the perturbation. As a consequence of both (sharpening and broadening), the perturbation either vanishes or increases steadily, depending on a and b. Provided that a influences the sharpening more strongly than the uncertainty of oscillators, we expect stable asynchronous states to be observable for large b and small a.

We will now return to the loss of stability of asynchronous states in synaptic failure networks. The continuum model allows us to explain the emergence of the boundaries of the parameter regime with asynchronous states (as presented in Figure 3.16). For large coupling strengths, stationary solutions do not exist. We have characterized the boundary at which they appear in Eq. (3.58). When they do exist, they may be either stable or unstable. Continuation of the stationary solution (via finite difference and AUTO) reveals a locus of AHB points. The Hopf points have a positive first Lyapunov coefficient, which implies that limit cycles are generated beyond the critical parameter at which stability is lost. This locus moves closer to the lower boundary of the parameter region with asynchronous solutions that we observe in synaptic failure networks.

Note that the states with recurring avalanches, that we described in 3.3 (see Figure 3.19) cannot be described with the framework so far. For avalanches, the firing rate as defined in Eq. (3.38) is negative and an integration in the same way as before would lead to phase distributions with negative values. However, it is probably possible to extend the model by defining the dynamics for the time

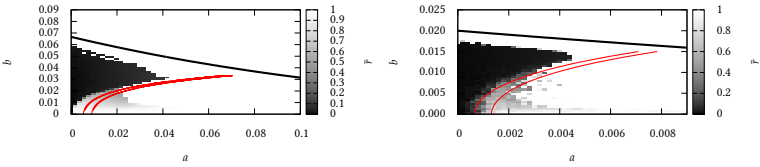

Figure 3.32: Mean Kuramoto's order parameter averaged over the time interval $t \in [100, 200]$ of synaptic failure networks ($N = 10000$) of linear IF oscillators for a mean degree of $m = 15$ (left) and $m = 50$ (right). The black line indicates the boundary up to which stationary solutions exist (according to Eq. (3.58)). The red line indicates the locus of supercritical AHB points obtained by AUTO via finite difference discretizations of the continuum model to 150 and 250 dimensions in the left plot and to 1000 and 2000 dimensions in the right plot.

intervals at which λ is infinite or negative. At the avalanche the distribution $\rho(\phi)$ is changed discontinuously. However, we can connect the discontinuity by a smooth change if we introduce an auxiliary time variable which increases linearly with firing oscillators. During the avalanche no time passes and convection plays no role. We could, therefore, assume for time of avalanches the differential equation in Eq. (3.37) without the convection term. After the avalanche the firing rate is again finite, and all oscillators that fired are injected as a δ-peak at $\phi = 0$. Note that we did not observe irregular behavior without avalanches. The equations of the continuum model are non-linear, and it is conceivable that it is able to produce chaotic dynamics for other parameter or PRCs. The dynamics of the states with recurring avalanches (Figure 3.19) do not decrease in irregularity even for larger network sizes (up to 10^7) and depend sensitive on initial conditions. It seems sensible to compare them to other chaotic behaviors that can be observed in PDEs. However, this point needs further investigations. The behavior at the upper boundary of the regime with asynchronous solutions is not related to a bifurcation in the strict sense. Asynchronous solutions become impossible due to diverging firing rates. Shortly below this divergence, they show large fluctuations and are therefore easily left due to finite size fluctuations which are seen in simulations of synaptic failure networks. Note that we find no correspondence in terms of bifurcations to the fine structure that we observed at the upper boundary (see Figure 3.13 and 3.16). Even for high dimensional discretizations ($N = 1000$) no loss of stability can be observed before the

divergence of the asynchronous solution.

3.4.2 Dense random networks

In this chapter, we will discuss the master equation for a continuum model of oscillators whose dynamics is described by the deterministic differential equation (3.23). The model is meant to describe the limit of both dense random and synaptic failure networks, as well as the dynamics for all-to-all coupling. The obtained equation has been investigated in [108] where the authors were able to describe the dynamical behavior for PRCs which are monotonous as being dichotomous: For increasing $\Delta(\phi)$ the probability density concentrates to a single phase in finite time for arbitrary initial distributions. In particular, partially synchronous states as in Figure 3.17 do not exist for dense connectivity. For decreasing $\Delta(\phi)$, solutions converge to the stationary solution, for initial conditions which do not immediately lead to avalanches. The excitatory linear IF oscillators that we study in this thesis, have a linearily increasing PRC and synchronize thus completely in the dense limit. Similar as in the sparse limit, stationary solutions exist for small coupling strengths. However, here they are unstable for arbitrary $a, b > 0$. In the following, we will derive the evolution equations for the continuum with dense connectivity and calculate the asynchronous solutions and the parameter regime in which they exist. Additionally, we provide a linear stability analysis which reproduces the results in [108] for the special case of linear IF oscillators and allows us to determine the stability when oscillators are endowed with time delays and refractory periods. The continuity equation which describes the macroscopic dynamics can be directly obtained from the deterministic motion of single units. We can however, also consider dense networks as limit of the continuum model for sparse networks which we described in the last chapter. We choose the latter as it illustrates what happens to solutions (and in particular to the bifurcation diagrams in Figure 3.32) for large m. Let m_i be a sequence of mean degrees such that $m_i \to \infty$ and let $\Delta_i(\phi)$ be a sequence of PRCs such that $\Delta_i(\phi)m_i$ converges to the limiting PRC $F(\phi)$. Furthermore, let $J_i(\phi, t)$ be the flux of the continuum with sparse connectivity as defined in Eq. (3.31) for the PRC $\Delta_i(\phi)$.

We define the dynamics of the continuum model with dense connectivity by assuming a probability flux $J(\phi, t)$ which is the limit of $J_i(\phi, t)$ for $i \to \infty$. Our assumptions for the sparse limit were continuity of the flux $J_i(\phi, t)$ and its definition as given in Eq. (3.31). The boundary conditions and the partial differential equation were derived from these assumptions. In a similar way all properties of this model will be deduced from the definition and the continuity of $J(\phi, t)$. The excitation rate for sparse connectivity is defined as $\lambda(t) = mJ_i(1, t)$. For dense connectivity ν diverges, and we will instead use the excitation rate $\nu(t) = J(1, t)$.

As the phase response curves $\Delta_i(\phi)$ vanish in this limit, the sets $I_{\rightarrow}(\phi)$ and $I_{\leftarrow}(\phi)$ only contain elements in close proximity to ϕ, so that we can, for large i, assume that the integrands in Eq. (3.31) are constant and we have:

$$J_i(\phi,t) \approx \rho(\phi,t) + \nu(t)\rho(\phi,t)\left(\left|I_{\rightarrow}(\phi)\right| - \left|I_{\leftarrow}(\phi)\right|\right). \tag{3.62}$$

When we exclude pathological examples of highly fluctuating PRCS, we can assume that in addition to $\Delta_i(\phi)$ also its derivative vanishes for $i \to \infty$. Under this assumption we have $R_i'(\phi) = 1 + \Delta_i'(\phi) \approx 1$, and $R(\phi)$ is monotonous, invertible and preserves distances between pairs of oscillators. If $\Delta_i(\phi)$ is positive (negative) the set $I_{\leftarrow}(\phi)$ ($I_{\rightarrow}(\phi)$) vanishes. The size of the other set can then be calculated as

$$\begin{aligned} |I_{\rightarrow}(\phi)| &= |\{\varphi < \phi | R(\varphi) \geqslant \phi\}| = \left|\{\varphi < \phi | \varphi \geqslant R^{-1}(\phi)\}\right| \\ &\approx |R^{-1}(\phi) - \phi| = |\phi - R(\phi)| = |\Delta(\phi)| \end{aligned} \tag{3.63}$$

.

Setting Eq. (3.63) into Eq. (3.62) we obtain

$$J_i(\phi,t) \approx \rho(\phi,t)\left(1 + J(1,t)m_i\Delta_i(\phi)\right) \tag{3.64}$$

which converges for $i \to \infty$ because of our assumptions on the PRCs to

$$\rho(\phi,t)\left(1 + J(1,t)F(\phi)\right) =: J(\phi,t). \tag{3.65}$$

The flux is given as the product of the density ρ and an effective oscillator velocity $v(\phi,t) := 1 + J(1,t)$ which accounts for the intrinsic dynamics and for excitations between oscillators. If we assume a firing rate of $\nu(t) = J(1,t)$ and evaluate the flux as defined in Eq. (3.65) at $\phi = 1$, we get the following equation for $\nu(t)$:

$$\nu(t) = J(1,t) = \rho(1,t)\left(1 + F(\phi)J(1,t)\right) \to \nu(t) = \frac{\rho(1,t)}{1 - F(1)\rho(1,t)}. \tag{3.66}$$

The continuity equation which corresponds to the flux in Eq. (3.65) takes the following form:

$$\partial_t\rho(\phi,t) = -\partial_\phi\left[\left(1 + F(\phi)\frac{\rho(1,t)}{1 - F(1)\rho(1,tf)}\right)\rho(\phi,t)\right]. \tag{3.67}$$

We focus our investigations on oscillators for which excitations are limited to the firing threshold. Note, that the slope of -1 ending in $\phi = 1$, which is present in $\Delta_i(\phi)$ will usually not be present in the limit $F(\phi)$ as the excitation strength vanishes. For example, if we chose an function $F(\phi)$, rescale it to the mean degree

and limit it to the firing threshold $\Delta_i(\phi) = \min\left\{F(\phi)/m_i, 1-\phi\right\}$ then the product $\Delta_i(\phi)m_i$ will converge pointwise to the function $F(\phi)$:

$$\Delta_i(\phi)m_i = \min\{\Delta(\phi), m_i(1-\phi)\} \to F(\phi). \tag{3.68}$$

If the slope of -1 was present in $\Delta_i(\phi)$ in the sequence, then we have a value $F(1) \neq 0$ in the dense limit. Analogously as for sparse connectivity, this can give rise to diverging firing rates and avalanches if $F(1)\rho(1) \geqslant 1$.

As in the case for the sparse limit, we deduce boundary conditions from the continuity of the flux $J(\phi, t)$; for phase response curves $F(\phi)$ with a discontinuity at some $\phi = \varphi$, continuity leads to a jump at $\phi = \varphi$ in the phase distribution $\rho(\phi, t)$:

$$J(\varphi^+, t) = \rho(\varphi^+, t)\left(1 + F(\varphi^+)\nu(t)\right) = \rho(\varphi, t)\left(1 + F(\varphi)\nu(t)\right) = J(\varphi, t). \tag{3.69}$$

This equation reflects the fact that if the convection velocity is abruptly increased, than the density of oscillators will be stretched proportionally to the velocity. For absorbing oscillators we have $F(0) = 0 \neq F(1)$ such that we obtain for $\varphi = 1$ from Eq. (3.69)

$$\rho(0, t)\left(1 + F(0)\nu(t)\right) = \rho(1, t)\left(1 + F(1)\nu(t)\right). \tag{3.70}$$

which using the definition of $\nu(t)$ in Eq. (3.66) simplifies to:

$$\rho(0, t) = \frac{\rho(1, t)}{1 + \rho(1, t)\left(F(0) - F(1)\right)}. \tag{3.71}$$

Eqs. (3.70) and Eq. (3.67) define the continuum model in the sparse limit. It may seem surprising that we can investigate synchronization even with this simple equation. Note that a non-trivial evolution depends crucially on the intrinsic motion of oscillators. In fact, if we leave the 1 in Eq. (3.67) out, the oscillator velocity decomposes into a product by factors which depend on t or ϕ only. We can then get rid of both by a transformation of t and ρ and obtain trivial convection with no change of the shape of the distribution.

Stationary solutions

In contrast to the continuum model with sparse connectivity, we can easily express the stationary solutions analytically if we set $0 = \partial_t \rho_0(\phi)$ in Eq. (3.67):

$$\rho_0(\phi) = \frac{c}{1 + F(\phi)\nu} \tag{3.72}$$

Here, c is an integration constant, which has to be chosen such that $\rho_0(\phi)$ is normalized. Evaluating ρ_0 at $\phi = 1$ and compairing with Eq. (3.66) yields $\nu = c$. If we define $I(\nu)$ as

$$I(\nu) = \int_0^1 \frac{\nu}{1 + F(\phi)\nu} d\phi, \tag{3.73}$$

we have to chose a positive firing rate ν such that $I(\nu) = 1$. If such a choice is not possible, than the continuum model does not have a stationary solution. Note that $I(\nu)$ is defined in analogy to Eq. (3.45) for the case of sparse connectivity. Similar as there, we here also relate uniqueness and existence of stationary solutions to $I(\nu)$. There exist at most one choice for ν which fulfulls $I(\nu) = 1$ as $I(\nu)$ depends monotonously on ν which can be seen by the following calculation:

$$\partial_\nu I(\nu) = \int_0^1 \frac{1}{1 + F(\phi)\nu} - \frac{\nu F(\phi)}{(1 + F(\phi)\nu)^2} d\phi = \int_0^1 \frac{1}{(1 + F(\phi)\nu)^2} d\phi > 0. \tag{3.74}$$

However, depending on $F(\phi)$ the continuum model with dense connectivity may not have an acceptable stationary solution. Before performing a stability analysis for the stationary solution, we will bring Eq. (3.67) into a slightly simpler form:

$$\partial_t \rho(\phi, t) = \frac{1}{1 - F(1)\rho(1, t)} - \partial_\phi \left[\Big(1 - F(1)\rho(1, t) + F(\phi)\rho(1, t) \Big) \rho(\phi, t) \right]. \tag{3.75}$$

Note that the factor which now appears at the beginning of the right side of Eq. (3.75) just corresponds to a transformation of the time t. It does not influence the distribution of phases that are obtained in solutions $\rho(\phi, t)$ of Eq. (3.75), only the times t at which they appear. We can get rid of the factor by going over to $\tilde{\rho}(\phi, t) = \rho(\phi, \int_{t_0}^{t} 1 - F(1)\rho(1.t)dt)$. As the integrand is always positive for physical relevant solutions, this defines a one-to-one relationship. If $\rho(\phi, t)$ is a solution of Eq. (3.76) then the so defined $\tilde{\rho}$ will be a solution of the simpler equation:

$$\partial_t \rho(\phi, t) = -\partial_\phi \left[\Big(1 + \rho(1, t)(F(\phi) - F(1)) \Big) \rho(\phi, t) \right]. \tag{3.76}$$

We will omit the ˜ in the following and use $\bar{F}(\phi) := F(\phi) - F(1)$ for ease of notation.The stationary solution of the simplified equation read:

$$\rho_0(\phi) = \frac{\nu}{1 + \nu \bar{F}(\phi)}. \tag{3.77}$$

Again, we define ν by requiring that ρ_0 has an integral of 1. Note that Eq. (3.77) is in fact identical to Eq. (3.72). Our transformation of time changes the firing rate and thus the normalization factor, not the spatial form.

Linear Stability Analysis

To determine the stability of the stationary solution, we consider a small, arbitrary variation $\eta(\phi, t)$ around the stationary solution $\rho(\phi, t) = \rho_0(\phi) + \eta(\phi, t)$. From the partial differential equation which describes the evolution of $\rho(\phi, t)$ (Eq. (3.76)), we intent to obtain a similar evolution equation for the variation $\eta(\phi, t)$, which is linear. The approximation will thus only hold for small variations. In return, we obtain a simpler problem which can be solved by methods from linear algebra:

$$\partial_t \rho(\phi, t) = \partial_t(\eta(\phi, t)) = -\partial_\phi \left[\left(1 + \bar{F}(\phi)\left(\rho_0(1) + \eta(1, t)\right)\right)\left(\rho_0(\phi) + \eta(\phi, t)\right)\right]. \quad (3.78)$$

Using the stationarity of $\rho_0(\phi)$ and neglecting terms which are quadratic in η (e.g.: $\eta(\phi, t)\eta(1, t)$) we get:

$$\partial_t \eta(\phi, t) = -\partial_\phi \left[\left(1 + \nu\bar{F}(\phi)\right)\eta(\phi, t) + \eta(1)\frac{\nu\bar{F}(\phi)}{1 + \nu\bar{F}(\phi)}\right]. \quad (3.79)$$

From the boundary condition for ρ in Eq. (3.69), we derive the corresponding boundary condition for the perturbation:

$$\left(\rho_0(\varphi^+) + \eta(\varphi^+, t)\right)\left[1 + \bar{F}(\varphi^+)\left(\nu + \eta(1, t)\right)\right] = \left(\nu + \eta(\varphi, t)\right)\left[1 + \bar{F}(\varphi)\left(\rho_0(1) + \eta(1, t)\right)\right]. \quad (3.80)$$

The boundary condition also needs to be linearized. We thus ignore terms which are quadratic in η, subtract Eq. (3.69) and replace all occurences of $\rho_0(\phi)$ by the expression in Eq. (3.77):

$$\eta(\varphi^+, t) = \frac{1 + \bar{F}(\varphi)\nu}{1 + \bar{F}(\varphi^+)\nu}\left[\eta(\varphi, t) + \nu\eta(1, t)\frac{\bar{F}(\varphi) - \bar{F}(\varphi^+)}{\left(1 + \nu\bar{F}(\varphi^+)\right)\left(1 + \nu\bar{F}(\varphi)\right)^2}\right] \quad (3.81)$$

Note that the size of the jump at some phase $\varphi \neq 1$ depends on $\varphi(1)$, which was not the case for jumps in the phase density. Applying this equation to the firing threshold ($\varphi = 1$), Eq. (3.81) simplifies to:

$$\eta(0, t) = \frac{\eta(1, t)}{\left(1 + \nu\bar{F}(0)\right)^2}. \quad (3.82)$$

The boundary value problem defined by Eqs. (3.79), (3.81), and (3.82)) is linear and determines the time evolution of the variation $\eta(\phi, t)$. In contrast to $\rho(\phi, t)$, however, we do not expect the norm $\int_0^1 \eta(\phi, t) d\phi$ to be constant with time. The stationary solution is stable if all functions $\eta(\phi, t)$ vanish over time. Note that Eq. (3.79) is again a contininuity equation, however the boundary conditions are not defined as to guarantee conservation flux. We will denote the linear differential operator at the right side of Eq. (3.79) as L. As the defining equation for its eigenfunctios is a ordinary differential equation of 1st order, we have one degree of freedom. However, as we are only interested in functions which satisfy the boundary conditions, we have to choose the solution accordingly and can expect the eigenvalues spectrum of L to be discrete. Let $\alpha_j(\phi)$ and be a complete set of its eigenfunctions with corresponding eigenvalues λ_j. We can thus express an initial variation $\eta_0(\phi) := \eta(\phi, 0)$ in terms of its eigenfunctions $\eta_0(\phi) = \sum_i \alpha_j(\phi)$. The time evolution can then be expressed as

$$\eta(\phi, t) = \sum_i \alpha_j(\phi) e^{\lambda_j t}. \tag{3.83}$$

A variation vanishes over time only if all eigenfunctions, which appear in its expansion have eigenvalue with negative real part. We thus have in this way expressed the stability of the stationary solution by a condition on the spectrum of L. A stationary solution is stable for all variations iff all eigenvalues of L have negative real part. The defining differential equation for the eigenfunctions can be simplified to

$$\alpha_j'(\phi) + \alpha_j(\phi) \frac{\lambda_j + cF'(\phi)}{1 + \nu \bar{F}(\phi)} + \alpha(1) \frac{\nu F'(\phi)}{\left(1 + \nu \bar{F}(\phi)\right)^3} = 0 \tag{3.84}$$

and is a linear differential equation with varying coefficients and a function evaluation at $\phi = 1$. Its solution can be expressed by integrals using an integration factor, which for most choices of $\bar{F}(\phi)$ is unlikely to lead to analytic expressions. Intriguingly, for linear IF oscillators, we can perform the integrations analytically. We will drop the general approach at this point and discuss the dynamics for linear IF oscillators with PRC $F(\phi) = a\phi + b$.

Linear IF oscillators with refractory period and time delay

For the case of linear IF oscillators, we can determine the firing rate ν for the stationary solutions explicitly:

$$1 = \int_0^1 \frac{\nu}{1 + (a\phi + b)\nu} d\phi = \frac{1}{a} \ln\left(1 + (a\phi + b)\nu\right)\Big|_0^1 = \frac{1}{a} \ln\left(\frac{1 + (a + b)\nu}{1 + bc}\right). \quad (3.85)$$

Similar as in the continuum with sparse connectivity, asynchronous solutions exist for small coupling strength only. For large values of b, the firing rate ν as determined by Eq. (3.85)

$$\nu = \frac{e^a - 1}{a - b\,(e^a - 1)} \quad (3.86)$$

turns negative and the stationary solutions defy a stochastic interpretation. For the parameter regime we are considering ($a, b > 0$), Eq. (3.86) is positive if the parameters satisfy:

$$b < \frac{a}{e^a - 1}. \quad (3.87)$$

In Figure 3.33 right, we show the firing rates of the stationary solutions in dependence on a and b (cmp. Figure 3.28). Near this boundary in the (a, b)-plane at which solutions are lost, the firing rate diverges. In Figure 3.33 left, we show asynchronous solutions of the model with sparse connectivity together with their limit which is the asynchronous solution for dense connectivity. Note that solutions do not converge for $\phi = 0$ where we observe large excursions in $\rho(\phi)$ which increase in frequency with m. However, the phase interval around $\phi = 0$ with excursions shrinks for larger m.

We now investigate stability of the stationary solutions by calculating the spectrum of the linear operator L. Inserting the PRC $F(\phi) = a\phi + b$ of linear IF oscillators into the simplified equation (3.76), we get:

$$\partial_t \rho(\phi, t) = -\partial_\phi \left[\left(1 + a\left(\phi - 1\right)\rho(1, t)\right)\rho(\phi, t)\right] \quad (3.88)$$

This equation does not depend on b, and the stability of the asynchronous state obviously is only determined by the parameter a. For simplicity, we will use the parameter $\kappa = ca = 1 - e^{-a}$ for the following calculation of the linear stability problem. κ can again be interpreted as coupling strength, which is normalized in such a way that $\kappa = 0$ corresponds to no coupling and $\kappa \to 1$ corresponds to the limit of large a. The defining equation for the eigenfunctions (3.84) takes the

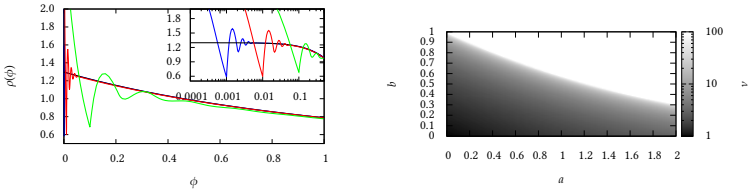

Figure 3.33: Left: Stationary solutions for the continuum model of linear IF oscillators with dense connectivity(Eq. (3.77), $a = b = 0.5$, black) and with sparse connectivity ($a = b = 0.5/m$ for $m = 500$ (blue), $m = 50$ (red) and $m = 5$ (green)). Right: firing rate $\nu(t)$ for stationary solutions of the dense connectivity in dependence on oscillator parameters a and b. Parameter for which no stationary solution exists, are marked in white.

following form:

$$\alpha_j'(\phi) + \alpha_j(\phi)\frac{\kappa + \lambda_j}{1 + \kappa(\phi - 1)} + \alpha_j(1)\frac{\kappa}{(1 + \kappa(\phi - 1))^3} = 0 \tag{3.89}$$

Let us first – as a simple check of consistency – consider the uncoupled case ($\kappa = 0$). From Eq. (3.89) we get $\alpha_j'(\phi) + \lambda_j\alpha_j(\phi) = 0$ which has $\alpha_j(\phi) = e^{\lambda_j\phi}$ as solution, which are either waves or exponential functions (depending on λ_j). The boundary condition, however, implies $1 = \alpha_j(0) = \alpha_j(1) = e^{\lambda_j}$, which means that the eigenvalues are of the form $\lambda_j = 2\pi\mathbb{Z}i$. The spectrum is thus purely imaginary, which reflects the marginal stability of solutions for the case without coupling.

We now calculate the eigenfunctions in Eq. (3.89) for $\kappa \neq 0$. The appearance of the evaluation of α at $\phi = 1$ can be removed by the substitution $\beta_j(\phi) = \frac{\alpha_j(\phi)}{\alpha_j(1)}$

$$\beta_j'(\phi) + \beta_j(\phi)\underbrace{\frac{\kappa + \lambda_j}{1 + \kappa(\phi - 1)}}_{G(\phi)} + \underbrace{\frac{\kappa}{(1 + \kappa(\phi - 1))^3}}_{H(\phi)} = 0. \tag{3.90}$$

We obtain a inhomogeneous linear differential equation of first order with varying coefficients $G(\phi)$ and $H(\phi)$. The solution can be expressed using an integrat-

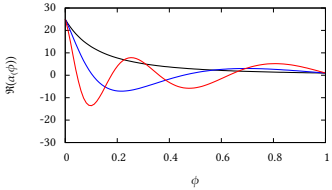

Figure 3.34: Real part of the eigenfunctions α_j of the linear stability problem for linear IF oscillators with $\kappa = a\nu = 0.8$ according to Eq. (3.93) for the three lowest eigenvalues (λ_0 (black), λ_1 (blue) and λ_2 (red)).

ing factor:

$$\beta_j(\phi) = \frac{\int H(\phi) e^{\int G(\phi)} + C}{e^{\int G(\phi)}}. \tag{3.91}$$

Fortunately, the integrals can be treated analytically in our case. A straightforward calculation yields

$$\beta_j(\phi) = \frac{C - \frac{\kappa}{\lambda_j - \kappa}\left(1 + \kappa\left(\phi - 1\right)\right)^{\frac{\lambda_j - \kappa}{\kappa}}}{\left(1 + \kappa\left(\phi - 1\right)\right)^{\frac{\lambda_j + \kappa}{\kappa}}}. \tag{3.92}$$

The integration constant C can be determined by setting $\beta_j(1) = 1$ which follows directly from our definition of β_j. We obtain $C = 1 + \frac{\kappa}{\lambda_j - \kappa}$. Using this value of C, $\beta_j(\phi)$ is a solution of the original equation Eq. (3.89), which is normalized in such a way that it takes a value of 1 at $\phi = 1$

$$\alpha_j(\phi) = \frac{1 - \frac{\kappa}{\lambda_j - \kappa}((1 + \kappa(\phi - 1)^{\frac{\lambda_j - \kappa}{\kappa}} - 1)}{(1 + \kappa(\phi - 1))^{\frac{\lambda_j + \kappa}{\kappa}}}. \tag{3.93}$$

For linear IF oscillators, the boundary condition for the variation in Eq. (3.82) takes the form:

$$\frac{\alpha_j(0)}{\alpha_j(1)} = \frac{1}{(1 - \kappa)^2} \tag{3.94}$$

Combining (3.94) and (3.93) we get the condition for the eigenvalues

$$\frac{1}{(1-\kappa)^2} = \frac{1 - \frac{\kappa}{\lambda_j - \kappa}((1-\kappa)^{\frac{\lambda_j-\kappa}{\kappa}} - 1)}{(1-\kappa)^{\frac{\lambda_j+\kappa}{\kappa}}} \tag{3.95}$$

which simplifies to

$$\frac{\kappa}{\kappa - \lambda_j}(e^{\ln(1-\kappa)\frac{\lambda_j-\kappa}{\kappa}} - 1) = (e^{\ln(1-\kappa)\frac{\lambda_j-\kappa}{\kappa}} - 1). \tag{3.96}$$

We can immediately read the solutions of this equation. For

$$\lambda_j = \kappa + i\frac{2\pi\kappa}{\ln(1-\kappa)}j, \quad j \in \mathbb{Z} \tag{3.97}$$

both sides vanish. Additionally for $\lambda = 0$ the factor at the front of the left side is 1 and we have equality. The zero eigenvalue can be related to the symmetry of the original problem which does allow for solutions with different integral. A speciality of the PRC we consider is that the real part is identical for all eigenvalues. An perturbation from the asynchronous solution will thus always increases with the same speed, independent on its shape.

For excitatory oscillators ($\kappa > 0$) we have eigenvalues with positive real part and the stationary solution is thus unstable even for arbitrary small coupling strength. In Figure 3.34, we show the real part of first three eigenfunctions as given in Eq. (3.93). These eigenfunctions present perturbations of the stationary solution which grow and reassume their shape after some time which is given by the imaginary part of the eigenvalue.

Linear IF oscillator with refractory periods and time delay

In the following, we will discuss the case of linear IF oscillators with time delays τ and refractory periods ϑ.

$$\partial_t \rho(\phi, t) = -\partial_\phi \left[\Big(1 + \rho(1)(F(\phi) - F(1))\Big)\rho(\phi, t)\right]. \tag{3.98}$$

Interpreting $\rho(\tau)$ as firing rate is only possible if oscillators are not excitable in the interval $\phi \in [0, \tau]$, such that solutions are only subject to convection in this interval and we have $\rho(\tau, t) = \rho(1, t-\tau)$. Again, we can only consider time delays which are shorter than refractory periods in this way.

In the following, we will discuss stability of asynchronous solutions of Eq. (3.98)

for PRCs $F(\phi)$ given by:

$$\bar{F}(\phi) = \begin{cases} 0 & 0 < \phi < \theta - \tau \\ a(\phi - \theta + \tau) + b & \theta - \tau < \phi < 1 - \tau \\ 0 & 1 - \tau < \phi < 1 \end{cases} \tag{3.99}$$

We will use the notations $V(\phi) = 1 + \nu\bar{F}(\phi)$ and $\phi_1 = \vartheta - \tau, \phi_2 = 1 - \tau$ in the following to keep formulas concise. Note that $V(\phi_1) = V(\phi_2^+) = 1$. With this definition Eq. (3.84) takes the form $\alpha_j'(\phi) + \alpha_j(\phi)\lambda_j$ for the intervals where $F(\phi)$ vanishes reads

$$\alpha_j'(\phi) + \alpha_j(\phi)\frac{\nu a + \lambda_j}{V(\phi)} + \alpha_j(1)\frac{\nu a}{V^3(\phi)} = 0 \tag{3.100}$$

otherwise. We have to solve each of the three parts seperately and choose parameters in such a way, that the function α_j solves the boundary condition for discontinuities in $F(\phi)$ in Eq. (3.81). The solutions in $[1-\tau, 1]$ and $[0, \vartheta - \tau]$ are exponential function, while the solution $[\vartheta - \tau, 1 - \tau]$ is obtained analogously as for the undelayed case (see Eq. (3.92). As the boundary value problem which defines $\alpha_j(\phi)$ is linear, we can choose a normalization $\alpha_j(\phi)$ by fixing $\alpha_j(\phi)$ at some phase. We choose $\alpha_j(1) = 1$, which simplifies Eq. (3.100) and allows us to express the solution in $[\vartheta - \tau, 1 - \tau]$ by

$$\alpha_j(\phi) = \frac{C - \frac{\nu a}{\lambda_j - \nu a} V(\phi)^{\frac{\lambda_j - \nu a}{\nu a}}}{V(\phi)^{\frac{\lambda_j + \nu a}{\nu a}}}. \tag{3.101}$$

Using the simple form of the solutions in $[0, \vartheta - \tau]$ and $[1-\tau, 1]$ and the boundary condition Eq. (3.81), we can calculate the values of of $\alpha(\phi_2)$ and $\alpha(\phi_1+)$:

$$\begin{aligned} \alpha_j(\phi_2) = &\quad \tfrac{1}{V(\phi_2)}\left[\alpha_j(\phi_2^+) + \alpha_j(1)\tfrac{1-V(\phi_2)}{V(\phi_2)}\right] = \alpha_j(1)\left[\tfrac{e^{\tau\lambda}}{V(\phi_2)} + \tfrac{1-V(\phi_2)}{V^2(\phi_2)}\right], \\ \alpha_j(\phi_1^+) = &\quad \tfrac{1}{V(\phi_1^+)}\left[\alpha_j(\phi_1) + \alpha_j(1)\tfrac{1-V(\phi_1^+)}{V(\phi_2^+)}\right] = \alpha_j(1)\left[\tfrac{e^{-(\vartheta-\tau)\lambda}}{V(\phi_1^+)} + \tfrac{1-V(\phi_1^+)}{V^2(\phi_1^+)}\right]. \end{aligned} \tag{3.102}$$

Enforcing these two relations on the solution for the interval $[\vartheta - \tau, 1 - \tau]$, allows us to eliminate C and finally determine the eigenvalues λ_j for which solutions are possible. Solving Eq. (3.93) with respect ot C, we obtain

$$\alpha(\phi_1^+)V(\phi_1^+)^{\frac{\lambda_j+\nu a}{\nu a}} + \frac{\nu a}{\lambda_j - \nu a}V(\phi_1^+)^{\frac{\lambda_j-\nu a}{\nu a}} = \alpha(\phi_2)V(\phi_2)^{\frac{\lambda_j+\nu a}{\nu a}} + \frac{\nu a}{\lambda_j - \nu a}V(\phi_2)^{\frac{\lambda_j-\nu a}{\nu a}} \tag{3.103}$$

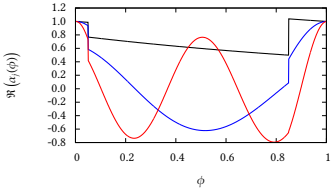

Figure 3.35: Real part of the eigenfunctions α_j of the linear stability problem for linear IF oscillators with $(a, b, \tau, \theta) = (0.2, 0.2, 0.15, 0.2)$ according to Eq. (3.93) for the three lowest eigenvalues (λ_0 (black), λ_1 (blue) and λ_2 (red)).

which using the expressions in Eq. (3.102) simplifies to the desired condition for the eigenvalues:

$$\left(\frac{V(\phi_1^+)}{V(\phi_2)}\right)^{\frac{\lambda_j - \nu a}{\nu a}} = \frac{1 + \left(e^{\tau\lambda} - 1\right) V(\phi_2) + \frac{\nu a}{\lambda_j - \nu a}}{1 + \left(e^{-(\vartheta-\tau)\lambda} - 1\right) V(\phi_1^+) + \frac{\nu a}{\lambda_j - \nu a}} \tag{3.104}$$

Note that we lost the solution $\lambda_j = 0$ in the transformations between Eq. (3.103) and (3.103), which is related to the symmetry of the original equation allowing solutions with different mass.

When we choose refractory periods, the real parts of eigenvalues take different values, which is plausible as depending on the eigenmode, the eigenfunctions take different contributions in the intervals where $\bar{F}(\phi)$ vanishes and where it does not. When we then introduce time delays $\tau < \vartheta$ (see Figure 3.36) some of the eigenmodes are stabilized. However, independently on our choices for τ and ϑ, we cannot stabilize all eigenmodes. In fact, the first eigenmode, which is not oscillatory and has a real eigenvalue, will remain unstable for arbitrary $\tau < \vartheta$. To show this, we assume that λ were a real and negative solution of Eq. (3.104). Then the term in paranthesis in the nominator of the r.h.s. is positive, while the term in the numerator is negative. The r.h.s is thus smaller than one. Solving this inequation with respect to λ, and therby considering that $V(\phi_1^+)/V(\phi_2) < 1$ for excitatory oscillators ($a > 0$), we obtain $\lambda > \nu a$ which is greater than zero in contradiction to our assumption. As long as a single eigenmode is unstable, the stationary solutions of the continuum model are unstable. Therefore, the continuum model with dense connectivity does not allow for stable stationary solutions for linear IF oscillator with arbitrary values of $a, b > 0$ and $\tau < \vartheta$. The

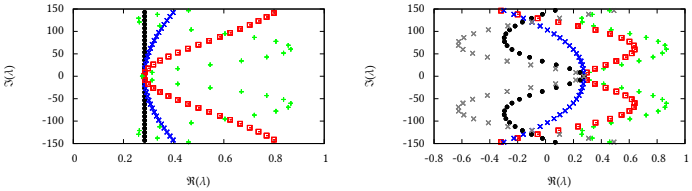

Figure 3.36: Eigenvalue spectra of the linear stability problem for linear IF oscillators ($a = 0.2, b = 0.2$) according to Eq. (3.104). Different values for time delay τ and refractory periods ϑ were chosen. Left: $\tau = 0$; black :$\vartheta = 0$, blue: $\vartheta = 0.005$, red: $\vartheta = 0.015$, green: $\vartheta = 0.05$. Right: $\vartheta = 0.05$; green: $\tau = 0.0$, red: $\tau = 0.01$, blue: $\tau = 0.02$, black: $\tau = 0.03$, grey: $\tau = 0.04$

stationary solution of the continuum model with sparse connectivity rely on sparseness and on the non-local terms. We cannot describe them by considering the much simpler equation that we investigated in this chapter.

3.4.3 Sparse Erdős-Rényi networks

For synaptic failure networks, every excited oscillator is chosen randomly from the network. This means that the distribution of phases of excited oscillators is the same as the distribution of oscillators in the network. This allowed us to assume, for the sparse limit of synaptic failure networks (Chapter 3.4.1), the same excitation rate for all oscillators in the network, independently on their phase. For Erdős-Rényi networks, however, connections are static, and it is conceivable that two oscillators which are connected have a different expected phase difference than oscillators which are not connected. In particular, the subset of oscillators which are connected to firing oscillators, may have a different distribution of phases than the distribution of all phases in the network (see Figures 3.3 and 3.4). Therefore, the excitation rate λ depends on the phase of the excited oscillator.

In the following, we will derive a two-dimensional kinetic equation which accounts for this dependence and which is intended to approximate the limiting dynamics of large, sparse Erdős-Rényi networks. With dimension, we mean here the number of dimensions of the flux, or equivalently the number of arguments of the distribution function under study. Using this equation, we can reproduce the qualitative behavior of the distribution of excited phases as shown

in Figures 3.3, 3.4, and 3.5. The kinetic equation is no exact description of the network dynamics but a refinement of the continuum with sparse connectivity in the sense that it accounts for phase dependent excitation rates observable in Erdős-Rényi networks. Instead of considering the distribution of phases $\rho(\phi)$, we here consider the density $\varrho(\psi, \phi)$ of edges in the network which have source and target nodes with phases ψ and ϕ, respectively. We norm this density to the mean degree m: $\int_0^1 d\psi \int_0^1 d\phi \varrho(\psi, \phi) = m$. When we identify 0 and 1, the phases ψ and ϕ form a torus. In absence of excitations, phase difference between ψ and ϕ stay constant, and the distribution $\varrho(\psi, \phi)$ is transported parallel to the diagonal characterized by $\psi = \phi$. The excitation rate in the network can be expressed by the edges which are connected to an oscillator with phase 1. Note that the density $\varrho(\psi, \phi)$ carries no information about the degree distribution in the network. Therefore, we have no exact way of calculating the phase distribution $\varrho(\phi)$ from $\varrho(\psi, \phi)$; a large value of $\varrho(\psi, \phi)$ could in principle go along with just a single oscillator with phase ϕ if all edges which contribute to $\varrho(\psi, \phi)$ connect to this same oscillator. However, for networks with a narrow degree distribution (like Erdős-Rényi networks), it may be justified to assume that the distribution of phases in the network can be obtained by integrating $\rho(\psi, \phi)$ over one of the two variables:

$$\rho(\phi) = \frac{1}{m} \int_0^1 d\psi \varrho(\psi, \phi) = \frac{1}{m} \int_0^1 d\phi' \varrho(\phi, \phi'). \tag{3.105}$$

The desired equations which govern the evolution of ϱ are as before described by a continuity equation:

$$\partial_t \varrho(\psi, \phi) = -\partial_\psi J_1(\psi, \phi) - \partial_\phi J_2(\psi, \phi) \quad \vec{J}(\psi, \phi) = \begin{pmatrix} J_1(\psi, \phi) \\ J_2(\psi, \phi) \end{pmatrix}. \tag{3.106}$$

The excitation rate for oscillators with phase ϕ is determined by the flux of edges which cross the boundary $\psi = 1$ of the unit square:

$$\lambda(\phi) = J_1(1, \phi). \tag{3.107}$$

It remains to define the probability flux $\vec{J}(\psi, \phi)$ and the boundary conditions. The choice of the exact definition here will allow us to distinguish between directed and undirected networks, and to reproduce the dynamics of the synaptic failure model in higher dimensions.

Two-dimensional description of synaptic failure networks

Let us—for comparison with the models to follow—derive a two-dimensional representation of the synaptic failure network model (presented in Chap. 3.4.1). In such a network, excitations are distributed evenly among oscillators, and the notion of connections between oscillators does not apply. However, if we imagine that every excitation to an oscillator with phase ϕ would be mediated by a connection, then the number of connections would be proportional to the product of the density of firing oscillators $\rho(1)$ and the density at phase ϕ. Therefore, it is plausible to define the two dimensional density $\varrho(1,\phi)$ in such a way that it decomposes into a product of $\rho(1)$ and $\rho(\phi)$. Our ansatz for the two-dimensional representation is to generalize this product to arbitrary phases by defining:

$$\varrho(\psi,\phi) = m\rho(\psi)\rho(\phi). \tag{3.108}$$

As a consistency check for the two-dimensional equations of synaptic failure networks, we can investigate if this factorization property is preserved if we chose initial conditions which fulfill it. We compute the time evolution of the product in Eq. (3.108) assuming that $\rho(\phi)$ solves the one-dimensional continuity equation of the continuum model with sparse connectivity (Eq. (3.31)):

$$\partial_t\varrho(\psi,\phi) = m\rho(\phi)\partial_t\rho(\psi) + m\rho(\psi)\partial_t\rho(\phi) = m\rho(\phi)\partial_\psi J(\psi) + m\rho(\psi)\partial_\phi J(\phi). \tag{3.109}$$

Comparing with (3.106) we conclude that

$$\vec{J}(\psi,\phi) = \begin{pmatrix} m\rho(\phi)J(\psi) \\ m\rho(\psi)J(\phi) \end{pmatrix}. \tag{3.110}$$

Using the definition for the flux of the continuum model with sparse connectivity (Eq. (3.31), we obtain:

$$\vec{J}(\psi,\phi) = \begin{pmatrix} \varrho(\psi,\phi) + m\int\limits_{I_\rightarrow(\psi)} J(1)\rho(\psi')\rho(\phi)d\psi' - m\int\limits_{I_\leftarrow(\psi)} J(1)\rho(\psi')\rho(\phi)d\psi' \\ \varrho(\psi,\phi) + m\int\limits_{I_\rightarrow(\phi)} J(1)\rho(\phi')\rho(\psi)d\phi' - m\int\limits_{I_\rightarrow(\phi)} J(1)\rho(\phi')\rho(\psi)d\phi' \end{pmatrix}. \tag{3.111}$$

As we intend to define an equation for the edge density $\varrho(\psi,\phi)$, we have to eliminate all appearances of the first order density and flux; Using

$$\rho(\phi) = \rho(\phi)\frac{\rho(\psi)}{\rho(\psi)} = \frac{\varrho(\psi,\phi)}{\int_0^1 d\phi'\,\varrho(\psi,\phi')} \tag{3.112}$$

we finally obtain

$$\vec{J}(\psi,\phi) = \begin{pmatrix} \varrho(\psi,\phi) + m\Big(\int\limits_{I_{\rightarrow}(\psi)} - \int\limits_{I_{\leftarrow}(\psi)}\Big)\frac{J_1(1,\psi')\varrho(\psi',\phi)}{\int_0^1 \varrho(\psi',\phi)d\phi}d\psi' \\ \varrho(\psi,\phi) + m\Big(\int\limits_{I_{\rightarrow}(\phi)} - \int\limits_{I_{\rightarrow}(\phi)}\Big)\frac{J_1(1,\phi')\varrho(\psi,\phi')}{\int_0^1 \varrho(\psi,\phi')d\psi}d\phi' \end{pmatrix}. \tag{3.113}$$

We endow the flux with the boundary conditions of a torus:

$$\vec{J}(0,\phi) = \vec{J}(1,\phi), \quad \vec{J}(\psi,0) = \vec{J}(\psi,1). \tag{3.114}$$

The problem defined by Eqs. (3.113) and (3.114) is entirely equivalent to the one-dimensional problem we studied in Chapter 3.4.1, and we cannot expect new dynamics from it. Let us interpret the formula with a Erdős-Rényi network in mind, to see in which way Eq. (3.113) needs to be changed as to break the factorization property in Eq. (3.108) and to yield a more accurate description for Erdős-Rényi networks. The first term of the r.h.s. of Eq. (3.113) represents convection in direction of the diagonal $\psi = \phi$. The second term describes the influence of excitations.

The first component of $\vec{J}$ defines the flux in direction of the ψ-axis. In this component we integrate over phases at which oscillators are moved past ψ by a single excitation. $J_1(1,\psi')$ is the flux of edges across $(1,\psi')$ in direction of the phase variable of source nodes. Every crossing edge has a firing source node while the target node is excited and of phase ψ'. We have to account for the change of $\varrho(\psi,\phi)$ due to every excited oscillator. The oscillator will have other edges attached to it, both ingoing and outgoing. However, we have no knowledge about the phases of the oscillators at the other side of these edges. At this point, we make the assumption that the attached edges are random and distributed homogeneously among possible ones. This assumption makes the description inexact when we compare it to Erdős-Rényi networks. In fact, the assumption is similar, as when we approximate a Erdős-Rényi network by a synaptic failure network. For synaptic failure networks we do not know the phases of excited oscillators and assume that the phases are chosen randomly. For the two-dimensional model, we do know the phase ψ' of an excited oscillators, but have no knowledge of the phases of those oscillators excited oscillators are connected to. We can, however, make an educated guess using $\varrho(\psi,\phi)$.

Suppose an oscillator o with phase ϕ_o is excited and we are interested in the influence of o's changed phase on $\varrho(\psi,\phi)$. Let us first consider the edges which have o as a source node. All edges which could fit this description are accounted for in $\varrho(\psi',\phi), \phi \in [0,1]$. If we assume that o's edges are some random subset of

these possible edges, we can express the possibility that o connects to an edge with phase ϕ by

$$P_1(\phi_o, \phi) = m \frac{\varrho(\phi_o, \phi)}{\int_0^1 \varrho(\phi_o, \phi) d\phi} \tag{3.115}$$

Analogously, we can represent the probability $P_2\psi'(\phi)$, that o is the target oscillator of an oscillator with phase ϕ by

$$P_2(\phi, \phi_o) = m \frac{\varrho(\phi, \phi_o)}{\int_0^1 \varrho(\phi, \phi_o) d\phi} \tag{3.116}$$

We can conceive the products $J_1(1, \psi)P_1(\psi, \phi)$ and $J_1(1, \phi)P_2(\psi, \phi)$ as excitation rates for edges in the sense that they describe the rates with which edges are moved discontinuously on the (ψ, ϕ)-torus due to excitation of source and target oscillator, respectively. These excitations rates are exactly the terms that we integrate over in Eq. (3.113). In the following, we will use the two-dimensional description of synaptic failure networks (Eqs. (3.113) and (3.114)) as starting point to derive equations tailored to Erdős-Rényi networks.

Two-dimensional description of undirected Erdős-Rényi networks

Let us consider the dynamics of an undirected Erdős-Rényi network. As every connection in such a network is bidirectional, we have $\varrho(\psi, \phi) = \varrho(\phi, \psi)$ and the defined probability flux has to preserve this property. Compared to the two-dimensional description of synaptic failure networks, we have to change two things. Firstly, when an edge with oscillator phases $(1, \phi)$ crosses the boundary of the unit square, the target oscillator is excited and has a phase of $R(\phi)$ afterwards. The edge thus reappears at $(0, R(\phi))$ afterwards. As we here discuss undirected networks, we can argue analogously for an edge at $(\psi, 1)$ which crosses the boundary. We obtain the following boundary conditions

$$\vec{J}(0, \phi) = \vec{J}(1, R^{-1}(\phi)), \quad \vec{J}(\psi, 0) = \vec{J}(R^{-1}(\psi), 1) \tag{3.117}$$

Secondly, when an oscillator is excited, it is by necessity connected to an oscillator with phase 1. Therefore, if we assume an average degree of m in the network, it only has $m-1$ connections which connect it to other oscillators with unknown phases. We thus scale the interaction terms in the definition of the flux by $m-1$

instead of m.

$$\vec{J}(\psi,\phi) = \begin{pmatrix} \varrho(\psi,\phi) + (m-1)(\int\limits_{I_{\rightarrow}(\psi)} - \int\limits_{I_{\leftarrow}(\psi)}) \frac{J_1(1,\psi')\varrho(\psi'\phi)}{\int_0^1 \varrho(\psi'\phi)d\phi} d\psi' \\ \varrho(\psi,\phi) + (m-1)(\int\limits_{I_{\rightarrow}(\phi)} - \int\limits_{I_{\rightarrow}(\phi)}) \frac{J_1(1,\phi')\varrho(\psi\phi')}{\int_0^1 \varrho(\psi,\phi')d\psi} d\phi' \end{pmatrix} \tag{3.118}$$

For the continuum model for synaptic failure networks, we were able to express the firing rate explicitly in terms of the phase density. Note that depending on the PRC, the same may be impossible for the continuum model for directed and undirected Erdős-Rényi networks. Setting $\psi = 1$ in Eq. (3.118), we obtain a Fredholm integral equation of second kind:

$$J_1(1,\phi) = \varrho(1,\phi) + (m-1)(\int\limits_{I_{\rightarrow}(1)} - \int\limits_{I_{\leftarrow}(1)}) \frac{J_1(1,\psi')\varrho(\psi'\phi)}{\int_0^1 \varrho(\psi'\phi)d\phi} d\psi', \tag{3.119}$$

This equation determines the excitation rate $\lambda(\phi) = J_1(1,\phi)$ which appears both inside and outside the integral. The solution of such an equation can be expressed by the Liouville-Neumann series. The implementation of finite size discretizations nevertheless is hindered by this. We restrict ourselves here to the case of linear IF oscillators with delay and refractory periods, for which $I_{\rightarrow}(1) = 0$ and Eq. (3.119) reduces to $J(1,\phi) = \varrho(1,\phi)$.

Two-dimensional description of directed Erdős-Rényi networks

We will now define the flux for directed Erdős-Rényi networks. As for the description tailored to undirected Erdős-Rényi networks, we consider the influence of an edge contributing to $\varrho(1,\phi)$ whose source and target oscillators have phases 1 and ϕ respectively. The target oscillator with phase ϕ is excited and we calculate the influence of its changed phase on the distribution ϱ. For a directed network, the number of incoming and outgoing edges per node have the same average value m. The excited oscillator has 1 incoming edge coming from the firing oscillator and $m-1$ incoming edges coming from other oscillators. In addition, we have to account for—on average—m outgoing edges of the excited oscillator.

$$\vec{J}(\psi,\phi) = \begin{pmatrix} \varrho(\psi,\phi) + m(\int\limits_{I_{\rightarrow}(\psi)} - \int\limits_{I_{\leftarrow}(\psi)}) \frac{J_1(1,\psi')\varrho(\psi'\phi)}{\int_0^1 \varrho(\psi'\phi)d\phi} d\psi' \\ \varrho(\psi,\phi) + (m-1)(\int\limits_{I_{\rightarrow}(\phi)} - \int\limits_{I_{\rightarrow}(\phi)}) \frac{J_1(1,\phi')\varrho(\psi\phi')}{\int_0^1 \varrho(\psi,\phi')d\psi} d\phi' \end{pmatrix} \tag{3.120}$$

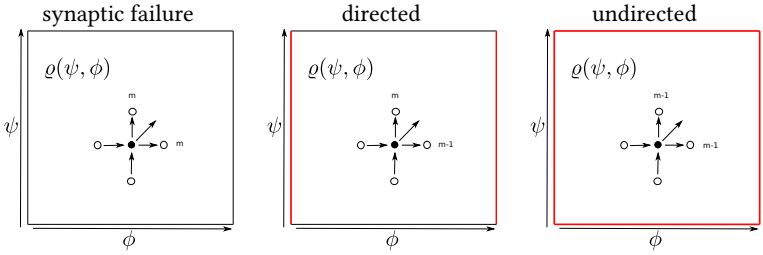

Figure 3.37: Schematic comparison of two-dimensional models for the three considered types of networks. All three models have convection parallel to the diagonal $\psi = \phi$ of the unit square. Additionally, we have jumps in direction of the axes due to excitations to the source or target oscillators of edges. For synaptic failure networks, both types of excitations scale with the mean degree m. For directed Erdős-Rényi networks excitations to the source oscillator scales with m while excitations to the target oscillator scale with $m - 1$. For undirected Erdős-Rényi networks, both types of excitations scale with $m - 1$. Continuous boundary conditions at the edges of the unit square are marked in black, while boundary conditions at which the flux is mapped by the PTC are marked in red.

The different factors make it obvious that the evolution equation which results from Eq. (3.118) will lead to phase densities which are not symmetric under exchange of the arguments ψ and ϕ. For the boundary conditions, we know that an edge with phases $(1, \phi)$ is injected at $(1, R(\phi))$. In contrast to undirected networks, we cannot conclude that the source oscillator of an edge $(\psi, 1)$ is excited at threshold crossing. At this boundary, we thus have to choose the simpler boundary condition.

$$J(0,\phi) = J(1, R^{-1}(\phi)), \quad J(\psi, 0) = J(\psi, 1) \tag{3.121}$$

This concludes the definition of the model for directed Erdős-Rényi networks which is defined by Eqs. (3.120) and (3.121). The integral equation which determines the firing rate is the same as for undirected Erdős-Rényi networks. In Figure 3.37, we show a graphical comparison of the three defined two-dimensional fluxes. Note, that the difference between all three two-dimensional continuity equations obviously vanishes in the limit of large m. The equations can be discretized analogously as for the continuum model with sparse connectivity aimed

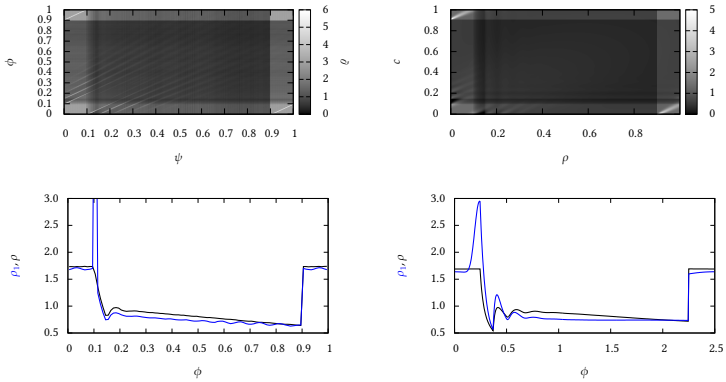

Figure 3.38: Top left: Distribution $\varrho(\psi, \phi)$ of edges with given source and target phases ψ and ϕ in asynchronous states of directed Erdős-Rényi Networks ($m = 10, N = 10^6$) of linear IF oscillators $(a, b, \tau, \vartheta) = (0.05, 0.05, 0.1, 0.2)$. Bottom left: distribution of oscillator phases $\rho(\phi)$ and distribution of phases of excited oscillators $\rho_1(\phi)$. Left: Histogram obtained from a network of 10^6 oscillators. Right: Finite size discretization to $500 \cdot 500$ dimensions of the two-dimensional continuum model tailored towards undirected Erdős-Rényi networks.

at synaptic failure networks, which allows us to reproduce, qualitatively, the observed behavior of the asynchronous states of Erdős-Rényi networks. In Figure 3.39 and 3.38, we show a comparison of $\varrho(\psi, \phi)$ as assessed from asynchronous states of Erdős-Rényi networks with $\varrho(\psi, \phi)$ as produced by the kinetic equations derived in this chapter. The kinetic equations are able to reproduce the characteristic features that we observed in Erdős-Rényi networks. An detailed analysis of differences in dynamical behaviors that emerge from the kinetic equations and from Erdős-Rényi networks is left for future study. Although the kinetic equations, we present here, possibly provide a better description to the dynamics of Erdős-Rényi networks, it can not be expected that the description is exact. Other influencing factors like the degree distribution are known to have a large impact on the dynamical behavior and are not accounted for by our approach [32].

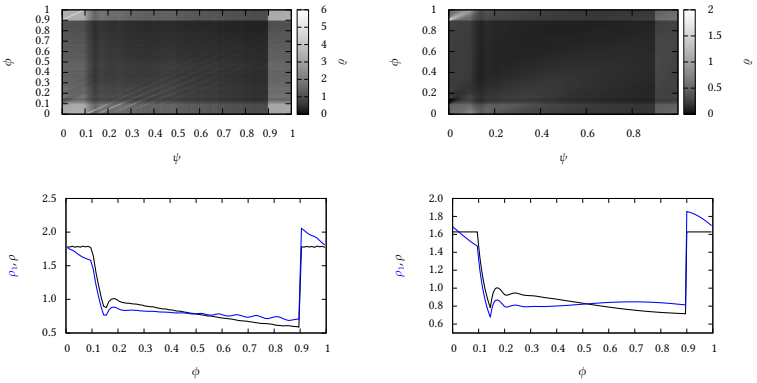

Figure 3.39: Same as Figure 3.38 but for directed Erdős-Rényi networks .

3.5 Summary

We investigated and compared the dynamics of integrate-and-fire-like oscillators coupled onto Erdős-Rényi - and synaptic-failure random networks. These networks are defined under the assumption that

each two nodes in the network have the same probability for a connection (for Erdős-Rényi networks) or for an interaction (for synaptic failure networks). We defined interaction of oscillators by δ-pulses and endowed them with time delayed interactions and refractory periods $\vartheta > \tau$.

For the same parameters, these oscillator networks are able to support both stable synchronous motion and chaotic transients to synchrony whose length grows exponentially with the network size. Similar behavior has been observed for comparable δ-pulse coupled systems in Refs. [74, 78]. However, the larger network sizes that we are considering here allowed us to describe the observed behaviors by distributions of the oscillator phases, and thus to provide a macroscopic point of view on the dynamics. During the transients, oscillators show nearly constant statistics and we thus related the transient behavior to an equilibrium phase density distribution. Using statistical properties (the distribution of phases of excited oscillators) we estimated the largest non-vanishing Lyapunov exponent in such states, which confirmed that the transient asynchronous behavior can be considered as chaotic.

Furthermore, we investigated different kinds of continuum models which represent the network dynamics in the limit of large networks. Such continuum models allow the definition of evolution equations for the distribution of oscillator phases. Similar approaches have furthered insights into the dynamics of excitatory integrate-and-fire neurons [109, 110], oscillators coupled by short-decaying pulses [42], and of continuously interacting oscillators like those of Kuramoto type [59].

Note that we cannot investigate the dynamics in the commonly assumed mean- or fluctuation-driven limits. Investigating the continuum model for the mean-driven limit (which corresponds to dense networks), we linearized the evolution equations near the stationary solution and found that the latter is unstable for the oscillators we are considering. The mean-driven limit is thus not sufficient to describe asynchronous or phenomena neartheir loss of stability.

For synaptic failure networks, we were able to describe the equilibrium phase distribution analytically, and show that it is unique. Two different mechanism may prevent the emergence of asynchronous behavior in these networks. Firstly, the equilibrium solutions do not exist for arbitrary parameters. When they do not, networks synchronize nearly instantaneous, similar as in a chain reaction or avalanche. Secondly, the equilibrium solution may turn unstable via an Andronov-Hopf bifurcation, leading to small oscillations around it and eventually to irregular more complicated behaviors (cf. [111]).

Generally, synaptic failure networks and Erdős-Rényi networks show for the most part very similar dynamical behaviors. Therefore, we are confident that descriptions and notions still are useful to understand the dynamics of Erdős-Rényi networks, although they present only an approximation here. Moreover, we defined a continuum model tailored towards Erdős-Rényi networks, which provides a further refinement towards their dynamics. The main dynamical variable here is not a distribution of phases but a distribution of edges in the network. Although the description is not exact, it is able to reproduce further statistical properties that can be measure in Erdős-Rényi networks, namely the distribution of phases of excited oscillators. Although a detailed analysis of this equation still has to be done, we are confident that further studies into the presented equations may improve our understanding of the emerging dynamics of systems coupled onto random networks.

Near the loss of stability of the equilibrium phase distribution, we observed various kinds of more complicated behaviors which emerge when oscillators fulfill the condition for a chain reaction; If every firing oscillator will excite on average one other oscillator beyond its firing threshold, then a macroscopic amount of oscillator fires in unison much like in an avalanche. While such avalanches

may lead to a rapid convergence to synchrony, it may also lead to irregular behavior in which *continuous dynamics* and avalanches interplay continuously, leading to irregular macroscopic behavior in which synchrony builds up and is recurrently diminished by the occurrence of avalanches.

4 Dynamics on spatial networks

In the following chapter, we investigate the dynamics of linear IF oscillators on networks with a spatial structure. Lattices with nearest neighbor-coupling are the simplest of such networks and have been studied extensively in the context of condensed matter. Due to their homogeneity and the large amount of symmetries, they are amenable to analytical approaches which aim at predicting critical parameter values, at which the site's states organize either globally or locally ([112]). However, even simple node dynamics easily leads to difficult problems. One of the more famous examples is the Ising model which for three or more spatial dimensions, has defied an analytical treatment despite intense effort. Oscillators as considered by Peskin have been shown to synchronize completely for nearest neighbor coupling in 1 spatial dimension [79], however starting from two dimensions, stable firing configurations have been found which do not lead to synchrony [71].

The situation gets even more complicated, when timescales are chosen for the oscillators as we did by introducing time delays τ and refractory periods ϑ. As distant oscillators on a lattice can only communicate via several intermediating oscillators, delays between these oscillators add up, making global synchrony an unlikely scenario. Instead, local synchrony and phase-locking can be observed in various types of wave-dominated states [113, 114]; two distant oscillators which communicate via waves traveling recurrently between them may lock their phases to a constant difference. We expect the typical phenomena known from excitable media like spiral waves [46]. For nearest neighbor coupling, a wave front may travel into the direction of one of the lattice's axis with a speed of one site per time delay. It is followed by a tail of refractory oscillators. For a stable wavefront, we need $\tau < \vartheta$ and a large coupling strength such that a single excitation suffices to make the excited oscillator fire immediately. When we consider a lattice defined by a radius of influence such that each oscillator is connected to more than the nearest four neighbors in a network, smaller coupling strengths may suffice, as each oscillator is excited several times due to the firing of the oscillators on the wavefront. In this case the possibility for wave propagation and the wave speed depend on the oscillator phases of the lattice sites the wave travels on; waves may travel faster on a region with large phases as then even the second-next neighbors in direction of wave prop-

agation may be excited by the wavefront. When two wavefronts collide, they annihilate, as the refractory tails of both waves come from both sides and the wave cannot spread in either direction. Our oscillators do not allow for total quiescence. Nevertheless, they can be expected to behave similar as excitable elements when excitations dominate over the intrinsic charging, which may be the case for wave-dominated states.

Small-World Media

Natural networks that are studied in the life and social sciences often contain a lattice-like structure which is complemented by some amount of connections between distant nodes. Many recent studies have constructed and studied the dynamics of model networks which mimic this property. A popular construction scheme is to start with a lattice, remove a certain number of connections and introduce the same number of connections between randomly chosen source and target nodes. The newly introduced connections will, with large probability, connect nodes which are far apart on the lattices; simplifying, we will denote them as long-ranged connections. Varying the fraction of long-ranged connections ρ between 0 and 1 allows to interpolate continuously between regular lattices and random networks while keeping the total number of connections in the network fixed. The generated networks are denoted as small-worlds because replaced connections [11] may be considered as short-cuts and lead to short paths between pairs of nodes in the network, even for small ρ. The archetypical dynamical behavior of lattices are waves, while for random networks synchronization phenomena are prevalent. Both behaviors can be expected to be carried over to spatial networks with short- and long-ranged connections, which allows us to study the interplay of local patterns and global oscillations. The influence of the described replacement on synchronization has many facets. Firstly, replaced connections allow nodes to communicate more immediate. Secondly, the distribution of node degrees in the networks becomes inhomogeneous, which usually hinders synchronization, similar as many other sources of inhomogeneity in complex networks. In many studies the coupling strength per node is normalized to account for that. Thirdly, the lattice structure is weakened, which may change the spatial patterns in the network which in turn may promote or hinder the global organization of the networks.

When we replace connections with probability $\rho = 1$, the spatial structure is completely destroyed and we obtain some random networks. We will construct and study three different kinds of small-world networks such that for $\rho = 1$ each of the three types of random networks is obtained that we discussed in Chapter 3.

All three kinds of small-world networks are based on a bidirectionally connected square lattice that we construct as follows:

- We start with a square arrangement of nodes, in which every node is connected bidirectionally to its k nearest neighbors. In case k does not define a unique set of neighbors, we choose randomly between nodes with the same distance.
- We use cyclic boundary conditions such that the lattice forms a torus.

For example for $k = 5$, we will connect each nodes to its 4 nearest neighbors and choose for each node one of the 4 diagonal neighbors randomly. The replacement is performed according to one of the three following rules, yielding directed and undirected networks as well as networks which interpolate between lattices and synaptic failure networks.

directed For each directed connection in the network and with probability ρ, we remove it and introduce a connection between randomly chosen source and targets nodes.

undirected For each directed connection and its counterpart with reverse direction and with probability ρ, we remove it both with probability ρ and introduce a bidirectional connection between randomly chosen source and targets nodes.

synaptic failure For each directed connection in the network, we remove it with probability ρ. Every firing oscillator o will distribute m excitations randomly among oscillators where m is the number of removed connections with o as source node.

The construction schemes depend on the fraction of long-ranged connections ρ and on the number of nearest neighbors k. Constructed networks with the same parameters may differ, even for the third rule concerning synaptic failure networks. For large networks, however, the dynamical behavior of these networks will be very similar. In addition, for larger k, we generate networks in which different nodes have similar amounts of short- and long-ranged connections. The synaptic failure variants of small-world networks then are approximately translation invariant. However, even for the Erdős-Rényi networks the target nodes of the replaced connections are well distributed over the network. We can think of it as an excitable medium in which the mean activity is coupled to every site. We will used the term small-world medium, which underlines this spatial homogeneity of the network.

We start with a discussion of the dynamics of linear IF oscillator endowed with time delays τ and refractory periods ϑ. Compared to plain IF oscillators, they show a richer dynamical spectrum, allowing for various kinds of wave dominated states that we cannot observe for plain IF oscillators. Furthermore, the generated non-converging behaviors that we report on seem less irregular for the more complicated oscillators. In Chapter 3, we have discussed two distinct mechanism that may lead to synchrony. In parameter space, we found two boundaries at which the asynchronous behavior was lost (see Figs. 3.13, 3.16, and 3.23). Depending on the type of random network, the oscillators show complicated states of partial synchrony at the lower boundary (which lies at smaller values of b) whereas the behavior at the upper boundary consisted of spontaneously initiated fast transient to complete synchrony. As the behavior at the upper boundary seems easier, we focus – as a first step – on this transition, and investigate how the dynamics is changed when we replace some amount of the random connections by a lattice structure. For comparability with the findings presented in Chapter 3.3, we choose a mean degree m of 50, $\tau = 0.01$, and $\vartheta = 0.05$. Furthermore, we chose a linear dependence between a and b such that the corresponding line in the (a, b)-plane intersects with the upper boundary of the parameter regime with asynchronous states. Note that the dynamical behaviors we describe here do not depend on leakyness in the sense of integrate-and-fire neurons. In fact, we can observe all behaviors for $a = 0$, i.e., for non-leaky oscillators. As can be seen in Figure 3.23, directed and undirected Erdős-Rényi networks undergo—with increasing oscillator parameters satisfying $a = 0.5b$—a transition from asynchronous states to synchrony. Near the boundary long, chaotic transients can be observed which end in a spontaneous and rapid transition to complete synchrony. In contrast, synaptic failure networks with $\tau = 0.01$ and $\vartheta = 0.05$ synchronize completely independent on the coupling strength.

In the following, we investigate the emerging network behavior in dependence on the fraction of long-ranged connections ρ and on the oscillator parameter b . In dependence on ρ and b, the networks show a large spectrum of dynamical behaviors which are crucially influenced by the formation of spatial patterns. For small timescales τ and ϑ, wave phenomena are fast compared to the intrinsic frequency of oscillators, and wave-dominated states are possible in which oscillators mostly fire because they are excited and not because of their intrinsic dynamics. The dynamics of the wave dominated states then is similar to what can be observed for excitatory IF neurons [115].

Macroscopically, we observe partially synchronous states with nearly constant firing rate and states with periodic time evolutions of the firing rate. Additionally, we observe a regime in which the oscillators show irregular behavior

with no convergence to limit cycles even for large networks. To characterize the global network behavior, we assess the order parameter $r(t)$ and the firing rate $\nu(t)$ when starting from distributed phases. A visual inspection of statistical properties of $r(t)$ and $\nu(t)$ (Figure 4.1 and Figure 4.2) allows us to distinguish different regions in parameter space spanned by b and ρ which are separated by boundaries and differ in the dynamical behavior.

In Figure 4.3, we show a schematic with a separation of the parameter space into regimes according to the dynamical behavior. The scheme is representative for either directed, undirected, or synaptic failure small-world media, which show for the most part similar progressions of the boundaries between behaviors and show qualitatively the same dynamical behaviors, the exception being the absence of asynchronous states for small coupling strengths in synaptic failure small-world media.

We provide a description of the different dynamical behaviors and start with cyclic wave states that can be observed for spatial network with a strong lattice structure (small ρ and large values of a and b).

4.1 Wave pattern

Cyclic waves

A traveling wavefront of firing oscillators excites other oscillators which lie in the direction of wave propagation. Oscillators which lie in the opposite direction are refractory. For cyclic waves, firing oscillators on the wave front must distribute enough excitation as to make other oscillators in direction of wave propagation fire, independently of the oscillator phases of the medium before arrival of the wave. When the coupling strength is large enough, cyclic waves are ignited at some site in the lattice, the focus, and spread outwards. The same wave cannot return to any point it has previously reached and for cyclic boundary conditions, it eventually extinguishes itself. While spreading, the wave resets the phases in the network according to the distance to the focus.

For regular lattices ($\rho = 0$), we observe cyclic waves, which quickly cover the whole network, and quiescence in which the phases of oscillators increase until the same waves are ignited again (see Figure 4.4 left). After waves have travelled the network once, all lattice sites have adapted their phases accordingly and oscillators would fire by themselves anyway at the arrival of the next wave. After a few collective oscillations, the lattices are phase-locked and show constant values of $r(t)$. Cyclic wave foci emit waves with a frequency of 1. In this time the wave front may travel a hundred times to new lattice sites (assuming $\tau = 0.01$).

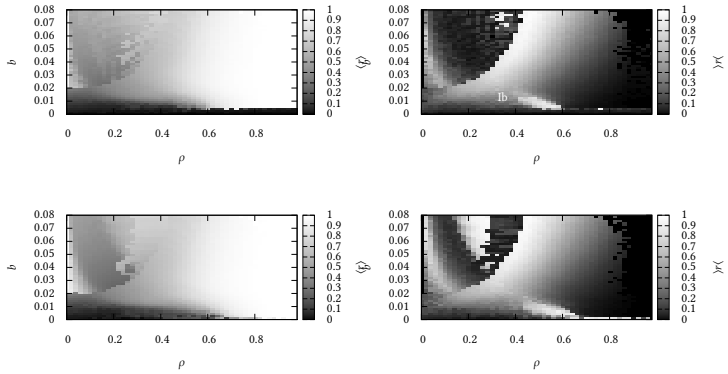

Figure 4.1: Statistical properties of the order parameter $r(t)$ of small-world networks ($N = 250 \times 250, m = 50$) of linear IF oscillators in dependence on the fraction of long-ranged connections ρ and the oscillator parameter b. Other oscillator parameter: $a = 0.5b, \tau = 0.01, \vartheta = 0.05$. Left: average value $\langle r \rangle$, Right: range of observed values $\rangle r \langle$. Values were obtained for $t \in [100, 200]$ to avoid influence of transients. Top: directed small-world media, bottom: synaptic failure small-world media. Undirected small-world media show very similar results as directed small-world media (data not shown).

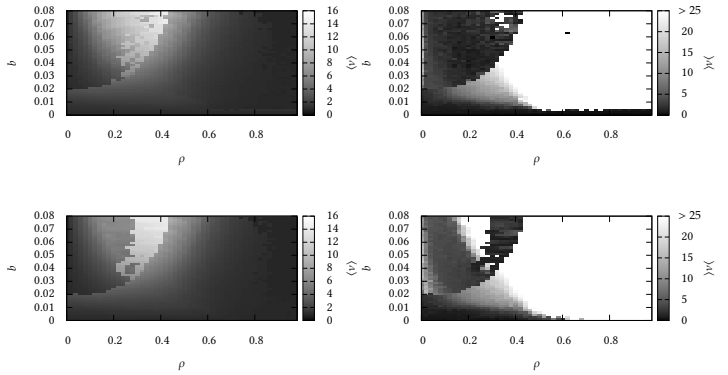

Figure 4.2: Same as Figure 4.1 but for the firing rate ν

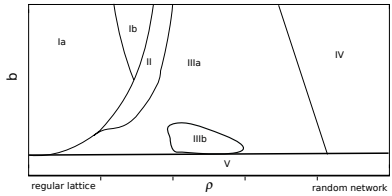

Figure 4.3: Schematic of the parameter regimes with different dynamical behaviors in dependence on the fraction of long-ranged connections and on oscillator parameters $b = 0.5a$ (cf. Figures 4.1 and 4.2). All three investigated types of small-world media of linear IF oscillators show qualitatively similar behaviors with the exception that regime V cannot be observed for synaptic failure media (for the chosen parameters). The observed behaviors show different spatial patterns which may or may not co-occur with periodic behavior of global observables: Ia: cyclic waves without global synchrony, Ib: cyclic waves with global synchrony, II: spiral waves without global synchrony, IIIa: networks split into synchronous regions and asynchronous regions which are unstructured for smaller phase responses and take the form of turbulent-like waves for larger ones. The relative size of synchronous and asynchronous regions is fixed. IIIb: networks split into synchronous and unstructured asynchronous regions which fluctuate in both size and shape. IV: almost complete synchronization, V: asynchronous state with constant firing rate and distribution of phases.

Therefore, very few waves will travel the networks at the same time for the lattice sizes we can investigate numerically. The phase-locked states thus have large order parameters.

For $\rho > 0$ the lattice structure of the networks is weakened and we need larger coupling strengths to observe cyclic waves. At the same time the translation symmetry of the lattices is broken and the dynamics did not reach any periodic attractor during the times we observed the networks. With increasing fraction of long-ranged connections, oscillators on wavefronts distribute a large number of excitations via long-ranged connections. As these are distributed homogeneously over the network, they increase the effective frequency of oscillators and thus decrease the time T between emitting of cyclic waves from the wave focus. When T comes into the same order of magnitude as the wave speed, we can observe states in which many waves travel the network at the same time (see

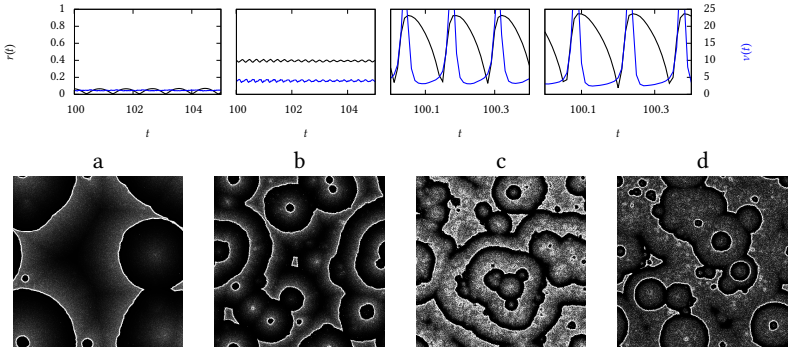

Figure 4.4: Top: Order paramter $r(t)$ and firing rate $\nu(t)$ for linear IF oscillators coupled onto directed small-world networks ($N = 500 \times 500, m = 50$). Bottom: Snapshot of the spatial distribution of phase values for linear IF oscillators coupled onto directed small-world networks ($N = 500 \times 500, m = 50$). Oscillator parameters: a: $\rho = 0.04, b = 0.0592$, b: $\rho = 0.2, b = 0.04$, c: $\rho = 0.34, b = 0.0752$, d: $\rho = 0.32, b = 0.072$. The dynamics shows cyclic waves which dominate the dynamics (a and b) or co-occur with collective firing of large parts of the network (c and d).

Figure 4.4 b). When the mean firing rate is much larger than 1 (see Figure 4.2 left), the phase change due to excitations outweighs the phase change due to the intrinsic dynamics. In this case, it can be expected that the observed dynamics is similar to the one for excitable elements. The situation is comparable as in [116] where small-world networks of excitable units where shown to exhibit sustained activity on one-dimensional networks. To obtain an indication, if the states for $\rho > 0$ also settle onto a limit cycle or possibly are chaotic, we estimated the largest Lyapunov exponent λ as described in chapter 3.2 (see Figure 4.5).

To our surprise the parameter regime with cyclic waves, splits into two regions. For small ρ, we observe $\lambda = 0$, while for larger ρ, trajectories diverge indicating a chaotic dynamics. A negative or vanishing largest Lyapunov exponent indicates that will vanish to a fixed point or a limit cycle. However, the corresponding transients can be very long for high dimensional systems as it is the case for systems showing stable chaos [95]. Most oscillators in the cyclic wave states fire because they receive a supra threshold excitation. The dynamics

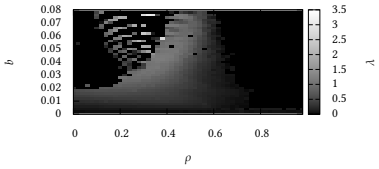

Figure 4.5: The largest Lyapunov exponent λ in dependence on ρ and $a = 0.5b$ for directed small-world media ($m = 50, N = 100 \times 100$) of linear IF oscillators. The dynamical regimes IIIa and IIIb as defined in Figure 4.3 are revealed to be chaotic. Cyclic wave states have converging trajectories for small ρ and diverging trajectories for larger ρ. For large ρ the lattices synchronize completely leading to $\lambda = 0$.

is thus insensitive to a perturbation in the phases of these oscillators. Only the oscillators which fire when reaching the threshold due to their intrinsic dynamics may propagate a perturbation of the oscillator phase.

The propagation of a cyclic wave depends little on the oscillator phases of the network sites it travels on. After the wave passes some position, phases of oscillators are reset to 0, independently on the phases before the passing. As long as the number of wavefronts is large enough to clear the network of the charging repeatedly, the network shows no global oscillations and is wave-dominated. For larger coupling strengths, however, we observe states with global oscillations and cyclic waves (see Figure 4.4 c and d) in a small range of rewiring probabilities around $\rho \approx 0.25$. A wave in an oscillating medium increases its speed with the oscillator phase of the collective oscillation. At the point of collective firing, only the oscillators which just left their refractory periods, can support wave propagation. The wave is thus moved back by a distance which is given by the size of its refractory tail. The parameter region for cyclic waves co-occurring with collective firing is much larger for synaptic failure small-world networks as these have to a much lesser degree inhomogeneities in the lattice structure which possible serve as wave foci for cyclic waves.

Spiral waves

In a spiral wave focus, excitation spreads along a cycle whose size is determined by the refractory period ϑ; if excitation reaches back to some oscillator on the

circle, the refractory period ϑ of that oscillator just ended (otherwise the excitation would spread on a larger cycle). The speed with which the excitation spreads on the cycle is determined by the time delay τ. The size of the cycle and the frequency with which waves are emitted from the focus is thus determined by the timescales of the oscillators and independent on the intrinsic dynamic of oscillator in contrast to cyclic waves. For our parameter, the emitting of spiral waves is much faster than for the cyclic wave states, which is why spiral wave states have much higher firing rates and are stable once created. Note that spiral waves are supported whenever cyclic waves are supported by our networks. Their generation, however, is unlikely when starting from uniformly distributed phases in the regime with cyclic waves (regime Ia of Figure 4.3). A spiral wave can be generated by choosing initial conditions, which generate a wave that ends at some point [115]. Starting from such initial conditions, the cyclic wave states cannot be observed anymore and the dynamics is dominated by spiral waves.

Additionally, Spiral waves are generated reproducibly even for distributed initial conditions in a small region around $\rho \approx 0.3$. We describe the mechanism which lead to this generation in Figure 4.6. To the left of the region, networks have a strong lattice structure, such that waves are fast even directly after collective firings. To the right of the region, the number of generated turbulent-like waves is too small and they are too slow to continuously reset the network and keep it from firing collectively.

Turbulent-like patterns

We now describe the dynamical behavior for networks in which the lattice structure does not allow for wave phenomena to dominate the dynamics (small coupling strengths and large fractions of long-ranged connections ρ). For $b = \rho = 0$ oscillators are uncoupled and maintain their random initial phases. With increasing coupling strength, the phases organize locally. Small worm-shaped regions are formed in which oscillators fire subsequently (see Figure 4.7 a). The regions retain their shape over many firing cycles. When the coupling strength is further increased, patterns become more volatile and obtain the form of turbulent-like waves (see Figure 4.7 b). In these states, wave propagation is only possible at regions where the oscillators already have large phases. At other regions waves die out leaving the medium partially excited. This leads to irregular patterns which show bending wave fronts which at times resemble spiral waves.

For $\rho = 0$, these states show no global organization and we observe only small fluctuations in network observables, possibly related to finite-size effects. In the small-world regime, however, similar wave phenomena co-occur with

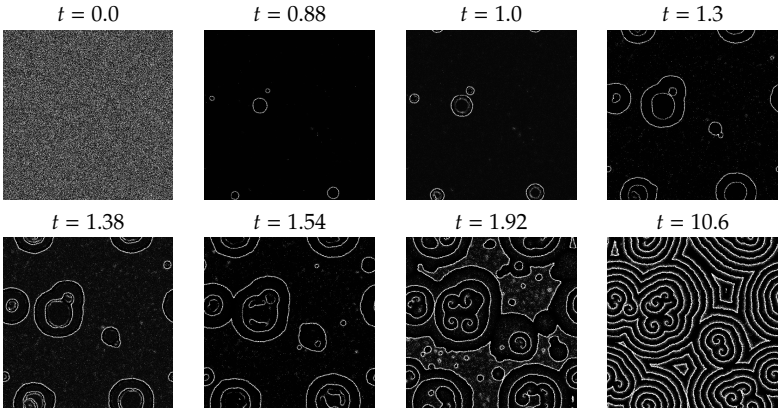

Figure 4.6: Consecutive snapshots of the spatial distribution of phases for linear IF oscillators coupled onto directed small-world networks ($N = 500 \times 500$, $m = 50$) for $\rho = 0.32$ and $b = 0.056$ starting from uniformly distributed phases. The dynamics shows the generation of spiral wave foci. At $t = 0.88$, the lattice shows a few wavefronts in a synchronized background. The lattice structure of the networks is too weak to allow for supra threshold excitation of oscillators ahead of the wavefronts. These oscillators, however, are left with large phases and fire soon, reaching the firing threshold due to their intrinsic dynamics. In this way, waves travel with a speed of less than one site per time delay. For the chosen parameters, the waves are so slow that oscillators behind wavefronts leave their refractory period and are excited, leading to the *double* wavefront structure seen at $t = 1.0$ or $t = 1.38$. The inner wavefront collides with the outer leading to spiral wave foci (seen at $t = 1.92$) which soon dominate the lattices ($t = 10.6$)

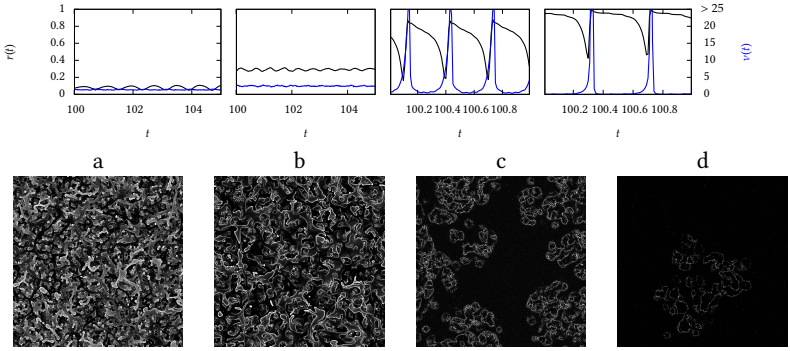

Figure 4.7: Top: Order paramter $r(t)$ and firing rate $\nu(t)$ for linear IF oscillators coupled onto directed small-world networks ($N = 500 \times 500$, $m = 50$). Bottom: Snapshot of the spatial distribution of oscillator phases for directed small-world media. Values range from 0 (black) to 1 (white). Different oscillator parameters were chosen for a ($b = 0.0064$, $\rho = 0.0$), b ($b = 0.0176$, $\rho = 0.0$), c (b=0.0352, $\rho = 0.4$), and d ($b = 0.064$, $\rho = 0.6$). The dynamics shows turbulent-like patterns without (a, b) and with collective firing (c, d).

partial synchronization, such that the time-resolved firing rate shows a periodic behavior with alternating times of low and high activity (see Figure 4.7 c and d).

The networks splits into synchronous parts and parts with spatial patterns, whereby the oscillators in the synchronous parts share a common phase. For a given set of parameters, the networks have preferred relative sizes of synchronous parts and wave patterns. The frequency of collective firings in the network increases with the size of wave patterns; oscillators which are part of the spatial patterns fire and excite oscillators in the synchronous parts. As the excitations are distributed in time, only few are received by oscillators shortly before or after firing for which the phase response is either small (due to absorption) or vanishes (due to refractory periods). This is in contrast to excitations which originate and are received by oscillators in the synchronous part, which do not increase the frequency of collective firing as the receiving oscillators are refractory. In the completely synchronized state, oscillators fire with their eigenfrequency in our model. The collective firing in turn suppresses wave propagation as wavefronts are moved back to the lattice sites where oscillators leave their

refractory periods. This feed-back mechanism allows for an equilibrium; whenever the size of wave patterns grows large, the frequency of collective firings is increased and the size of wave patterns shrinks. Then again if we start with few wave patterns, the frequency of collective firings is small, which gives wave patterns time to invade the synchronous regions and increase in size. The preferred size of wave patterns increases with increasing ρ as does the order parameter (see Figure 4.1).

With weaker lattice structure, (smaller b and larger ρ) wave patterns become more stationary, less wave-like, and change form and shape over many firing cycles only. For $\rho > 0.5$ and b shortly above the synchronization threshold, the spatial patterns in the asynchronous parts of the network show distributed phases with nearly no distinctive structure. Depending on parameters, these asynchronous patterns may evolve in size and shape, or may lead to some configuration which changes little after the transient. We will first describe the latter case.

4.2 Chimera states

In a chimera state a network of identical oscillators splits into two domains, one of which is synchronized and phase-locked while the other is asynchronous and chaotic [64, 65, 117–123]. In many studies, the considered networks are lattices such that the domains are separated in space. Chimera states have been observed first in lattices of identical Kuramoto oscillators and have been met with surprise by the community as they present a form of symmetry breaking: the equations of motions are translation invariant while the chimera state, which often emerges in a self-organized way, is not.

Starting from uniformly distributed phases, networks of linear IF oscillators may split into some partition of asynchronous and synchronous regions. For $\rho > 0.6$ and small coupling strengths, the partition is frozen after the transient. The directed and undirected small-world media that we study have construction rules which are translation invariant. In addition, for larger mean degrees constructed networks are fairly homogeneous and *almost* translation invariant, more so the synaptic failure small-world networks. The frozen pattern is thus determined by the initial condition and not by inhomogeneities in the network; the same region in the network which is asynchronous after some transient may be synchronous when starting from a different initial condition. Networks prefer a certain size of asynchronous patterns, similar as for the aforedescribed, turbulent-like patterns that can be observed for larger coupling strengths. If we start with a small asynchronous region, it will grow until it reaches a certain

size. Then again the same total size of asynchronous regions is reached if we start from distributed phases. In Figure 4.8 and 4.9, we show transients which start from a small localized disturbance in an otherwise synchronous network for a directed small-world network and a synaptic failure small-world network, respectively. For the chosen parameters, the disturbance grows in size via the short-ranged connections. Moreover, excitations via long-ranged connections lead to a small jitter in the synchronized background. At times additional disturbances may be created, which also grow in size. Intriguingly, the speed of growth is not constant but diminishes with the increase of the asynchronous regions. When a critical size is reached, the growth stops which leads to the frozen partition of the network. The different asynchronous regions do not form perfect circles, which we relate to inhomogeneities in the network structure. Note that the disturbances which are created later stop growing at a size when the first disturbances still were growing. We can thus conclude that the growing of an asynchronous region is influenced by the overall distribution of patterns, by the relative fractions of synchronous and asynchronous regions.

An Oscillator in the network is connected by long-ranged connections to other oscillators which are distributed randomly over the network. For larger mean degrees m, the incoming excitations of an oscillator can be considered as a sampling of the mean firing rate in the network. Neighboring oscillators will be subject to sequences of excitations by long-ranged connections which are different but which have similar statistical properties. As approximation, we can assume that every oscillator in the network is subject to a Poisson process which we can regard as a kind of mean field mediated by excitations via long-ranged connections. For a given fraction of long-ranged connections ρ, this Poisson process has a rate of $m\rho\nu(t)$ determined by the firing rate $\nu(t)$ in the network. Similar as for our discussion of continuum models in Chapter 3.4, the assumption of the Poisson process is only exact for the limit of large synaptic failure small-world networks whereas it presents an approximation for Erdős-Rényi small-world networks.

The firing rate $\nu(t)$ of a network in a chimera state consists of distributed firings of the oscillators in the asynchronous regions and a collective pulse originating from the synchronous part (see Figure 4.8 and 4.9 top right). With increasing size of the asynchronous part, the collective pulse will decrease in favor of the distributed excitations. However, also the frequency of the collective pulses changes (see Figure4.8 and 4.9 top left), which we relate to excitations from the asynchronous to the synchronous part of the network. These excitations are received when oscillators in the synchronous part are not refractory and may thus decrease the time to the next collective firing. This is in contrast

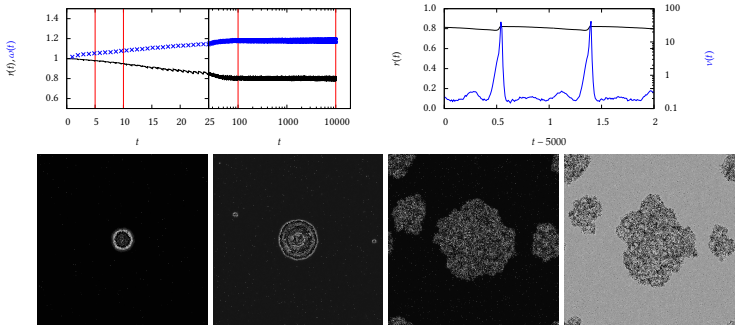

Figure 4.8: Snapshots of the spatial distribution of oscillators phases taken from a spatial network ($N = 500 \times 500, \rho = 0.64, m = 50$) of linear IF oscillators ($\tau = 0.01, \vartheta = 0.05, a = 0.004, b = 0.008$). Phase values range from 0 (black) to 1 (white). As initial condition we chose a small circle of radius 10 with uniformly distributed oscillator phases, other oscillators start with phase 0. Times of snapshots are marked as vertical lines in the top left plot, which shows the time evolution of the order parameter $r(t)$ and the inverse ω ot times between collective firings. The small disturbance with distributed phases grows in size, other asynchronous regions are generated. After asynchronous regions reach a certrain size, their shape is frozen. The top right plot shows a closer view on the firing rate ν and the order parameter $r(t)$ for $t \in [5000, 5002]$.

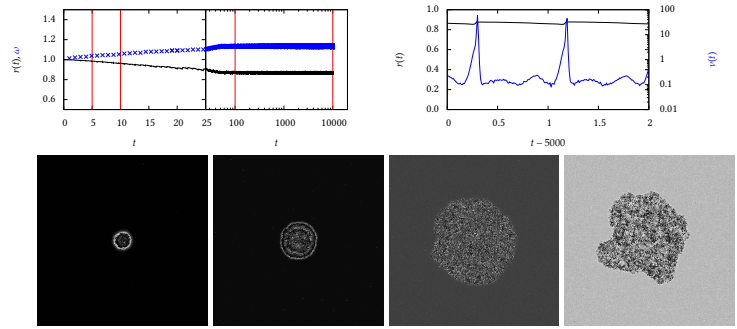

Figure 4.9: Bottom: Same as Figure but for synaptic failure small-world networks with ($\rho = 0.7, m = 50, N = 500 \times 500$).

to excitations which originate from and are received by oscillators in the synchronous parts. As those excitations are received by refractory oscillators, they cannot increase the frequency of the collective firing. In short, the collective pulse becomes weaker and more frequent which changes the local conditions at the boundary of asynchronous regions and influences the speed and the possibility of their growth. When the asynchronous regions reach a critical size, the growth stops and the partition of the network into synchronous and asynchronous regions is frozen. For Erdős-Rényi small-world network additional asynchronous regions were created at inhomogeneities in the network which was not observed for synaptic failure networks which are much more homogeneous. After the partition is frozen, we observe changes in the spatial pattern only on a much larger time scale. Note that the dynamics of the networks in the frozen states is still chaotic (see Figure 4.5), although the dynamics is trapped on a lower dimensional subspace due to the synchronous parts.

We will now investigate the behavior when the size of the synchronous part of the network is much smaller than the preferred size (for the parameters used in Figure 4.8 and 4.9). Note that for Erdős-Rényi small-world networks, the critical coupling strength up to which asynchronous states remain stable is nearly independent on $\rho \in [0.6, 1.0]$. We thus assume that the dynamical behavior is similar to what we can study with random networks. For large coupling strengths these show fast avalanche-like synchronization in which large parts of the network are entrained to a synchronous part during a few oscillations. For small-world media, the emerging spatial patterns are different compared to those that are generated by growing of asynchronous regions. During an avalanche, only those oscillators will be entrained, which also are shortly before the firing threshold. Due to the irregular dynamics such oscillators are distributed all over the network. Accordingly, the emerging synchronous part is distributed over the network, contrasting the connected asynchronous regions that are formed by the growing of asynchronous regions (see Figures 4.10 and 4.11). The large *surface* between the synchronous part and the asynchronous regions seems to favor synchronization as oscillators may be entrained to via short-ranged connections in addition to long-ranged connections; when we compare spatial distributions of oscillator phases with the same order parameter $r(t)$ then $r(t)$ will decrease if the asynchronous regions form connected regions and $r(t)$ will increase if asynchronous and synchronous regions are intertwined. For the transient starting from uniformly distributed phases, this will lead to an overshoot behavior in $r(t)$ (see Figure 4.10).

Synchronization is not complete. As discussed, the size of the collective pulse increases, while its frequency diminishes. At some point, the spatial-temporal

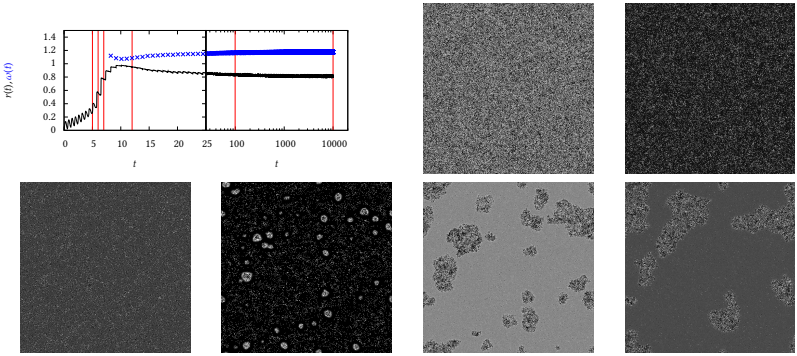

Figure 4.10: Snapshots of the spatial distribution of oscillators phases taken from a directed small-world medium ($N = 500 \times 500, \rho = 0.64, m = 50$) of linear IF oscillators ($\tau = 0.01, \vartheta = 0.05, a = 0.004, b = 0.008$). Phase values range from 0 (black) to 1 (white). Times of snapshots are marked as vertical, red lines in the top left plot, which show the time evolution of the order parameter $r(t)$ and the inverse $\omega(t)$ of times between collective firings. Note the change of scaling at $t = 25$. Starting from uniformly distributed phases, oscillators synchronize rapidly but not completely. A few asynchronous regions remain which grow until they reach a critical size. Afterwards smaller regions shrink and vanish in favor of the larger ones until a partition of the network into synchronous and asynchronous parts is frozen.

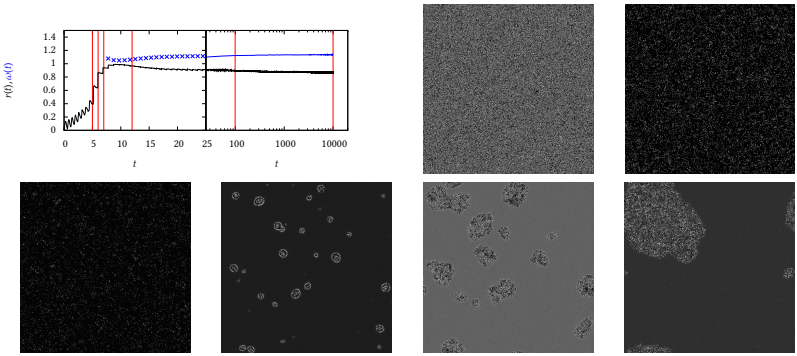

Figure 4.11: Same as Figure 4.10 but for synaptic failure small-world networks with $\rho = 0.7, m = 50, N = 500 \times 500$.

chaotic dynamics becomes resistant to the collective pulse. Synchronization stops when only a few asynchronous regions remain. Afterwards, they grow in size as described before until the stable size of asynchronous regions is reached and the partition is again frozen. On a much longer timescale, the shape and distribution of asynchronous regions also has an influence on their stability and evolution. Even after long periods of time, smaller asynchronous shrink and vanish in favor of larger ones. For synaptic failure small-world networks (see Figure 4.11), the distribution of oscillator phases eventually showed a single connected asynchronous region. This was, however, not observed for directed small-world media during the observation time, in which the dynamics is to a larger degree influenced by inhomogeneities. A circular arrangement of the asynchronous region, minimizes its surface to the synchronous region. It is plausible that such an arrangement is preferred; Assuming this configuration, every deviation from this shape will create an insular which receives more excitations from the synchronous part than other regions. This insular is thus more likely to be entrained than other regions, leading back to the circular shape. However, the chaoticity of the asynchronous region does allow for deviations from the preferred shape to some degree (see Figure 4.11).

We claim that the incompleteness of synchronization can be understood as a resonance phenomenon. A single oscillator has an eigenfrequency of one and is thus best entrained by repeated excitations which arrive with a frequency of one. However, oscillators in a asynchronous region with spatial-temporal dynamics fire on average with a larger frequency and are not susceptible to entrainment by a collective pulse with frequency near 1. To test this hypothesis, we construct lattices with only short-ranged connections in which oscillators are subject to a periodic forcing. The lattices are meant to describe a small region in a small-world network whose influence on the whole network can be neglected. The forcing consists of, firstly, Poissonian excitations which represent excitations originating from other asynchronous regions in the network, and secondly, a collective pulse consisting of a large number of concurrently arriving excitations distributed randomly over the small network. The latter represents excitations from other synchronous parts of the large network. In a way the considered lattices represent small-world media which are simplified in such a way that we have constant conditions. In Figure 4.12, we show the influence of the time T between collective pulses on the emerging order parameter of the network. As initial condition, we chose a distribution of phases which contains both synchronous and asynchronous regions.

As expected, the lattice synchronizes according to this external forcing only for frequencies of the collective pulse in a small range of values below 1. For

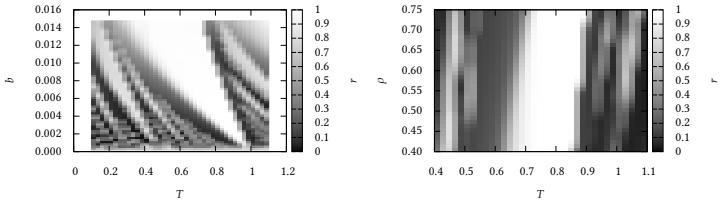

Figure 4.12: Average order parameter r assessed in $t \in [100, 200]$ of lattices of linear IF oscillators ($a = 0.0055, b = 0.011, \vartheta = 0.05, \tau = 0.01$) subject to external forcing. Starting from a square lattice ($N = 150 \times 150$) in which each oscillator is connected to its 50 nearest neighbors, a fraction ρ of connections is removed without subsequent addition of connections. The lattices are forced by collective pulses with period T in which $25N$ times a randomly chosen oscillators is excited. Furthermore, every oscillator in the lattice is subject to Poissonian excitations with rate 12.5. Left: influence of T and b on r for $\rho = 0.65$, right: influence of T and ρ on r for $b = 0.005$.

$T \approx 1$, the networks are not susceptible to the applied forcing as the effective frequency of oscillators mismatches the pulse frequency. The range of values of T which lead to synchronization shifts to smaller frequency values when the lattice structure is strengthened, either by increasing the number of local connections or by increasing the coupling strength. This can be expected as both increase the effective frequency of oscillators in asynchronous regions. In addition to the region in which frequencies match, we observe emerging order in the lattices also, when the frequencies satisfy simple rational relationships, which correspond to synchronization phenomena in which the modelled lattices produces a rhythm which coincides with the external pulse only for some subset of the collective firings.

For the chimera states, we have described an entrainment to the asynchronous part mediated by short-ranged connections (see Figure 4.8 and Figure 4.9) and an entrainment to the synchronous part mediated by long-ranged connections (see Figure 4.10 and Figure 4.11). However, for the forced lattices we can also observe the other two cases of entrainment to the synchronous part via short-ranged connections and entrainment to the asynchronous part via long-ranged connections. In Figure 4.13, we show snapshots of the time evolution of the 4 cases of synchronization/desynchronization mediated by short/long-ranged connections. Interestingly, we observe different behaviors at both bound-

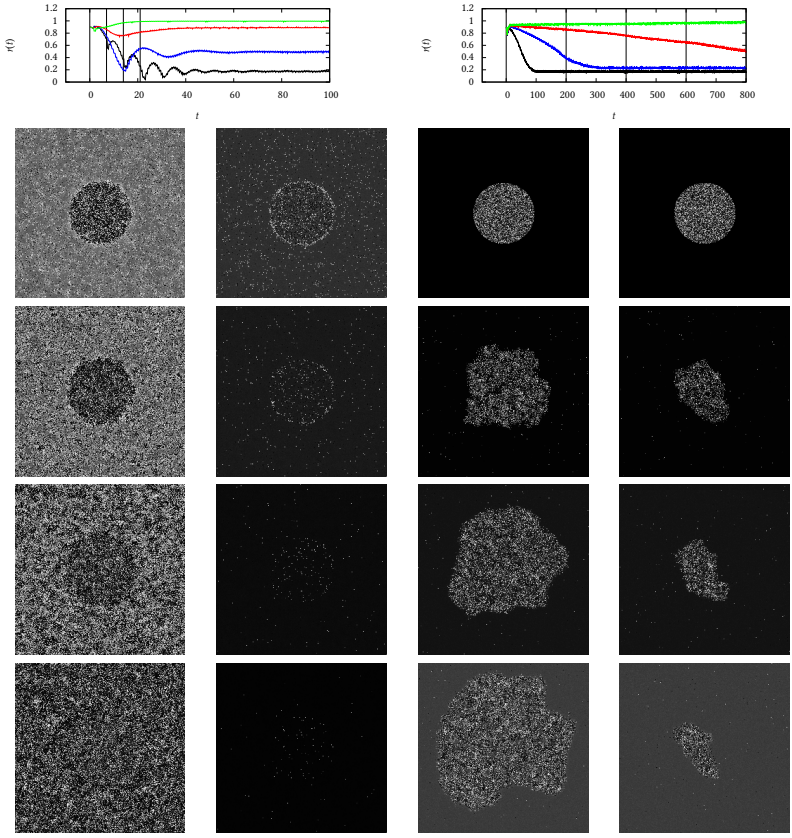

Figure 4.13: : exemplary time evolutions of the order parameter taken from the parameter scan presented in Figure 4.12. Left: parameter values at the left boundary of the range of period durations T which leads to synchronous states for $\rho = 0.65, b = 0.004$, black: $T = 0.7$, blue: $T = 0.74$, red: $T = 0.76$, green: $T = 0.79$. Right: $b = 0.005, T = 0.9$ which is at the right boundary of the range of period durations which lead to synchronous states. Black: $\rho = 0.65$, blue: $\rho = 0.7$, red: $\rho = 0.72$, green: $\rho = 0.73$. Bottom: Snapshots of the spatial distribution of oscillator phases taken from the black curve in the top left plot (1st column), green curve top left plot (2nd column), red curve top right plot (3rd column), green curve top right plot (4th column). Times of snapshots are indicated as vertical lines in the top plots.

aries of the resonance region. When T is too small, the synchronous regions become unstable. At this boundary we observe states in which all regions in the lattices, locally, show similar amounts of order. The order parameter can take any value and synchronization and desynchronization depends on the long-ranged connections. At the other boundary, we observe no partially synchronous states. When starting from a state which is split into synchronous and asynchronous regions, we observe either growing or shrinking of asynchronous regions. Although transients can become quite long, the dynamics eventually settles to synchrony or asynchrony.

Let us return to the small-world media and be a bit more concrete how these compare to the forced lattices. For large networks, we can consider point process of incoming excitations as a mean field which is mediated by long-ranged connections. This mean field consists of concentrated excitations due to the firing of the synchronous part complemented by distributed excitations due to the firing of the asynchronous part. The mean field depends on the relative sizes of synchronous and asynchronous parts (which can be related to the order parameter) and only marginally on the spatial pattern they form. We will thus write $F_r(t)$ to denote the periodic mean field that is generated for a given order parameter r, assuming the sizes of synchronous and asynchronous regions were stationary. Note that the adaption of the frequency of the collective pulse is related to the refractory periods that we chose for the oscillators and can probably not be observed without them. When oscillators are excitable at the moment of firing, the timing of excitations has a much smaller influence on the frequency as with increasing size of the synchronous part, the synchronous part receives more and more self-excitations which increase the frequency just as excitations from asynchronous regions do.

For the forced lattices, we can observe synchronization and desynchronization both as volume and as surface phenomenon. For small-world networks in the parameter regime spanned by ρ and b, however, only synchronization as a volume phenomenon and desynchronization as a surface phenomenon seems to play a role. With an eye on the non-converging behaviors that we shall describe in the next chapter, we define two sets S and D, which will aid us in our explanation in which way non-converging behaviors are generated. Note that we do not measure or calculate S and D. Let us assume a distribution of oscillator phases in which synchronous and asynchronous regions are separated. We define

$D \subset [0, 1]$ set of order parameters r, for which the mean field $F_r(t)$ generated by excitations via long-ranged connections allows for growing of asynchronous regions,

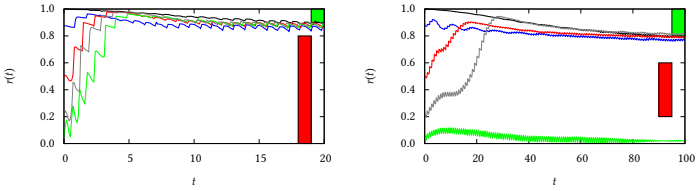

Figure 4.14: Time evolution of the order parameter $r(t)$ for directed small-world media ($N = 500 \times 500, \rho = 0.65, m = 50$) of linear IF oscillators ($\tau = 0.01, \vartheta = 0.05$). Other oscillator parameters were $a = 0.005, b = 0.01$ for the left and $a = 0.00175, b = 0.0035$ for the right plot. Initial condition: uniformly distributed phases for all oscillators within a distance R of some chosen oscillator, $\phi = 1$ for other oscillators. Different radii R were chosen for the circular, asynchronous region: black: $R = 10$, blue: $R = 100$, red: $R = 200$, grey: $R = 250$, green: $R = 300$. The red and green bars outline S and D, respectively (see text). As both bars do not overlap, we can observe chimera states for both parameter choices of the left and right plot. For the right plot asynchronous states are also stable.

$S \subset [0, 1]$ set of order parameters r for which the mean field $F_r(t)$ generated by excitations via long-ranged connections allows for entrainment of oscillators in the asynchronous regions to the synchronous part.

Note that once entrainment of asynchronous regions (as defined in S) sets in, the distribution of patterns shows no longer a separation of synchronous and asynchronous regions such that r will increase above values which are no longer part of S. Regarding time evolutions of $r(t)$, we can interpret S and D graphically: S can be regarded as the set of values from which the order may jump to a larger value, while order parameters in D allow for a steady decrease of $r(t)$. Chimera states and a preferred size of asynchronous regions in the network, can be related to the fact that S and D do not overlap. In Figure 4.14, we show time evolutions of $r(t)$ starting from initial conditions with different order parameters. Both routes to the chimera state—starting from asynchronous regions which are either smaller or larger than the preferred size—rely on different dynamical mechanism: The growing of asynchronous regions is a surface effect between the different regions and relies on the short-ranged connections. Synchronization of asynchronous regions from within, on the other hand, is mediated by

long-ranged connections. By changing the fraction of long-ranged connections, we can thus expect to control the relative strength of both mechanism. It is conceivable that we can, for a given partition into synchronous and asynchronous regions, chose parameters such that only one or both mechanism are possible. Moreover, it seems conceivable that the growing of asynchronous regions does not stop but continues until the network is again susceptible to the forcing of the mean field which is created by the long-ranged connection, which means that the sets S and D overlap. This is what happens in the small regions with non-converging behavior we are left to describe.

4.3 Non-converging behavior

It is a common observation in dynamical systems which are designed to model spatially extended, natural systems that local observables are a lot more irregular and fluctuating than macroscopic ones. Although the local dynamics may be stochastic (as for Brownian motion) or chaotic (as for turbulent flows), governing equations for global observables of large systems often show convergence to either fixed points or simple limit cycles. Intriguingly, small-world networks of linear IF oscillators support different kinds of non-converging collective behaviors when the number of short- and long-ranged connections is comparable ($\rho \approx 0.5$). The order parameter in these states also shows small amplitude oscillations, which reflect the average phase velocity of oscillators. However, these oscillations range around absolute values which themselves may exhibit complicated time evolutions. To distinguish non-converging from limit cycles behavior, we calculate the series of local maxima $\bar{r}(t)$ of $r(t)$. In this way, we have eliminated the small amplitude oscillations. Both asynchronous states and limit cycles will lead to constant values of $\bar{r}(t)$, while more complicated time evolutions can be assessed by a statistical property of $\bar{r}(t)$ which characterizes fluctuation. In Figure 4.15, we show the range of assumed values of $\bar{r}(t)$ after transients for different network sizes. While the mean of $\bar{r}(t)$ provides similar information as the mean of $r(t)$ itself (see Figure 4.1 top left), the range of assumed values reveals a region around $\rho = 0.5$ with non-converging network activity. For the considered network sizes N, the fluctuations in $\bar{r}(t)$ do not decrease with N, nor does the size of the region in parameter space decrease. We therefore assume, that the behavior is not a consequence of finite-size effects but has a different dynamical origin. In Figure 4.15 bottom right, we show a closer view of the parameter region with non-converging behavior. Compared to the chimera states, the non-converging collective behaviors are observed at smaller ρ at which asynchronous regions

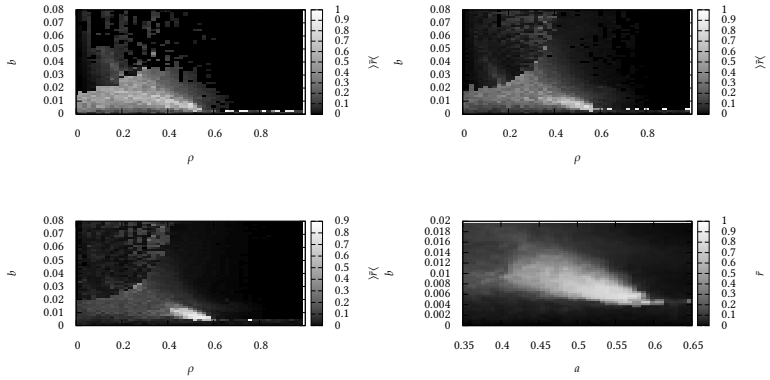

Figure 4.15: Range $\langle \bar{r} \rangle$ of local maxima of r observed in $t \in [100, 200]$ for directed small-world media ($m = 50$) of linear IF oscillators ($\tau = 0.01, \vartheta = 0.05$) in dependence on the fraction of long-ranged connections ρ and oscillator parameters $b = 2a$. Different lattice sizes were chosen: $N = 50 \times 50$ (top left), $N = 100 \times 100$ (top right), $N = 250 \times 250$ (bottom left and right). Bottom right: Closer view of the region with non-converging behavior.

are growing until synchronization may set in, leading to a constant interplay of synchronization and desynchronization phenomena. In the following, we will discuss now the different dynamical behaviors that emerge, traversing the region with non-converging behavior in direction of increasing b.

For small b directed and undirected small-world media exhibit asynchronous behavior which is for all practical purposes stable; transients starting from some distribution of synchronous and asynchronous regions show growing of the latter until they cover the whole network (see Figure 4.16). Regarding our definitions, S is empty, while D covers nearly the whole unit interval.

When we increase the coupling strength, the asynchronous states loose stability and their lifetimes assume values such that we can observe transitions. The networks show long periods of asynchronous behavior before a phase cluster is formed and the networks spontaneously start to synchronize. The behavior is similar to the chaotic transients leading to complete synchrony that can be observed for random networks (see Figure 3.14 top left and Figure 3.15, and

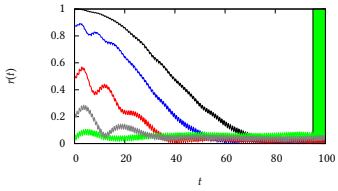

Figure 4.16: Time evolution of the order parameter $r(t)$ for directed small-world media ($N = 500 \times 500, \rho = 0.5, m = 50$) of linear IF oscillators ($\tau = 0.01, \vartheta = 0.05, a = 0.00175, b = 0.0035$). Initial condition: uniformly distributed phases for all oscillators within a distance R of some chosen oscillator, $\phi = 1$ for other oscillators. Different radii R were chosen for the circular, asynchronous region: black: $R = 10$, blue: $R = 100$, red: $R = 200$, grey: $R = 250$, green: $R = 300$. The green bar outlines D (see text). S is empty as Synchronization along long-ranged connections is not possible for the chosen parameters. (cmp. Figure 4.14).

Figure 3.23). Here, synchronization is not complete but stops when the networks exhibit only a few small asynchronous regions embedded in a synchronized background. These asynchronous regions grow until they cover the whole network, and the dynamics reenters the quasi-stable asynchronous state. The emerging network behavior can be described as short, spontaneously generated events of synchrony which are embedded into extended periods of asynchronous behavior. In Figure 4.17 top, we show a time evolution of the order parameter for this behavior. For larger lattice sizes, the macroscopic observables of events show very similar progressions. However, the spatial patterns which are formed by the oscillator phases are different for every event. Note that for synaptic failure small-world media, asynchronous states are unstable even for arbitrary small phase responses. Therefore, we cannot observe events in those networks for our choice of parameters. When we further increase the coupling strength, the frequency of events increases (see Figure 4.17 bottom right). The escape from the quasi-stable asynchronous state becomes faster, similar as we observed for random networks where transients lead to complete synchrony. The shape and dynamics during events, however, is nearly unaffected. The rewiring probability has an influence on the duration of events (see Figure 4.17 bottom left); when the lattice structure is weakened, growing of asynchronous regions becomes slower and eventually stops. At this point, the event is turned into a

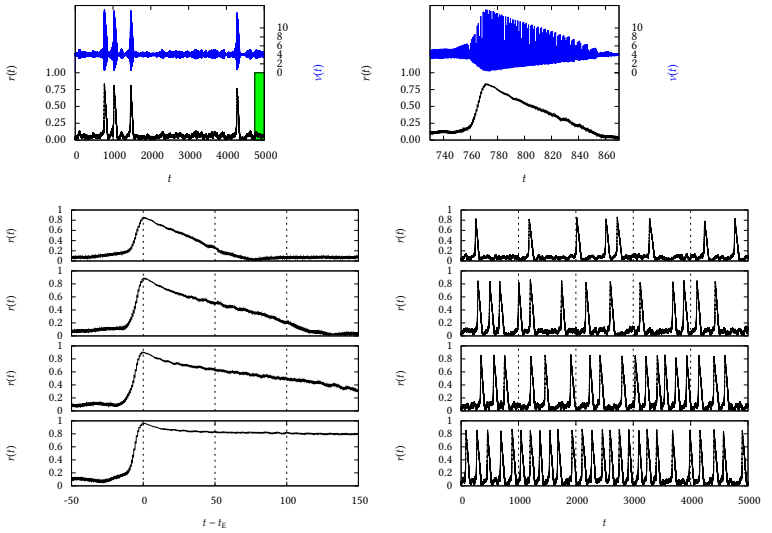

Figure 4.17: Top: Time evolution of the order parameter $r(t)$ and of the firing rate $\nu(t)$ for a directed small-world medium ($\rho = 0.56$) of linear IF oscillators ($b = 0.004$). The right plot shows a closer view on the first event of synchronous behavior. For the chosen parameters D (indicated as the green bar) contains the whole unit interval. Synchronization is not possible and S is therefore empty. However, the asynchronous states are unstable synchronize spontaneously with a small probability. Initial condition: uniformly distributed phases. Bottom left: $r(t)$ obtained from small-world media of linear IF oscillators ($b = 0.0045$) with different fraction of long-ranged connections ρ. From top to bottom: $\rho = 0.55$, $\rho = 0.57$, $\rho = 0.59$, $\rho = 0.64$. Events are aligned such that the maximum value of $r(t)$ lies at $t = 0$. With increasing ρ growing of asynchronous regions slows down and eventually stops, leading to chimera states. Bottom right: $r(t)$ for $\rho = 0.56$ and different phase responses. From top to bottom: $b = 0.0042$, $b = 0.0044$, $b = 0.0046$ and $b = 0.0048$. With increasing coupling strength, the times of asynchronous behavior between events diminishes, while the shape of events is nearly unchanged. Additional parameters chosen for the networks in this plot were $a = 0.5b, \tau = 0.01, \vartheta = 0.05, m = 50, N = 250 \times 250$.

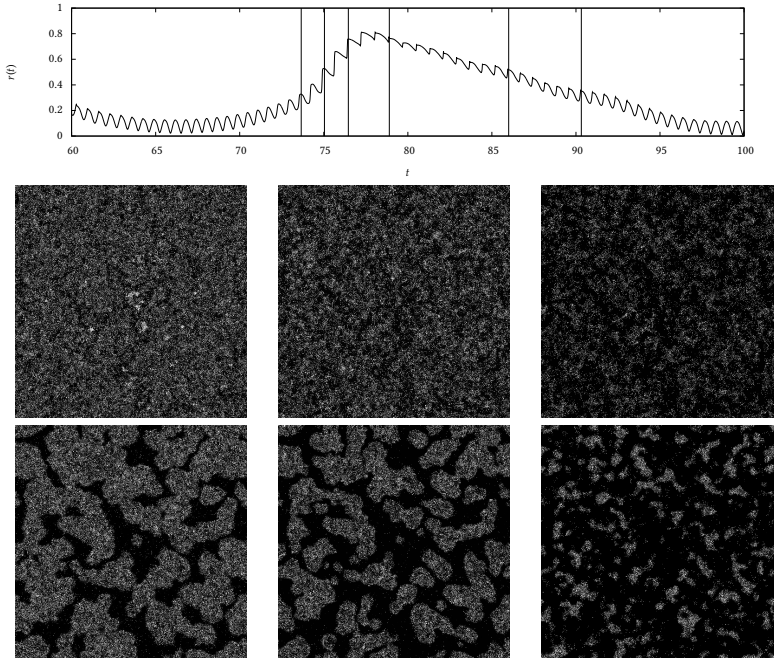

Figure 4.18: Top: Closer view of the first event of Figure 4.17 top left. Bottom: snapshots of the spatial distribution of oscillator phases. Times of snapshots are indicated as vertical lines in the upper plot. Times at which snapshots were taken increase in the first row and decrease in the second row, such that snapshots which lie under another relate to the same order parameter r.

transient to a chimera state, similar as described in Figure 4.10. In Figure 4.18, we show a closer inspection of the dynamics during a single event. Let us compare the distribution of patterns at times on the ascending and descending parts of events which have the same value of $r(t)$. Note that a snapshot of the spatial distribution of phases, as presented in the lower part of Figure 4.18 represents the complete state space of the system. The time evolution is thus fully determined by the pattern which must differ at the ascending and descending parts of events. Similar as for the transients to chimera states, the synchronous re-

gion is distributed over the network at the ascending parts and forms connected regions at the descending parts.

Note that the generation of the events does not rely on leakyness of oscillators; in fact, all of the dynamical behaviors that we discuss in this chapter can be observed for $a = 0$. For the sake of an investigation of statistical properties of the events, we searched for parameters for which events are generated by smaller network sizes, such that the characteristic behavior is not masked by finite-size effects. Observing networks of $N = 75 \times 75$ oscillators, we measure statistical properties of the distribution of events in time (see Figure 4.19).

The measured durations between events is consistent with an exponential distribution. Moreover, we find no correlation between subsequent durations between events. The events are thus distributed in time similarly as if generated by a Poisson process. This means, that the probability for an event to occur is constant during the time the networks show asynchronous behavior. Moreover, this can be regarded as an indication that events are difficult to predict. Events themselves show a duration T_E that is characteristic and varies little.

Due to the smaller network sizes, we can expect significant differences for networks which are constructed using the same parameters. In Figure 4.19 middle left, we show the mean duration between events for 15 networks starting from 15 different initial conditions. While the initial condition has only a minor influence on the distribution of durations between events T_A, different constructed networks show a large deviation of the average duration $\langle T_\mathrm{A} \rangle$ of a few hundred percent. Which differences in the constructed networks are responsible for these large differences requires further investigations.

With increasing b, $\langle T_\mathrm{A} \rangle$ decreases until events immediately start as soon as the whole network is covered with asynchronous regions. At this point the networks generate a periodic macroscopic behavior, which is much slower than the frequency of single oscillators and which is an emerging property of the network, not directly related to their timescales (τ and ϑ). In Figure 4.21, we show different examples of emerging rhythms. The dynamics during one oscillation is very similar as presented in our description of a single event (Figure 4.18). The frequency of the network rhythm is determined by the size of phase responses and thus by a and b. For small phase responses, patterns of arbitrary type change over the course of many oscillations only, and thus both the period duration of the rhythm or the duration of extreme events is large. We can shift the values of a, b which lead to oscillatory behavior to smaller values, by increasing τ and ϑ (and keeping their relation fixed). This allows us to control the frequency of the network rhythms. A further increase of b leads to non-converging behavior in which synchronization may set in even before the network is completely asyn-

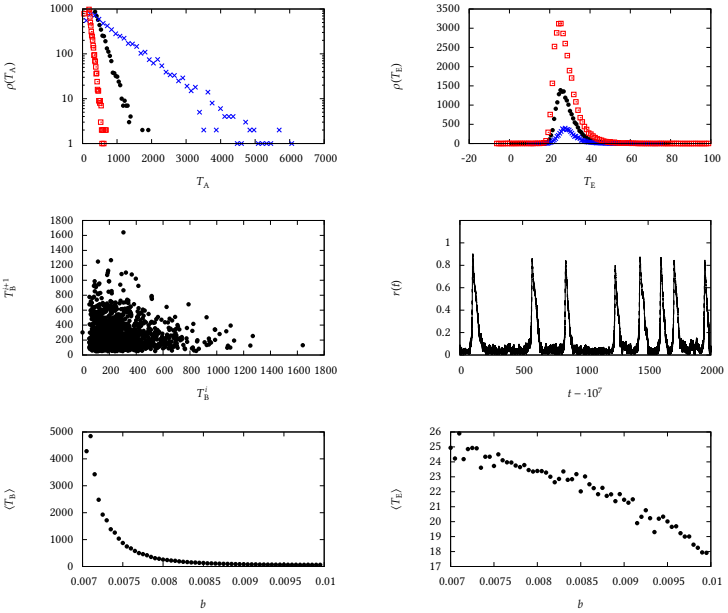

Figure 4.19: Top left: frequency distribution $\rho(T_A)$ of times between synchronous events T_A in directed small-world networks of non-leaky IF oscillators. Blue: $b = 0.0075$, red: $b = 0.008$, green: $b = 0.0085$. Top right: distribution of event durations T_E. Event beginnings and ends were determined by threshold crossings at $r = 0.2$. A single simulation was used for each of the given distributions. Middle left: correlation between subsequent inter event durations ($b = 0.008$). Middle right: exemplary section of the time evolution of $r(t)$ for $b = 0.008$. Bottom left: mean duration between events in dependence on b, bottom right: mean event duration in dependence on b. Other parameters used for the simulations in this plot: ($N = 75 \times 75, m = 50, \rho = 0.55, \tau = 0.01, \vartheta = 0.05, a = 0$).

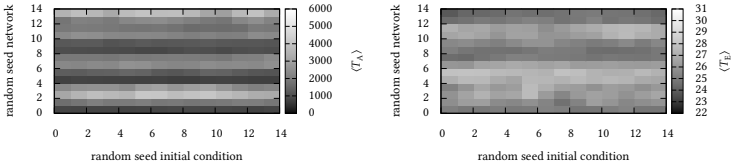

Figure 4.20: Mean duration between events $\langle T_A \rangle$ (left) and mean duration of events $\langle T_E \rangle$ (right) for different constructed networks of the same parameters ($N = 75 \times 75, m = 50, \rho = 0.55$) starting from different sets of uniformly distributed initial phases as initial conditions. Oscillator parameters:$\tau = 0.01, \vartheta = 0.05, a = 0, b = 0.0075$.

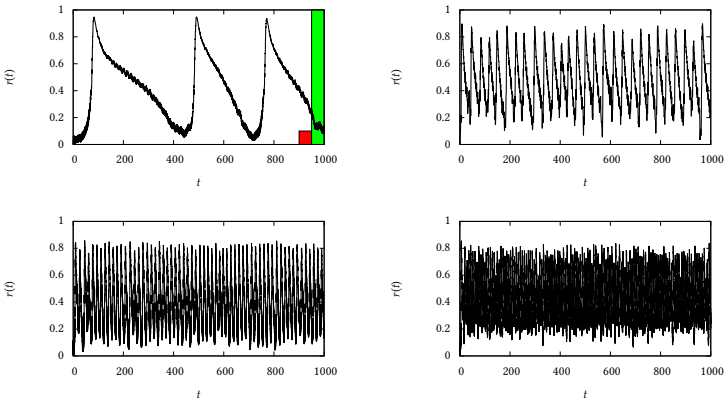

Figure 4.21: Time evolution of $r(t)$ for directed small-world media ($N = 250 \times 250, m = 50, \rho = 0.54$) of linear IF oscillators. Oscillator parameters: top left: $(a, b, \tau, \vartheta) = (0.0, 0.005, 0.02, 0.1)$, top right: $(0.0, 0.012, 0.01, 0.05)$, bottom left: $(0.0, 0.014, 0.005, 0.025)$, bottom right: $(0.0, 0.0165, 0.002, 0.01)$. The red and green bars outline S and D, respectively (see text).

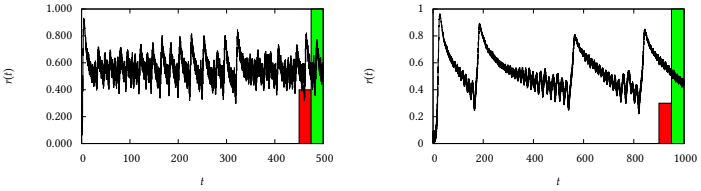

Figure 4.22: Time evolution of the order parameter $r(t)$ for directed small-world media ($N = 250 \times 250, m = 50, \rho = 0.54$). Left: oscillator parameter :$(a, b, \tau, \vartheta) = (0.007, 0.014, 0.01, 0.05)$, right: $= (0.00325, 0.0065, 0.02, 0.1)$. The red and green bars outline S and D, respectively (see text).

chronous. Naturally, this decreases the range of fluctuations that we observe in macroscopic observables and may lead to complicated and irregular behavior (see Figure 4.22).

If we further increase b, the range of fluctuations in $r(t)$ vanishes and we observe constant macroscopic observables in states in which synchronization and desynchronization phenomena continuously interplay. In contrast to the chimera states, however, these states are accompanied by highly volatile spatial patterns (see Figure 4.23) which grow at boundaries and are synchronized from within at the same time.

Let us summarize our observations of the different macroscopic behaviors which are generated when networks split into asynchronous and synchronous regions. In Figure 4.24 we show a closer view of the region in the (ρ, b)-plane in which networks show non-converging behavior with markers at the parameters that we used when describing the different dynamical behaviors.

In Figure 4.24 we show a schematic of the parameter regime with non-converging behavior. For our networks and in dependence on the parameters, the evolution of these patterns is determined by growing of asynchronous regions and synchronizations of these regions via long-ranged connections. The possibility for either of these phenomena is influenced by the amount of order in the network, i.e., the cumulative size of synchronous regions in the network. We described the possibility of both phenomena by the set of values of r for which avalanche-like synchronization may set in (S), and the set of values for which growing of asynchronous regions is possible D. Graphically, this means that if r is in D, then the order parameter r will decrease as asynchronous regions are growing. When r is in S, then r will *jump* to larger values during the next few oscillations due to

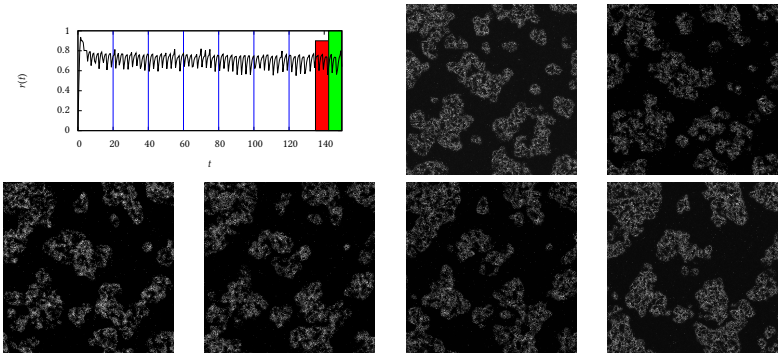

Figure 4.23: Snapshots of the spatial distribution of oscillators phases taken from a directed small-world medium ($N = 500 \times 500, \rho = 0.5, m = 50$) of linear IF oscillators ($\tau = 0.01, \vartheta = 0.05, a = 0.008, b = 0.016$). Phase values range from 0 (black) to 1 (white). Times of snapshots are marked as vertical lines in the top left plot, which shows the time evolution of the order parameter $r(t)$. The networks show volatile spatial patterns in which synchronization and desynchronization phenomena facilitate an equilibrium in the size of asynchronous pattern.

avalanche-like synchronization. The generation of the non-converging behavior, relies on the situation that exactly one of both phenomena is possible for a given amount of the order in the network, such that both synchronization and desynchronization phenomena may take turns. For ρ values which are larger than those of the region with non-converging behavior, S and D do not overlap such that growing of asynchronous regions is only possible for larger values of r and stops at some value of r which is neither in S nor in D. At this point the spatial pattern is frozen into a nearly immobile chimera state (regime II and I of Figure 4.24). For coupling strengths below the region with non-converging behavior, synchronization is not possible even when asynchronous regions cover the whole network. For b values above the circumscribed region both synchronization and desynchronization phenomena are possible at the time, leading to an equilibrium of asynchronous regions which are growing and are synchronized from within at the same time. Finally, for small values of ρ and large values of b, the lattice-structure is enforced and the networks eventually exhibit wave-like patterns at which point the dynamics is no longer governed by these

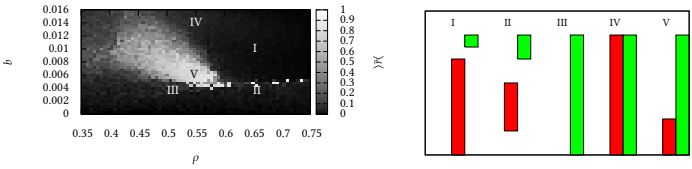

Figure 4.24: Left: Partition of the (ρ, b) into regimes according to the presence or absence of (de-)synchronization phenomena (cmp. Figure 4.15). I: chimera states (cmp. Figure 4.14 left), II: chimera states co-existing with asynchronous states (cmp. Figure 4.14 right), III: asynchronous states (cmp. Figure 4.16, IV: volatile asynchronous patterns (cmp. Figure 4.23), V: non-converging collective behavior (Figure 4.21 and 4.22). Right: sketch of the range of value of the order parameters S for which synchronization may set in (red) and range D for which growing of asynchronous regions is possible (green) indicated as bars schematically.

two distinct routes to synchrony that we described for the chimera states.

Linear IF oscillator without refractory periods and time delays

In Chapter 3.3, we described for random networks two transitions at which asynchronous states loose their stability. We investigated these transitions both for linear IF oscillators with and without refractory periods and time delays. In this chapter, we then chose one of the more simple transitions and continued it into the small-world regime. A detailed of the analysis of the dynamical behaviors that can arise at the other transitions, in particular those at which we observed partially synchronous states and irregular behavior, is left for future studies. We will, however, provide some indications which parts of the dynamical behaviors can be expected to carry over to linear IF oscillators without refractory periods. The line which is parallel to the b-axis and runs through $a = 0.004$ crosses both boundaries of the asynchronous regime with increasing b. We can thus continue both transitions into the small-world regime when we choose $a = 0.004$, and study the dynamical behavior in dependence on b and on the fraction of long-ranged connections ρ (see Figure 4.25). It suggests itself to compare the dynamics near the upper boundary with the dynamics of oscillators with refractory periods. From Figure 4.25, we find no indication for wave-dominated or

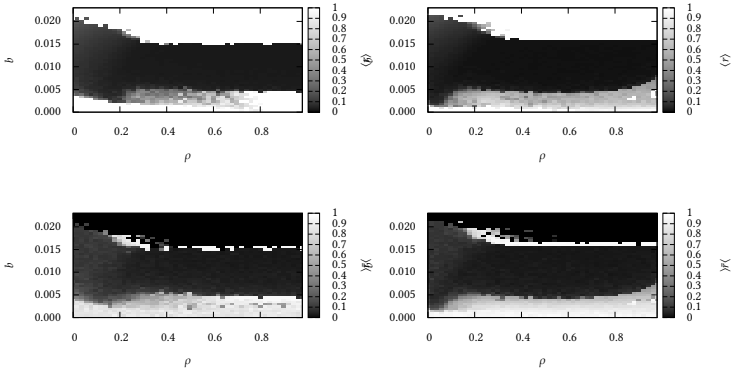

Figure 4.25: Statistical properties of the order parameter $r(t)$ of small-world networks of linear IF oscillators in dependence on the fraction of long-ranged connections ρ and the oscillator parameter b. Other oscillator parameter: $a = 0.004, \tau = 0.0, \vartheta = 0.0$. Network parameter: $N = 10000, m = 50$. Top: average order parameter $\langle r \rangle$, bottom: range $\rangle \bar{r} \langle$ of local maxima of r. Values were obtained for $t \in [100, 200]$. Left: directed small-world media, right: synaptic failure small-world media.

chimera states above the transition to synchrony at $b \approx 0.015$. We do, however, observe a small region with non-converging behavior around $\rho \approx 0.25$. In Figure 4.26 left, we show an exemplary time evolutions of the order parameter in this region. The behaviors seem comparable to the short events of synchronous firing that we described in this chapter. However, this point requires further investigations. Even more complicated behavior can be expected near the lower boundary. Note that the mechanism that lead to the irregular collective behaviors that we described, are different for random networks and for spatial networks. In random networks the irregular behaviors seemed related to a build up in synchrony and avalanches which introduce a gap in the phase distribution of oscillators. For spatial networks irregular behavior is generated due to the dual structure of the networks which allows for synchronization/desynchronization as mediated by either short- or long-ranged connections. It seems obvious that even more complicated behaviors can be observed when we choose parameters which enable both sources of irregularity, i.e. by continuing the irregular be-

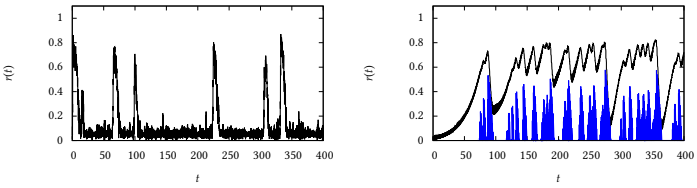

Figure 4.26: Top: Time evolutions of the order parameter $r(t)$ for linear IF oscillators without refractory periods and time delays. Left: directed small-world network with $a = 0.004, b = 0.016, m = 50, \rho = 0.26, N = 10000$, Right: synaptic failure small-world network with $a = 0.002, b = 0.003, m = 50.0, \rho = 0.5, N = 250000$. The right plot also contains Avalanche sizes indicated as blue lines.

havior that we observed near the lower boundary into to small-world regime (see Figure 4.26 right). Equally, the behaviors that can be observed here require further investigations.

4.4 Summary

We investigated the dynamics of linear integrate-and-fire-like oscillators coupled onto spatial networks which have both short and long-ranged connections (small-world networks). We focused on linear IF oscillators endowed with time delay and refractory periods.

Small-world networks represent a mixture of two well-studied organization structures, namely random networks and regular lattices. Accordingly, we can expect to observe their typical dynamical behaviors also for small-world networks. Moreover, we reported on several dynamical behaviors that uniquely rely on their dual structure and thus underline their importance for modeling, especially in contexts of social networks or neural networks. In the small-world regime, the formation of spatial patterns co-occurs with collective organization mediated by long-ranged connections. While lattices allow for different kinds of wave phenomena, random networks allow for synchronous and asynchronous collective motion. In small-world networks we can observe combinations of both behaviors co-occurring (e.g. cyclic waves with collective motion or turbulent-like waves without collective motion, etc.).

Furthermore, we observed dynamical behaviors, which rely on the co-occurrence of synchronous and asynchronous motion. In random networks, we can choose

parameters in such a way that both are stable. However, we did not observe both at the same time, because they are too tightly knit together. In contrast, networks with a spatial dimension as the small-world networks allow for the necessary spatial separation, that enables a self-organized split of the network into synchronous regions (sharing a common phase) and asynchronous region with distributed phases and unstructured spatial patterns. These split states are commonly denoted as chimera states [124], and they introduce two distinct routes to synchrony/asynchrony. Depending on parameters and dynamical properties, the asynchronous behavior may turn unstable and be entrained to the synchronous part of the network. Similarly, the synchronous behavior may turn unstable and be entrained to the asynchronous part of the network. In these cases entrainment is mediated by long-ranged connections. Moreover, we can observe entrainment at the boundaries between synchronous and asynchronous parts as a surface phenomenon; asynchronous regions may grow or shrink in which case entrainment is mediated by short-ranged connections. Both routes are influenced by network parameters and by the relative sizes of synchronous or asynchronous regions in the network. For example, we found parameters in which growing of asynchronous regions is only possible while their total size in the network is small, and asynchronous regions are only unstable when their total size is large. Depending on the possibility of (de-)synchronization over both routes, we can observe various kinds of non-converging macroscopic behaviors.

The dynamics of a neuronal network is the most obvious context for our dynamical system. In the following paragraphs we will interpret our findings with regard to such networks. One of these non-converging behaviors are events of partially synchronous firing which are embedded in extended periods of asynchronous behavior of variable length. From a quantitative point of view, this behavior is comparable to the dynamics seen in epilepsy patients: The standard accepted notion is that epileptic seizures represent short periods of overly synchronous firing, while the normal functioning of the brain is usually connoted with asynchronous firing. However, the mechanisms which lead to transitions into and out of seizures are still unclear for many types of epilepsy [125,126]. Recent computational models of epileptic brain networks usually consider a noise-induced attractor switching which leads to exponentially distributed seizure and inter-seizure times [127–130]. However, especially so-called focal epilepsies are often related to seizure-times which follow a modal distribution, which possibly points to a mechanism which is responsible for seizure termination. The merit of our work may be to display a mechanism for desynchronization which persists even without inhibitory interactions and noise, and which could be comparable to the dynamics seen during the initiation and termination of epileptic seizures.

A different non-converging behavior that can be observed in the small-world regime is an emergent rhythm which is much slower than the firing of single oscillators. By changing network or oscillator parameters, we can control the frequency of this rhythm nearly arbitrarily. The mechanism of this oscillation may improve, e.g., our understanding of the generation of the respiratory rhythm. The latter is generated in a small brain region, the so-called Pre-Bötzinger Complex, and persists in small slices even when inhibition is blocked pharmacologically [131]. The mechanisms which lead to this generation are unknown and are believed to be a network phenomenon.

5 Conclusions

In this thesis, we have investigated the dynamics and in particular synchronization phenomena seen in complex networks of pulse-coupled oscillators. Complex networks appear ubiquitously in nature. An important question is in which way their dynamical behavior and in particular macroscopic properties are influenced and determined by the structure of the network and by the dynamics of constituents.

A fundamental question is whether the dynamical systems allows for stable macroscopic behaviors such as stable equilibria or phase-locked states, or if fluctuations and/or chaotic motion extent to the macroscopic scale. Fluctuations and in particular extreme events (like epileptic seizures, stock market crashs or tornadoes) in macroscopic observables are often connected to disastrous financial and personal consequences. It is therefore important to understand the mechanism that lead to their emergence, and possibly, to predict or even control their occurrence. For our investigations, we focused on random networks and on spatial networks which reflect the strong prevalence towards short-ranged connections in many spatially extended networks. As random networks, we investigated the emerging dynamics of Erdős-Rényi and of synaptic failure networks. These networks assume that for each pair of nodes, a connection (for Erdős-Rényi networks) or an interaction (for synaptic failure networks) is equally likely, and they are obvious first candidates for modeling purposes when the knowledge about the underlying connection structure is limited. In addition, to synchronous and asynchronous states, we observed different kinds of more complicated behaviors which show irregular macroscopic behaviors even for large networks and after long periods of time. To improve our understanding of these networks, especially for larger arrangements, we investigated several continuum models, which provide a macroscopic point of view onto the dynamics. This investigation allowed us to provide statistical properties of oscillators (like their phase distribution) analytically and to unravel the mechanism that leads to the loss of stability of the asynchronous behavior.

For synaptic failure networks of integrate-and-fire-like oscillators, we found two different mechanisms that lead to synchronous motion in large networks. The equilibrium phase distribution that we associated with asynchronous behavior may disappear for certain choices of oscillator and network parameters,

or it may turn unstable leading first to oscillations and finally to irregular macroscopic behaviors which persist for large networks and after long periods of time. A specific dynamical feature of our oscillators are avalanches in which a macroscopic amount of oscillators fires in a short period of time. We related these avalanches to the generation of the irregular macroscopic behaviors in which synchrony builds up and is recurrently aborted by avalanches. Synaptic failure networks represent a significant simplification to Erdős-Rényi networks. Nevertheless, the generated dynamical behaviors that emerges from both types of networks is often surprisingly similar. The continuum model tailored to Erdős-Rényi networks that we proposed may further our understanding of the difference between both models. Although it cannot be expected to represent the limit dynamics of Erdős-Rényi networks completely, it yields a refined approximation. A detailed analysis of this equation is left for future studies. We are confident that the introduced methodology and the proposed continuum models could improve the understanding of other system that can be described by phase response curves.

In the second part of this thesis, we investigated the dynamics of small-world networks. These are networks with a lattice structure which is complemented by some amount of long-ranged connections. These networks represent a bridging generalization of regular lattices and random networks and allow for the interplay between synchronization phenomena and spatial patterns. We described different kinds of wave patterns which may co-occur with collective firing, or may dominate the dynamics in such a way that macroscopic observables show constant behavior. Additionally, we observed a variety of states in which asynchronous and synchronous behavior occurs at the same time in so-called chimera states [124]. As we found for random networks, synchronous and asynchronous states can be stable for the same networks, depending on initial conditions. Given a spatial dimension, networks split into synchronous and asynchronous regions. Moreover, such split states are generated generically and in a self-organized way. They add a new layer of complexity to (de-)synchronization phenomena, as entrainment to either the synchronous or asynchrous part of the network can occur either at the boundary or inside a region. The duality of the networks containing both short- and long-ranged connections is mirrored by the two distinct roads to synchrony/asynchrony, and allows for novel dynamical behaviors. In particular, we described extreme events of synchronous firing and a network rhythm which may emerge from these networks. We related the behaviors, to open problems of neural dynamics, namely epileptic seizures and the generation of the respiratory rhythm. The dynamical behaviors intimately rely on the dual structure of the considered networks containing both short- and

long-ranged connections. It remains to be investigated, however, if the described dynamics can be observed for other dynamical systems possibly described by ODEs. Or if not, to which extent the behaviors rely on singularities that are present in the studied integrate-and-fire systems.

In contrast to the our work on random networks, the definition of a continuum model, which captures the described dynamics on spatial networks is pending. It suggests itself to describe the continuum limit of a spatial network of phase oscillators by a complex-valued function. However, for asynchronous regions such a function will not be continuous and thus probably not very practical. The majority of the work that has been devoted to neural fields [132], reduces the state of neurons at some point in time, to a single value, the firing rate. While such models are able to describe excitation waves, it is probably necessary to extend them if they should be able to describe the evolution of the asynchronous regions that we reported on. Asynchronous and synchronous regions do not differ in their activity but in the local phase coherence, the amount of synchrony assessed near some position in the network. A continuum description of the investigated phenomena could possibly include a field of local synchrony.

There are several factors which influence synchronization phenomena in complex networks which we did not address here. The degree distribution of networks is known to have a large influence on synchronization phenomena, similar as assortativity, i.e., the correlation between the degrees of of connected nodes. Moreover, some variance between different units in a natural, complex network can often be assumed and the influence of this should be studied, especially for the dynamical behaviors that intuitively rely on homogeneity of parameters: The dynamics of avalanches is possibly changed when we assume distributed time delays for oscillators. Similarly, chimera states could be influenced by a distribution of oscillator frequencies. Other extensions of the studied model could include the study of negative phase responses either globally or in more complicated scenarios like negative phase responses for long-ranged connections and positive phase responses for short-ranged connections.

Most of the behaviors that we described probably do not rely on some attractor in phase space, but probably have to be considered as very long transient to synchrony. Similar as for turbulent flows, the high dimensionality of complex networks yields that transients often must be considered as the typical generic behavior of the systems. This underlines the importance of the investigation of large systems as some phenomena – like those with irregular macroscopic behaviors that we reported on in both random and small-world networks – might not be observable for small systems and thus are difficult to relate to the dynamics of the constituents.

Bibliography

[1] R. Gallagher and T. Appenzeller. *Complex Systems [Special Issue]*, volume 284. Science, 1999.

[2] A.-L. Barabási and R. Albert. Emergence of scaling in random networks. *Science*, 286:509–512, 1999.

[3] S. H. Strogatz. Exploring complex networks. *Nature*, 410:268–276, 2001.

[4] M. E. J. Newman. The structure and function of complex networks. *SIAM Rev.*, 45:167–256, 2003.

[5] S. Boccaletti, V. Latora, Y. Moreno, M. Chavez, and D.-U. Hwang. Complex networks: Structure and dynamics. *Phys. Rep.*, 424:175–308, 2006.

[6] E. N. Gilbert. Random graphs. *Ann. Math. Stat.*, 30:1141–1144, 1959.

[7] P. Erdős and A. Rényi. On random graphs I. *Publ. Math. Debrecen*, 6:290–297, 1959.

[8] MEJ Newman, DJ Watts, and SH Strogatz. Random graph models of social networks. *Proc. Natl. Acad. Sci. U.S.A.*, 99:2566–2572, 2002.

[9] S. Bornholdt, H.G. Schuster, and J. Wiley. *Handbook of graphs and networks*, volume 2. Wiley Online Library, 2003.

[10] V. Braitenberg and A. Schütz. *Anatomy of the cortex – statistics and geometry*. Springer, Berlin, 1991.

[11] D. J. Watts and S. H. Strogatz. Collective dynamics of 'small-world' networks. *Nature*, 393:440–442, 1998.

[12] A. Arenas, A. Díaz-Guilera, J. Kurths, Y. Moreno, and C. Zhou. Synchronization in complex networks. *Phys. Rep.*, 469:93–153, 2008.

[13] J. Buck and E. Buck. Mechanism of rhythmic synchronous flashing of fireflies. *Science*, 159:1319–1327, 1968.

[14] J. Buck. Synchronous rhythmic flsashing of fireflies. II. *Q. Rev. Biol.*, 63:265–289, 1988.

[15] L. Glass. Synchronization and rhythmic processes in physiology. *Nature*, 410:277–284, 2001.

[16] M. R. Guevara and T. J. Lewis. A minimal single-channel model for the regularity of beating in the sinoatrial node. *Chaos*, 5:174–183, 1995.

[17] D. Gonze, N. Markadieu, and A. Goldbeter. Selection of in-phase or out-of-phase synchronization in a model based on global coupling of cells undergoing metabolic oscillations. *Chaos*, 18:037127, 2008.

[18] K. Wiesenfeld, P. Colet, and S. H. Strogatz. Synchronization transitions in a disordered josephson series array. *Phys. Rev. Lett.*, 76:404–407, 1996.

[19] T. Sugawara, M. Tachikawa, T Tsukamoto, and T. Shimizu. Observation of synchronization in laser chaos. *Phys. Rev. Lett.*, 72:3502–3505, 1994.

[20] D Xenides, D S Vlachos, and T E Simos. Synchronization in complex systems following a decision based queuing process: rhythmic applause as a test case. *Journal of Statistical Mechanics: Theory and Experiment*, 2008:P07017, 2008.

[21] I. Farkas, D. Helbing, and T. Vicsek. Social behaviour: Mexican waves in an excitable medium. *Nature*, 419:131–132, 2002.

[22] S. H. Strogatz, D. M. Abrams, A. McRobie, B. Eckhardt, and E. Ott. Theoretical mechanics: Crowd synchrony on the millennium bridge. *Nature*, 438:43–44, 2005.

[23] Z. Li, Z. Duan, G. Chen, and L. Huang. Consensus of multiagent systems and synchronization of complex networks: A unified viewpoint. *Circuits and Systems I: Regular Papers, IEEE Transactions on*, 57:213 –224, 2010.

[24] Y.-W. Hong and A. Scaglione. A scalable synchronization protocol for large scale sensor networks and its applications. *Selected Areas in Communications, IEEE Journal on*, 23:1085–1099, 2005.

[25] Y. Kuramoto. Collective synchronization of pulse-coupled oscillators and excitable units. *Physica D*, 50:15–30, 1991.

[26] S. H. Strogatz. From Kuramoto to Crawford: exploring the onset of synchronization in populations of coupled oscillators. *Physica D*, 143:1–20, 2000.

[27] W. S. Lee, E. Ott, and T. M. Antonsen. Large coupled oscillator systems with heterogeneous interaction delays. *Phys. Rev. Lett.*, 103:044101, 2009.

[28] X. Guardiola, A. Díaz-Guilera, M. Llas, and C. J. Pérez. Synchronization, diversity, and topolgy of networks of integrate and fire oscillators. *Phys. Rev. E*, 62:5565, 2000.

[29] M. Barahona and L. M. Pecora. Synchronization in small-world systems. *Phys. Rev. Lett.*, 89:054101, 2002.

[30] T. Nishikawa, A. E. Motter, Y. C. Lai, and F. C. Hoppensteadt. Heterogeneity in oscillator networks: Are smaller worlds easier to synchronize? *Phys. Rev. Lett.*, 91:014101, 2003.

[31] M. Denker, M. Timme, M. Diesmann, F. Wolf, and T. Geisel. Breaking synchrony by heterogeneity in complex networks. *Phys. Rev. Lett.*, 92:074103, 2004.

[32] A. E. Motter, C. Zhou, and J. Kurths. Network synchronization, diffusion, and the paradox of heterogeneity. *Phys. Rev. E*, 71:016116, 2005.

[33] M. di Bernardo, F. Garofalo, and F. Sorrentino. Effects of degree correlation on the synchronization of networks of oscillators. *International Journal of Bifurcation and Chaos*, 17:3499–3506, 2007.

[34] M. Drew LaMar and Gregory D. Smith. Effect of node-degree correlation on synchronization of identical pulse-coupled oscillators. *Phys. Rev. E*, 81:046206, 2010.

[35] K. Yoshimura and K. Arai. Phase reduction of stochastic limit cycle oscillators. *Physical review letters*, 101:154101, 2008.

[36] J. n. Teramae, H. Nakao, and B. G. Ermentrout. Stochastic phase reduction for a general class of noisy limit cycle oscillators. *Phys. Rev. Lett.*, 102:194102, 2009.

[37] J. T. C. Schwabedal and A. Pikovsky. Phase description of stochastic oscillations. *Phys. Rev. Lett.*, 110:204102, 2013.

[38] C. S. Peskin. *Mathematical Aspects of Heart Physiology*. Courant Institute of Mathematical Sciences, New York, 1975.

[39] R. E. Mirollo and S. H. Strogatz. Synchronization of pulse-coupled biological oscillators. *SIAM J. Appl. Math.*, 50:1645–1662, 1990.

[40] M. Calamai, A. Politi, and A. Torcini. Stability of splay states in globally coupled rotators. *Phys. Rev. E*, 80:036209, 2009.

[41] C. van Vreeswijk. Partial synchronization in populations of pulse-coupled oscillators. *Phys. Rev. E*, 54:5522–5537, 1996.

[42] L. F. Abbott and C. van Vreeswijk. Asynchronous states in networks of pulse-coupled oscillators. *Phys. Rev. E*, 48:1483–1490, 1993.

[43] D. Zhou, A. V. Rangan, Y. Sun, and D. Cai. Network-induced chaos in integrate-and-fire neuronal ensembles. *Phys. Rev. E*, 80:031918, 2009.

[44] R. Brette, M. Rudolph, T. Carnevale, M. Hines, D. Beeman, J. Bower, M. Diesmann, A. Morrison, P. Goodman, F. Harris, M. Zirpe, T. Natschläger, D. Pecevski, B. Ermentrout, M. Djurfeldt, A. Lansner, O. Rochel, T. Vieville, E. Muller, A. Davison, S. El Boustani, and A. Destexhe. Simulation of networks of spiking neurons: A review of tools and strategies. *J. Comput. Neurosci.*, 23:349–398, 2007.

[45] D. Zhou, Y. Sun, A. Rangan, and D. Cai. Spectrum of lyapunov exponents of non-smooth dynamical systems of integrate-and-fire type. *J. Comp. Neurosc.*, 28:229–245, 2010.

[46] E. Meron. Pattern formation in excitable media. *Phys. Rep.*, 218:1–66, 1992.

[47] A. Bunde, J. Kropp, and H.-J. Schellnhuber, editors. *The Science of Disaster*. Springer, Berlin Heidelberg, 2002.

[48] D. Sornette. *Critical Phenomena in Natural Sciences*. Springer, Berlin Heidelberg, 2003.

[49] S. Albeverio, V. Jentsch, and H. Kantz. *Extreme Events in Nature and Society*. The Frontiers Collection. Springer, Berlin, 2006.

[50] J.-W. Kim and E. Ott. Statistics and characteristics of spatiotemporally rare intense events in complex Ginzburg–Landau models. *Phys. Rev. E*, 67:026203, 2003.

[51] M. A. Zaks, X. Sailer, L. Schimansky-Geier, and A. B. Neiman. Noise induced complexity: from subthreshold oscillations to spiking in coupled excitable systems. *Chaos*, 15:026117, 2005.

[52] V. Nagy and E. Ott. Control of rare intense events in spatiotemporally chaotic systems. *Phys. Rev. E*, 76:066206, 2007.

[53] A. Rothkegel and K. Lehnertz. Recurrent events of synchrony in complex networks of pulse-coupled oscillators. *Europhys. Lett.*, 95:38001, 2011.

[54] C. Bonatto, M. Feyereisen, S. Barland, M. Giudici, C. Masoller, J. R. Rios Leite, and J. R. Tredicce. Deterministic optical rogue waves. *Phys. Rev. Lett.*, 107:053901, 2011.

[55] Vimal Kishore, M. S. Santhanam, and R. E. Amritkar. Extreme events on complex networks. *Phys. Rev. Lett.*, 106:188701, 2011.

[56] P. So and E. Barreto. Generating macroscopic chaos in a network of globally coupled phase oscillators. *Chaos*, 21:033127, 2011.

[57] V. Kishore, M.S. Santhanam, and R. E. Amritkar. Extreme events and event size fluctuations in biased random walks on networks. *Phys. Rev. E*, 85:056120, 2012.

[58] J. Zamora-Munt, B. Garbin, S. Barland, M. Giudici, J. R. Rios Leite, C. Masoller, and J. R. Tredicce. Rogue waves in optically injected lasers: Origin, predictability, and suppression. *Phys. Rev. A*, 87:035802, 2013.

[59] J. A. Acebrón, L. L. Bonilla, C. J. Pérez Vicente, F. Ritort, and R. Spigler. The Kuramoto model: A simple paradigm for synchronization phenomena. *Rev. Mod. Phys.*, 77:137–185, 2005.

[60] C. van Vreeswijk. Analysis of the asynchronous state in networks of strongly coupled oscillators. *Phys. Rev. Lett.*, 84:5110–5113, 2000.

[61] S. H. Strogatz and R. E. Mirollo. Stability of incoherence in a population of coupled oscillators. *J. Stat. Phys.*, 63:613–635, 1991.

[62] Cheng Ly and G. Bard Ermentrout. Analysis of recurrent networks of pulse-coupled noisy neural oscillators. *SIAM J. Img. Sci.*, 3:113–137, 2010.

[63] K. A. Newhall, G. Kovacic, P. R. Kramer, D. Zhou, A. V. Rangan, and D. Cai. Dynamics of current-based, Poisson driven, integrate-and-fire neuronal networks. *Commun. Math. Sci.*, 8:541–600, 2010.

[64] D. M. Abrams, R. Mirollo, S. H. Strogatz, and D. A. Wiley. Solvable model for chimera states of coupled oscillators. *Phys. Rev. Lett.*, 101:084103, 2008.

[65] C. R. Laing. Chimera states in heterogeneous networks. *Chaos*, 19:013113, 2009.

[66] E. A. Martens, C. R. Laing, and S. H. Strogatz. Solvable model of spiral wave chimeras. *Phys. Rev. Lett.*, 104:044101, 2010.

[67] S. Olmi, R. Livi, A. Politi, and A. Torcini. Collective oscillations in disordered neural networks. *Phys. Rev. E*, 81:046119, 2010.

[68] R. Zillmer, R. Livi, A. Politi, and A. Torcini. Stability of the splay state in pulse-coupled networks. *Phys. Rev. E*, 76:046102, 2007.

[69] Jaeger D Schultheiss NW, Edgerton JR. Phase response curve analysis of a full morphological globus pallidus neuron model reveals distinct perisomatic and dendritic modes of synaptic integration. *J. Neurosci.*, 30:2767–2782, 2010.

[70] M. A. Farries and W. J. Charles. Phase response curves of subthalamic neurons measured with synaptic input and current injection. *J. Neurophys.*, 108:1822–1837, 2012.

[71] J. J. Hopfield and A. V. M. Herz. Rapid local synchronization of action potentials: Toward computation with coupled integrate-and-fire neurons. *Proc. Natl. Acad. Sci. U.S.A.*, 92:6655–6662, 1995.

[72] A. V. M. Herz and J. J. Hopfield. Earthquake cycles and neural reverberations: collective oscillations in systems with pulse-coupled threshold elements. *Phys. Rev. Lett.*, 75:1222–1225, 1995.

[73] U. Ernst, K. Pawelzik, and T. Geisel. Synchronization induced by temporal delays in pulse-coupled oscillators. *Phys. Rev. Lett.*, 74:1570–1573, 1995.

[74] M. Timme, F. Wolf, and T. Geisel. Coexistence of regular and irregular dynamics in complex networks of pulse-coupled oscillators. *Phys. Rev. Lett.*, 89:258701, 2002.

[75] A. N. Burkitt. A review of the integrate-and-fire neuron model: II. Inhomogeneous synaptic input and network properties. *Biol. Cybern.*, 95:97–112, 2006.

[76] A. N. Burkitt. A review of the integrate-and-fire neuron model: I. Homogeneous synaptic input. *Biol. Cybern.*, 95:1–19, 2006.

[77] K. V. Mardia. *Statistics of directional data.* Academic Press, London, 1972.

[78] A. Zumdieck, M. Timme, T. Geisel, and F. Wolf. Long chaotic transients in complex networks. *Phys. Rev. Lett.*, 93:244103, 2004.

[79] S. R. Campbell, D. L. Wang, and C. Jayaprakash. Synchrony and desynchrony in integrate-and-fire oscillators. *Neural Comput.*, 11:1595–1619, 1999.

[80] A. V. Rangan and D. Cai. Fast numerical methods for simulating large-scale integrate-and-fire neuronal networks. *J. Comput. Neurosci.*, 22:81–100, 2007.

[81] R. Brown. Calendar queues: a fast o(1) priority queue implementation for the simulation event set problem. *Commun. ACM*, 31:1220–1227, 1988.

[82] J. R. Driscoll, H.R. Gabow, R. Shrairman, and R. E. Tarjan. Relaxed heaps: an alternative to Fibonacci heaps with applications to parallel computation. *Commun. ACM*, 31:1343–1354, 1988.

[83] A. Rothkegel and K. Lehnertz. Conedy: A scientific tool to investigate complex network dynamics. *Chaos*, 22:013125, 2012.

[84] R. DeVille and C. Peskin. Synchrony and Asynchrony in a Fully Stochastic Neural Network. *Bull. Math. Biol.*, 70:1608–1633, 2008.

[85] C. Allen and C. F. Stevens. An evaluation of causes for unreliability of synaptic transmission. *Proceedings of the National Academy of Sciences*, 91:10380–10383, 1994.

[86] M. Volgushev, I. Kudryashov, M. Chistiakova, M. Mukovski, J. Niesmann, and U. T. Eysel. Probability of transmitter release at neocortical synapses at different temperatures. *Journal of neurophysiology*, 92:212–220, 2004.

[87] R. Botet and M. Płoszajczak. Universal features of fluctuations. *Nuclear Physics B-Proceedings Supplements*, 92:101–113, 2001.

[88] E. J. Hildebrand, M. A. Buice, and C. C. Chow. Kinetic theory of coupled oscillators. *Phys. Rev. Lett.*, 98:054101, 2007.

[89] E. Ott. *Chaos in Dynamical Systems*. Cambridge University Press, Cambridge, 1994.

[90] R. Zillmer, R. Livi, A. Politi, and A. Torcini. Desynchronization in diluted neural networks. *Phys. Rev. E*, 74:036203, 2006.

[91] Sven Jahnke, Raoul-Martin Memmesheimer, and Marc Timme. Stable irregular dynamics in complex neural networks. *Phys. Rev. Lett.*, 100:048102, 2008.

[92] R. Eichhorn, S. J. Lniz, and P. Hänggi. Transformation invariance of lyapunov exponents. *Chaos Solitons Fractals*, 12:1377–1383, 2001.

[93] R. Zillmer, N. Brunel, and D. Hansel. Very long transients, irregular firing, and chaotic dynamics in networks of randomly connected inhibitory integrate-and-fire neurons. *Phys. Rev. E*, 79:031909, 2009.

[94] A. Mauroy and R. Sepulchre. Clustering behaviors in networks of integrate-and-fire oscillators. *Chaos*, 18:037122, 2008.

[95] A. Politi and A. Torcini. Stable chaos. In M. Thiel, J. Kurths, M. C. Romano, G. Károlyi, and A. Moura, editors, *Nonlinear Dynamics and Chaos: Advances and Perspectives*, Understanding Complex Systems, pages 103–129. Springer Berlin Heidelberg, 2010.

[96] J.-P. Eckmann and D. Ruelle. Fundamental limitations for estimating dimensions and lyapunov exponents in dynamical systems. *Physica D*, 56:185, 1992.

[97] J. P. Crutchfield and K. Kaneko. Are attractors relevant to turbulence? *Phys. Rev. Lett.*, 60:2715–2718, 1988.

[98] T. Tel and Y. C. Lai. Chaotic transients in spatially extended systems. *Phys. Rep.*, 460:245–275, 2008.

[99] H.-L. Zou, M. Li, C.-H. Lai, and Y.-C. Lai. Origin of chaotic transients in excitatory pulse-coupled networks. *Phys. Rev. E*, 86:066214, 2012.

[100] S.M. Ross. *Stochastic Processes*. Wiley series in probability and mathematical statistics: Probability and mathematical statistics. Wiley, 1983.

[101] D.R. Cox and V. Isham. *Point Processes*. Monographs on applied probability and statistics. Chapman and Hall, 1980.

[102] N. Metropolis and S. Ulam. The monte carlo method. *Journal of the American statistical association*, 44:335–341, 1949.

[103] E. N. Brown, R. E. Kass, and P. P. Mitra. Multiple neural spike train data analysis: state-of-the-art and future challenges. *Nat. Neurosci.*, 7:456–461, 2004.

[104] S.P. Corwin, D. Sarafyan, and S. Thompson. Dklag6: a code based on continuously imbedded sixth-order runge-kutta methods for the solution of state-dependent functional differential equations. *Applied Numerical Mathematics*, 24:319–330, 1997.

[105] F. Hartung. *Differentiability of solutions with respect to parameters in differential equations with state-dependent delays*. Dissertation. University of Pannonia, Veszprém, Hungary, 2010.

[106] G. D. Smith. *Numerical solution of partial differential equations: finite difference methods*. Oxford University Press, 1985.

[107] Y. A. Kuzntsov. *Elements of applied bifurcation theory*, volume 112. Springer, 1998.

[108] A. Mauroy and R.J. Sepulchre. Global analysis of a continuum model for monotone pulse-coupled oscillators. *IEEE Trans. Autom. Control*, 58:1154–1166, 2013.

[109] L. Sirovich, A. Omurtag, and K. Lubliner. Dynamics of neural populations: stability and synchrony. *Comp. Neural Syst.*, 17:3–29, 2006.

[110] Grégory Dumont and Jacques Henry. Synchronization of an excitatory integrate-and-fire neural network. *Bull. Math. Biol.*, 75:629–648, 2013.

[111] W. Nicola and S. A. Campbell. Bifurcations of large networks of two-dimensional integrate and fire neurons. *J. Comput. Neurosci*, 35:87–108, 2013.

[112] P. Östborn. Renormalization of oscillator lattices with disorder. *Phys. Rev. E*, 79:051114, 2009.

[113] P. C. Bressloff. Resonantlike synchronization and bursting in a model of pulse-coupled neurons with active dendrites. *J. Comput. Neurosci.*, 6:237–249, 1999.

[114] D. Horn and I. Opher. Solitary waves of integrate and fire neural fields. *Neural Comput.*, 9:1677–1690, 1997.

[115] A. Rothkegel and K. Lehnertz. Multistability, local pattern formation, and global collective firing in a small-world network of non-leaky integrate-and-fire neurons. *Chaos*, 19:015109, 2009.

[116] A. Roxin, H. Riecke, and S. A. Solla. Self-sustained activity in a small-world network of excitable neurons. *Phys. Rev. Lett.*, 92:198101, 2004.

[117] Y. Kuramoto and D. Battogtokh. Coexistence of coherence and incoherence in nonlocally coupled phase oscillators. *Nonlinear Phenom. Complex Syst.*, 5:380–385, 2002.

[118] D. M. Abrams and S. H. Strogatz. Chimera states for coupled oscillators. *Phys. Rev. Lett.*, 93:174102, 2004.

[119] O. E. Omel'chenko, Y. L. Maistrenko, and P. A. Tass. Chimera states: The natural link between coherence and incoherence. *Phys. Rev. Lett.*, 100:044105, 2008.

[120] J. H. Sheeba, V. K. Chandrasekar, and M. Lakshmanan. Globally clustered chimera states in delay-coupled populations. *Phys. Rev. E*, 79:055203(R), 2009.

[121] M. Wolfrum and E. Omel'chenko. Chimera states are chaotic transients. *Physical Review E*, 84:015201, 2011.

[122] C. R. Laing, K. Rajendran, and I. G. Kevrekidis. Chimeras in random non-complete networks of phase oscillators. *Chaos*, 22:013132, 2012.

[123] M. Wildie and M. Shanahan. Metastability and chimera states in modular delay and pulse-coupled oscillator networks. *Chaos*, 22:043131, 2012.

[124] M. R. Tinsley, S. Nkomo, and K. Showalter. Chimera and phase-cluster states in populations of coupled chemical oscillators. *Nat. Phys.*, 2012.

[125] W. W. Lytton. Computer modelling of epilepsy. *Nat. Rev. Neurosci.*, 9:626–637, 2008.

[126] F. Mormann, R. Andrzejak, C. E. Elger, and K. Lehnertz. Seizure prediction: the long and winding road. *Brain*, 130:314–333, 2007.

[127] F. H. Lopes da Silva, W. Blanes, S. N. Kalitzin, J. Parra, P. Suffczynski, and D. N. Velis. Dynamical diseases of brain systems: different routes to epileptic seizures. *Biomedical Engineering, IEEE Transactions on*, 50:540–548, 2003.

[128] D. Takeshita, Y. D. Sato, and S. Bahar. Transitions between multistable states as a model of epileptic seizure dynamics. *Phys. Rev. E*, 75:051925, 2007.

[129] P. Suffczynski, F. H. Lopes da Silva, J. Parra, D. Velis, and S. Kalitzin. Epileptic transitions: Model predictions and experimental validation. *J. Clin. Neurophysiol.*, 22:288–299, 2005.

[130] P. Suffczynski, F. Wendling, J. J. Bellanger, and F. H. Lopes Da Silva. Some insights into computational models of (patho)physiological brain activity. *Proc. IEEE*, 94:784–804, 2006.

[131] J. L. Feldman and C. A. Del Negro. Looking for inspiration: new perspectives on respiratory rhythm. *Nat. Rev. Neurosci.*, 7:232–242, 2006.

[132] G. Deco, V. K. Jirsa Viktor, P. A. Robinson, M. Breakspear, and K. Friston. The dynamic brain: from spiking neurons to neural masses and cortical fields. *PLoS computational biology*, 4:e1000092, 2008.

Acknowledgements

This thesis would not have been possible without the support of many dear people. First of all I want to thank my supervisor and mentor Professor Klaus Lehnertz for his great support, the countless hours and patience he invested in me and for the encouragment and friendship throughout the years of my work. His way of scientific writing and thinking has defined my approach.I also want to thank Professor Carsten Urbach who agreed to serve as the co-examiner for this dissertation. I owe special gratitude to my parents Dorothea and Dr. Peter Rothkegel who have supported me all my life and shown me their unlimited encouragment and love and to my sister Steffi who always rushed to my side in ours of need. I owe great gratitude to Christoph Lindlahr and Noa Freudenthal for reading and correcting mistakes in grammar and style. Sincere thanks to my friends Henning Dickten, Christian Geier for their courageous commitment to the never-ending quest for the nerdiest tools and development environment. I want to thank Justus Schwabedal for his ongoing encouragment and friendship over the years. Special thanks to Gerrit Ansmann for teaching me the merits of a rational keyboard layout. I am indebted to all the past and present members of the Neurophysics research group. I will miss the place upon the Venusberg.